

**ORNL/TM-2001/2**

**Cooperative Research and Development  
Agreement Final Report  
for  
Cooperative Research and Development  
Agreement Number ORNL93-0237**

**ADHESIVE BONDING  
TECHNOLOGIES FOR AUTOMOTIVE  
STRUCTURAL COMPOSITES**

**February 2001**

**Unlimited Distribution**

## **DISCLAIMER**

This report was prepared as an account of work sponsored by an agency of the United States Government. Neither the United States Government nor any agency thereof, nor any of their employees, makes any warranty, expressed or implied, or assumes any legal liability or responsibility for the accuracy, completeness, or usefulness of any information, apparatus, product, or process disclosed, or represents that its use would not infringe privately owned rights. Reference herein to any specific commercial product, process, or service by trade name, trademark, manufacturer, or otherwise, does not necessarily constitute or imply its endorsement, recommendation, or favoring by the United States Government or any agency thereof. The views and opinions of the authors expressed herein do not necessarily state or reflect those of the United States Government or any agency thereof.

**ORNL/TM-2001/2**

**Cooperative Research and Development Agreement  
Final Report  
for  
Cooperative Research and Development Agreement  
Number ORNL93-0237**

**ADHESIVE BONDING TECHNOLOGIES FOR  
AUTOMOTIVE STRUCTURAL COMPOSITES**

R. G. Boeman  
D. L. Erdman  
L. B. Klett  
R. D. Lomax  
J. M. Starbuck  
F. L. Paulauskas  
Oak Ridge National Laboratory

J. A. Schroeder  
Automotive Composites Consortium

February 2001

Prepared by the  
OAK RIDGE NATIONAL LABORATORY  
Oak Ridge, Tennessee 37831

MANAGED BY UT-BATTELLE, LLC, FOR THE U.S. DEPARTMENT OF ENERGY  
UNDER CONTRACT DE-AC05-00OR22725

## TABLE OF CONTENTS

<b>LIST OF TABLES .....</b>	<b>V</b>
<b>LIST OF FIGURES .....</b>	<b>VII</b>
<b>LIST OF ACRONYMS.....</b>	<b>IX</b>
<b>ABSTRACT .....</b>	<b>XI</b>
<b>1. INTRODUCTION.....</b>	<b>1</b>
<b>2. OBJECTIVES .....</b>	<b>3</b>
2.1 Bulk Materials.....	3
2.2 Fracture Mechanics.....	4
2.3 Modeling/Characterization.....	4
2.4 Process Control and Nondestructive Evaluation.....	4
2.5 Crash Energy Management of Bonded Composites.....	4
2.6 Fatigue Durability of Bonded and Hybrid Joints.....	4
2.7 Alternate Processing .....	5
2.8 Manufacturability Demonstration.....	5
<b>3. ACCOMPLISHMENTS .....</b>	<b>7</b>
3.1 Bulk Materials.....	7
3.2 Fracture Mechanics.....	7
3.3 Modeling\Characterization.....	8
3.4 Nondestructive Evaluation.....	9
3.5 Crash Energy Management of Bonded Composites.....	9
3.6 Alternate Processing .....	9
<b>4. TECHNICAL DISCUSSION.....</b>	<b>11</b>
4.1 Technical Approach.....	11
4.2 Bulk Materials.....	11
4.3 Fracture Mechanics.....	23
4.4 Modeling/Characterization.....	54
4.5 Process Control and Nondestructive Evaluation.....	56
4.6 Crash Energy Management of Bonded Composites.....	59
4.7 Fatigue Durability of Bonded and Hybrid Joints.....	62
4.8 Alternate Processing .....	63
4.9 Manufacturability Demonstration.....	66
<b>5. INVENTIONS .....</b>	<b>69</b>
<b>6. COMMERCIALIZATION .....</b>	<b>71</b>
6.1 Bulk Material Data.....	71
6.2 Structural Mechanics Test Development.....	71
6.3 Predictive Modeling .....	71
<b>7. FUTURE COLLABORATION .....</b>	<b>73</b>

**TABLE OF CONTENTS CONTINUED**

**8. CONCLUSIONS .....75**  
    8.1 *Bulk Materials*..... 75  
    8.2 *Fracture Mechanics*..... 75  
    8.3 *Nondestructive Evaluation*..... 76  
    8.4 *Crash Energy Management* ..... 76  
    8.5 *Alternative Processing*..... 76  
**9. ACKNOWLEDGMENTS .....77**  
**10. REFERENCES .....79**  
**DISTRIBUTION .....81**

## LIST OF TABLES

Table 4.2.1. Room Temperature (21°C) Tensile Test Data .....	16
Table 4.2.2. Elevated Temperature (80°C) Tensile Test Data .....	16
Table 4.2.3. Creep Test Matrix .....	18
Table 4.2.4. Tensile Creep Power Law Fit Parameters.....	20
Table 4.3.1. Dimensions and Properties of Substrates for Backing Beam Determination .....	33
Table 5.1. Invention Disclosures Filed as a Result of CRADA Research .....	69



## LIST OF FIGURES

Figure 2.1. Task Areas for the Adhesive Bonding Technologies for Automotive Structural Composites CRADA.....	3
Figure 4.2.1. Bubble in the Cross-Section of a Failed Specimen.....	14
Figure 4.2.2. Particle Inclusion in the Cross-Section of a Failed Specimen.....	16
Figure 4.2.3. Stress-Strain Curves for BFG EXP582E, T=21°C (68°F).....	17
Figure 4.2.4. Stress-Strain Curves for BFG EXP582E, T=80°C (176°F).....	17
Figure 4.2.5. Creep Results for Loads at 40% of Ultimate Strength, 80°C.....	19
Figure 4.2.6. Creep Results for Loads at 60% of Ultimate Strength, 80°C.....	19
Figure 4.2.7. Creep Results for Loads at 40% of Ultimate Strength, 21°C.....	20
Figure 4.2.8. Incremental Loading/Recovery Test, Increasing Stress Levels.....	21
Figure 4.2.9. Incremental Loading/Recovery Test, Constant Stress Levels.....	22
Figure 4.3.1. The Three Modes of Fracture: (a) Opening or Mode I, (b) Sliding Shear or Mode II and (c) Transverse Shear or Mode III.....	24
Figure 4.3.2. Flexure Failure of the Substrate During Mode I Fracture Tests of SRIM Composites with Traditional DCB Geometry.....	26
Figure 4.3.3. Composite Beam Cross-Section Consisting of Backing Beam Rigidly Attached to a Substrate.....	29
Figure 4.3.4. Finite Element Analysis Depicting Mode-Mix Versus the Ratio of Substrate Heights for a Steel-Aluminum Specimen.....	30
Figure 4.3.6. Contoured Backing Beam.....	32
Figure 4.3.7. Schematic Representation of a Test Specimen with Dissimilar Substrates and Backing Beams.....	32
Figure 4.3.8. Load-Displacement Record for an Epoxy Mode I Test.....	34
Figure 4.3.9. Load-Displacement Record for a Composite Mode I Test.....	34
Figure 4.3.10. Load-Displacement Record for a Composite-Epoxy-Composite Mode I Test.....	34
Figure 4.3.11. Load-Displacement Record for a Steel-Epoxy-Steel Mode I Test.....	35
Figure 4.3.12. Load-Displacement Record for a Composite-Epoxy-Steel Mode I Test.....	35
Figure 4.3.13. Fiber Bridging in a Composite-Epoxy-Composite Mode I Test.....	36
Figure 4.3.14. Failure Surface for Mode I Fracture of Composite-Epoxy-Steel Specimen.....	37
Figure 4.3.15. Fracture Toughness Values Calculated with Several Analysis Methods.....	38
Figure 4.3.16. Fracture Toughness as a Function of Crack Length (Each Case Represents Several Specimens).....	39
Figure 4.3.17. Modified ENF Specimen.....	40
Figure 4.3.18. Load-Displacement Record for Mode II Composite Joint Test.....	41
Figure 4.3.19. Load-Displacement Record for Mode II Steel Joint Test.....	41
Figure 4.3.20. Load-Displacement Record for Mode II Epoxy Test.....	42
Figure 4.3.21. FEM Mode II Load-Displacement Results (No Adhesive or Initial Crack).....	43
Figure 4.3.22. FEM Determined Stresses (a=45mm, 1.75 in, No Insert, with Friction).....	44
Figure 4.3.23. FEM Determined Stresses (a=45 mm, 1.75 in, Insert, with Friction).....	45
Figure 4.3.24. FEM Determined Stresses (a=95 mm, 3.75 in, Insert, with Friction).....	46
Figure 4.3.25. FEM Mode II Load-Displacement Results (No Insert).....	46
Figure 4.3.26. FEM Mode II Load-Displacement Results (Insert).....	47
Figure 4.3.27. Mode II Fracture Toughness vs. Crack Length for Five Composite-Composite ENF Specimens.....	49

**LIST OF FIGURES CONTINUED**

Figure 4.3.28. Mode II Fracture Toughness vs. Crack Length for Three Composite-Composite ENF Specimens .....49

Figure 4.3.29. Mode II Fracture Toughness vs. Crack Length for Four Composite-Composite ENF Specimens .....50

Figure 4.3.30. Typical MMF Specimen .....51

Figure 4.3.31. Typical Load-Displacement Curve From a Pure Adhesive MMF Specimen .....52

Figure 4.3.32. Mixed Mode Model Geometry .....53

Figure 4.3.33. Test Case Specimen Geometry .....54

Figure 4.4.1 Von Mises Equivalent Stress Contours In A Composite/Epoxy Specimen With A Trapezoidal Interface Separation Law Under Mode I Loading .....56

Figure 4.5.1. Photo Results from Shearography NDT Trial: Dark Areas Indicate Good Adhesion. Small Black Circles Indicate Where Core Samples Were Removed .....58

Figure 4.6.1. Longitudinally Bonded SRIM Composite Hourglass Rails.....60

Figure 4.6.2. Dynamic Response Curves for Four Longitudinally Bonded Crush Rails.....61

Figure 4.6.3. Dynamic Response Curves for Ten Transversely Bonded Crush Rails .....61

Figure 4.8.1. Comparison of Lap-Shear Test Results for Adhesive Cured with Microwave Energy Under Various Operation Conditions .....64

Figure 4.8.2. Glass Fibers Exposed Through Laser Ablation in a SRIM Composite.....65

## LIST OF ACRONYMS

ACC: Automotive Composites Consortium  
CRADA: Cooperative Research and Development Agreement  
CSM: Continuous Strand Mat  
DAQ: Data Acquisition  
DMTA: Dynamic Mechanical Thermal Analyzer  
DOE: Department of Energy  
DCB: Double Cantilever Beam  
DSC: Differential Scanning Calorimeter  
EM: Energy Management  
EMRC: Engineering Mechanics Research Corporation  
ENF: End-Notched Flexure (Specimen)  
FEA: Finite Element Analysis  
FP II: Focal Project II  
FTIR: Fourier Transform Infrared Spectroscopy  
MMF: Mixed Mode Flexural  
MMPI: Michigan Materials and Processing Institute  
NCCST: National Center for Composite Systems Technology  
NDA: Nondestructive Analysis  
NDE: Nondestructive Evaluation  
NDT: Nondestructive Testing  
ORNL: Oak Ridge National Laboratory  
PC: Process Control  
P-FMEA: Processing-Failure Modes and Effects Analysis  
PI: Principle Investigator  
PMCs: Polymer Matrix Composites  
P/U: Pickup (truck)  
s-SMC: Simulated Sheet Molding Compound  
SMC: Sheet Molding Compound  
SRIM: Structural Reaction Injected Molded  
USAMP: United States Automotive Materials Partnership



## ABSTRACT

In 1993, the Oak Ridge National Laboratory (ORNL) entered into a Cooperative Research and Development Agreement (CRADA) with the Automotive Composites Consortium (ACC) to conduct research and development that would overcome technological hurdles to the adhesive bonding of current and future automotive materials. This effort is part of a larger Department of Energy (DOE) program to promote the use of lighter weight materials in automotive structures for the purpose of increasing fuel efficiency and reducing environmental pollutant emissions. In accomplishing this mission, the bonding of similar and dissimilar materials was identified as being of primary importance to the automotive industry since this enabling technology would give designers the freedom to choose from an expanded menu of low mass materials for component weight reduction.

The research undertaken under this CRADA addresses the following areas of importance: bulk material characterization, structural fracture mechanics, modeling/characterization, process control and nondestructive evaluation (PC/NDE), manufacturing demonstration, and advanced processing. For the bulk material characterization task, the individual material properties of the adherends and adhesives were characterized. This included generating a database of mechanical and physical properties, after identifying and developing standard test methods to obtain properties. The structural fracture mechanics task concentrated on test development to characterize the fracture toughness of adhesively bonded joints subjected to Mode I, Mode II and mixed-mode conditions. Standard test procedures for quantifying an adhesive/adherend system's resistance to crack growth were developed for use by industry. In the modeling/characterization task, fracture mechanics-based design guidelines and predictive methodologies have been developed which will facilitate iteration on design concepts for bonded joints while alleviating the need for extensive testing. Methods for nondestructive evaluation of adhesive bonds that can be used for process optimization, in-line process control and product validation were evaluated in the PC/NDE task. Promising NDE techniques were identified for additional development. In the advanced processing task, rapid-cure and advanced surface preparation processes were investigated with the goal of increasing the manufacturability and performance as well as reducing the costs of bonded composites. Demonstration that a "designed for composites" structure is manufacturable was undertaken in the manufacturability demonstration task.

In addition to the aforementioned efforts, ancillary topics that were coordinated by the CRADA partners will be discussed briefly. These include the performance of bonded composite structures in crashes and fatigue durability of bonded and hybrid joints. This report covers the activities undertaken during the CRADA through February 1997.



## 1. INTRODUCTION

In the future, automobiles will be required to travel further before refueling while discharging lower levels of pollutants. Currently, automobiles account for just slightly less than two-thirds of the nation's gasoline usage, and about one-third of the total United States energy consumption. By improving automotive fuel efficiency, the United States can lessen the impact that foreign oil prices have on our economy and lives. In addition, decreased emissions from reduced fuel consumption will provide a cleaner environment for future generations. At current usage rates, a 25% weight reduction in vehicles would save an estimated 750,000 barrels of oil each day, reduce the yearly domestic fuel consumption by 13% and eliminate 101 million tons of CO<sub>2</sub> emitted into the atmosphere each year. [1,2]

A significant reduction in fuel consumption can be achieved by three means: (1) improving engine and drivetrain efficiency; (2) reducing automotive component mass and thus vehicle weight; and (3) reducing the size and thus weight of an automobile. Engine efficiency improvements are being studied in a wide variety of industry and government programs and great strides are being made in this area. Vehicle downsizing has been undertaken since the gasoline crisis of the early '70s and is still occurring. However, consumers are reluctant to purchase increasingly smaller vehicles due to their transportation requirements. Reducing component weight and vehicle weight, without sacrificing vehicle size, reducing safety or increasing vehicle cost, can be accomplished by the use of alternate, lighter weight materials. The goal of this project is to provide one enabling technology, adhesive bonding, which will allow for the use of alternate materials, particularly reinforced polymer matrix composites (PMCs).

The commercial application of composites has an extensive history in the marine, aerospace and construction industries but has evolved relatively slowly in the automotive industry during the past 25 years. Composite use has traditionally been limited to secondary structures, such as appearance panels and dash boards, but PMCs are now being considered for weight reduction in future automotive structures and load-bearing components. A critical aspect of using these materials is the manner in which they are joined, since conventional attachment technologies, such as welding and bolting, are not suitable for PMCs and some other alternate materials. Adhesive bonding is an economical and structurally sound joining method that may overcome this major obstacle to the incorporation of lighter weight materials into automobiles. Adhesive bonding provides many benefits that will ultimately lead to lighter-weight vehicles, fuel savings, and reduced emissions. Among the benefits are design flexibility, opportunity for part consolidation, and joining of dissimilar materials. Additionally, adhesive bonding can result in stiffer assemblies and better load distribution regardless of the substrates. Consequently, bonded parts are typically smaller, thinner, and lighter without sacrificing load carrying capacity.

While much work has been conducted in adhesive bonding for the aerospace industry, the automotive industry does not currently have a full portfolio of processes and methods for evaluating candidate adhesives for use in bonding structural automotive components. Aerospace techniques and materials are not generally applicable, since the automobile industry must be more cognizant of cost and high volume production. Consequently, the charter of this project was to develop those processes and methods.

The following is the final report documenting work performed by the ORNL, and the ACC under the CRADA ORNL93-0237 titled "Adhesive Bonding Technologies for Automotive Structural Composites." The report describes the CRADA partners' results toward developing

adhesive bonding technologies that will facilitate the greater use of advanced materials and joining technologies. Discussion is limited to research activities completed through February 1997.

The enormous economic impact of this program on the automotive industry is apparent by the sheer size of the American automotive market. The technologies to be developed in this CRADA will enable the use of alternate, lighter weight components in future automobiles. In addition to the consumer benefit and environmental impact of lighter vehicles that have already been mentioned, successful deployment of these advanced technologies will help keep American automotive companies at the forefront of transportation technology, resulting in greater worldwide sales and more productive jobs for Americans.

## 2. OBJECTIVES

The overall objective of this cooperative effort between ORNL and the ACC was to develop and demonstrate adhesive bonding technologies for the design, manufacture, and assembly of composite automotive structures. Every attempt was made to develop technologies of a generic nature sufficient to cover future materials in addition to those available when this project was initiated.

Task areas were determined in cooperation with the CRADA partners. Project efforts were organized into six major tasks and coordinated with two additional efforts as shown in Figure 2.1.

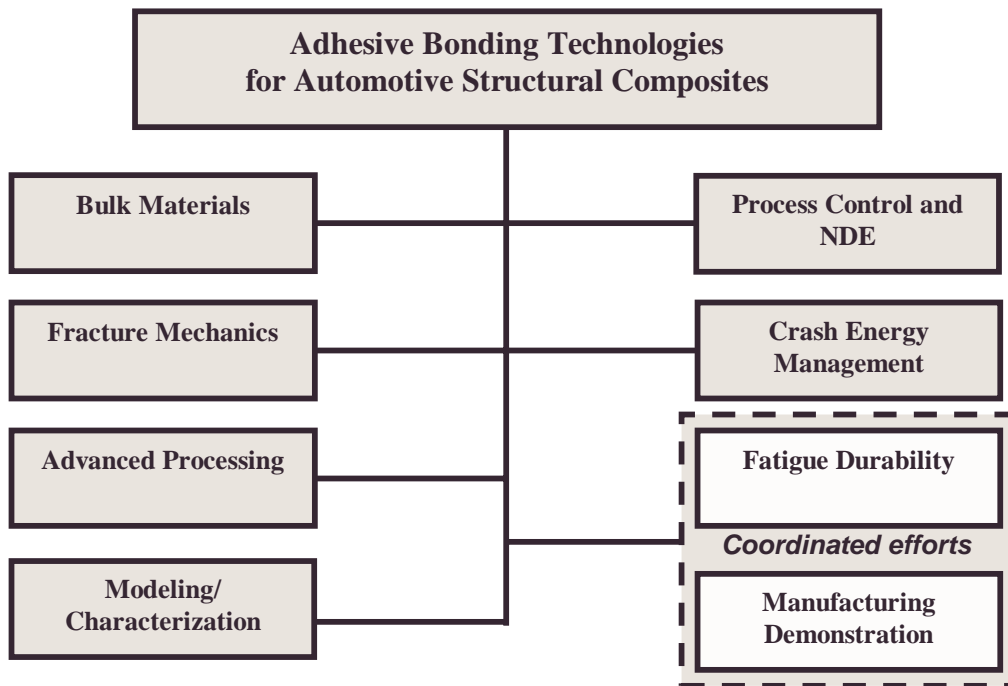


**Figure 2.1. Task Areas for the Adhesive Bonding Technologies for Automotive Structural Composites CRADA**

A brief description of the goal along with the organizational lead for each of the six major research tasks follows.

### 2.1 Bulk Materials

The goal of the bulk materials task was to characterize the properties of each of the joint constituents independent of one another or interfacial influences (when they are not combined to form an adhesive joint). Mechanical, thermal, and diffusion properties were obtained. The results were required for implementation into materials models as well as for defining operating parameters for the material systems investigated. The work in this task was led by the ACC with participation from suppliers and ORNL.

## **2.2 Fracture Mechanics**

The overall goal of the fracture mechanics task was to develop standardized and automated test procedures for characterizing the fracture toughness of joints for adhesively bonded automotive materials. The resultant test methods will be used by automotive companies and their suppliers to generate material property data to be incorporated into design codes to predict the performance of bonded joints. To successfully achieve the overall goal of this task, several objectives were established. (1) Resolve many theoretical and experimental issues associated with specimen design and data reduction schemes. (2) Develop test methods that will be valid for a wide range of both adherend and adhesive properties using standardized geometries, sizes, fixtures and procedures. (3) Establish and incorporate the most repeatable and accurate data reduction schemes. (4) Automate the test methods using commercial products suitable for technology transfer to industry. (5) Publish and issue a test manual to potential suppliers. The work in this task was conducted by ORNL.

## **2.3 Modeling/Characterization**

The objective of the modeling/characterization task was to develop predictive methodologies to describe the resistance of adhesively bonded joints to crack growth under general loading conditions. Additionally, fracture mechanics-based design guidelines for adhesively bonded automotive structures were sought. The work in this task was contracted to the University of Texas at Austin under the direction of Professor Ken Liechti. ORNL and ACC jointly monitored the progress of this subcontract.

## **2.4 Process Control and Nondestructive Evaluation**

The goal of this task was to identify and develop methods for nondestructive evaluation for process optimization, in-line production process control, and product validation. This task was led by the ACC with assistance from ORNL. A subcontract was awarded to Oakland University, under the direction of Professor Y.Y. Hung, for development of one of several possible NDE techniques, specifically shearography.

## **2.5 Crash Energy Management of Bonded Composites**

The goal of this task was to initiate a preliminary investigation to determine how various joint configurations performed in crash energy management structures. The ACC Joining and Energy Management Groups conducted this task.

## **2.6 Fatigue Durability of Bonded and Hybrid Joints**

The goal of this task was to investigate the fatigue performance of bonded and hybrid (bonded and bolted) composite joints. This task was conducted by the University of Michigan – Dearborn under the direction of Professor P. K. Mallick and monitored by the ACC.

## **2.7 Alternate Processing**

This task's objective was to identify and develop alternate adhesive processing methods to substantially reduce processing time and cost, while providing increased performance. The task was conducted by ORNL.

## **2.8 Manufacturability Demonstration**

The objective of this task was to demonstrate that a "designed for composites" vehicle, or major vehicle sub-assembly, is manufacturable, meets defined performance criteria, and achieves mass savings (relative to conventional steel structures) at minimum cost. The work in this task was primarily conducted by the ACC.



### 3. ACCOMPLISHMENTS

#### 3.1 Bulk Materials

Two adhesives were chosen for the fundamental, baseline work of the program: a tough urethane and a strong epoxy. These adhesives were characterized in order to obtain the bulk material properties needed for all modeling and analysis. A slightly modified version of the one part epoxy adhesive (654 ETG) was chosen as the adhesive for use in Focal Project II (FP II), the manufacturing demonstration project. The epoxy was characterized to obtain data necessary for Finite Element Analysis (FEA). Over the course of FP II, the structural reaction injected molded (SRIM) substrate was altered due to concerns about moisture, resulting in the qualification of a new substrate/adhesive system for FP II. The new version of the SRIM substrate was found to be compatible with the chosen adhesive. A simulated sheet molding compound (s-SMC) cross-sill material, which was hand-fabricated for FP II, was tested and yielded good adhesion results with the 654 ETG. Long-term stress/durability studies have been initiated to develop correlations between lab test results and field performance with respect to durability.

Methods for casting neat-adhesive panels for test coupons (dog-bone specimens) were developed to produce acceptable, consistent test specimens for static tensile and creep experiments. Significant effort was expended developing processing techniques to reduce trapped gas bubbles and maintain uniform specimen thickness. Specific processes investigated included centrifuging adhesives prior to molding between steel plates along with injection molding techniques. Resultant test coupons exhibited reduced scatter in mechanical property data.

Drying procedures were developed for the composite substrates to eliminate blistering and the subsequent loss of adhesive caused by the rapid expansion of trapped moisture during the heating phases of specimen manufacture.

Tensile test methods appropriate for the experimental adhesive considered in this study were developed to determine required mechanical properties. Specific concerns included stress-strain behavior, stiffness and strength measurements, and elongation to failure. Tests were conducted at room and elevated temperatures (80°C).

Creep testing procedures appropriate for this class of adhesive were developed. These procedures were essential due to the sensitivity of the adhesive to temperature and inelastic behavior indicated by non-recoverable strains observed during experiments. The latter behavior necessitated establishing specimen-preconditioning procedures to minimize scatter and establish permanent deformation thresholds.

A power law creep relationship was adopted to describe elongation-time behavior for adhesives. Testing at room and elevated temperatures over a range of creep stress levels was carried out to establish the creep-law parameters.

#### 3.2 Fracture Mechanics

##### 3.2.1 Mode I

Double cantilever beam specimens employing backing beams were adopted to facilitate Mode I fracture toughness testing of automotive adhesive joints. Procedures for manufacturing

and preparation to assure consistent specimen quality and uniformity were developed. Problematic issues associated with these specimens which were solved included: identifying acceptable adhesives and surface preparations to ensure good backing beam to substrate adhesion throughout the test, maintaining bond-line thickness, and reducing unfavorable effects due to moisture and air trapping during cure cycles.

A fracture toughness test procedure was developed to characterize Mode I fracture behavior for adhesive joints with similar and dissimilar substrates. Joint configurations included: bonded composites, bonded steel and composite bonded to steel joints as well as neat adhesives. All configurations were investigated through a comprehensive test matrix.

A compliance matching approach was developed to determine Mode I fracture toughness of adhesive joints comprised of dissimilar substrates (such as steel-composite joints). This approach utilizes the concept of varying backing beam height to achieve equivalent flexural stiffness in the dissimilar beams, thereby achieving the desired Mode I fracture condition.

A draft test manual for Mode I fracture toughness of adhesive joints has been developed and reviewed by the ACC Joining Group. Validation of the manual will be assessed through round robin testing. The procedures outlined in this manual include instructions for specimen preparation, testing and data reduction of all the aforementioned material combinations considered for automotive adhesive joints.

### **3.2.2 Mode II**

A test method to determine Mode II fracture toughness in adhesive joints was developed and evaluated through experimental tests. Observed hysteresis in experimental load-displacement records indicated the possibility of frictional forces at the fracture surface during crack extension. The presence of frictional forces was confirmed through a finite element analysis.

Guided by the finite element analysis, a modified edge notch flexural specimen, employing a roller-pin support was developed to reduce the undesirable frictional forces observed during crack growth.

### **3.2.3 Mixed Mode**

Preliminary mixed-mode fracture toughness tests were conducted employing a modified mixed-mode flexural specimen that made use of metallic backing beams. These tests explored fracture behavior with steel-steel, composite-composite and purely adhesive bonded joints (adhesive layer between two backing beams).

## **3.3 Modeling\Characterization**

A non-linear finite-element analysis incorporating a traction-law approach to model crack growth under applied load was conducted. Input parameters for this analysis required measurement of dynamic mechanical, strain rate and shear properties over a range of various frequencies and temperatures.

A fracture-based predictive methodology was proposed to determine critical load conditions necessary for crack growth. Implementation required development of a mixed-mode fracture envelope in conjunction with the aforementioned finite element analysis. Fracture

values for this analysis require toughness testing over a range of mode-mixes with both steel and composite adherends, with both epoxy and urethane adhesives.

### **3.4 Nondestructive Evaluation**

After examining a wide range of nondestructive evaluation techniques as candidates for on-line component/structural validation, a full-field technique was determined to be the appropriate approach for assessing the integrity of bonded composite joints. Of those techniques considered, laser shearography was identified and demonstrated to be an excellent candidate for this application.

### **3.5 Crash Energy Management of Bonded Composites**

Hourglass rail structures were fabricated with a variety of longitudinal and transverse joints. Drop tower testing was conducted, and the results indicate that certain longitudinal joint geometries result in stable crush and have potential for crash management applications.

### **3.6 Alternate Processing**

The application of single frequency and variable-frequency microwave technology for joining of substrates using epoxy-based adhesives significantly reduced the curing time by 66 to 75%. This was accomplished while maintaining equal or slightly higher values of the load carrying capability measured through the single lap-shear test.

Microwave processed samples, when tested as single lap-shear specimens exhibited less rigidity but more plasticity compared to conventionally processed samples. Coupling of the Goodrich EXP 582E epoxy based adhesive to the 2.45 GHz microwave radiation is extremely efficient and was enhanced with a carbon black additive.

A laser ablation technique was explored and demonstrated as a potential technique for automated rapid surface preparation. It resulted in bonded specimens that had better lap-shear strengths than specimens with solvent only preparation. Optimization of this process may lead to further improvements, especially for carbon-reinforced composites.



## 4. TECHNICAL DISCUSSION

The tasks under this program were executed by industry, university and government researchers and were managed in a joint effort between the ACC and ORNL staff members. During the execution of the CRADA, the partners published comprehensive quarterly reports containing detailed documentation of the research activities. In addition, several publications are available summarizing or detailing research findings. It is not the intent of this document to supplant those documents, but rather to summarize the salient aspects of the various tasks and provide references for the interested reader. In some cases where insufficient detail is contained in the aforementioned documents, the subject matter will be expounded upon in this document. Discussion is limited to research activities completed through February 1997.

### 4.1 Technical Approach

At the onset of this program, the ability to structurally bond composites for automotive applications was unproven. The issues involved in bonding SRIM composites include: initial adhesion, bulk properties of substrates and adhesives (initial and over time), methods of dealing with mold release, production processing capability, joint performance, and environmental durability. Systems with acceptable properties and performance were unknown. With this in mind, the primary goals of this work were to identify and characterize acceptable systems, develop appropriate screening tests, compile the necessary material databases, develop performance guidelines, and optimize processing. Every attempt was made to choose generic material systems that would typically be considered for automotive bonding applications such that results from this effort could be extrapolated to other material systems.

### 4.2 Bulk Materials

#### 4.2.1 Material Selection

Commercial and developmental adhesives from several suppliers were evaluated for their structural performance in bonding glass reinforced SRIM composites for automotive applications. The initial SRIM substrate of interest was DOW MM 364, a polyisocyanurate-based material. Adhesives from Dow-Essex, Ashland, SIA Inc. a subsidiary of Sovereign Specialty Chemicals (formerly B.F. Goodrich), Lord, 3M, and other suppliers were investigated. Generally, the adhesives were either epoxy or urethane-based. Ultimately, two adhesives were chosen for continuing work: a 2-part Ashland urethane (rated acceptable) and a 1-part Goodrich (now Sovereign) epoxy (rated excellent), designated BFG (SIA) EXP582E. All other adhesives evaluated at this time were found inappropriate for this specific (SRIM) application. Bulk properties required for modeling efforts, including moisture uptake, were obtained for the adhesives. Additionally, lap shear results were used to estimate acceptability in bonded joints.

In support of FP II, a bonded composite pick-up box, a newly reformulated adhesive with lower cure temperature and better sag properties was developed to address issues concerning production-capability. The resultant formulation, designated as Sovereign 654 ETG, was obtained and accepted as the adhesive for FP II based on material property evaluation and lap-shear results. FP II also required modifications to the composite substrate to address undesirable issues regarding moisture uptake. Moisture, which was absorbed into the original composite

substrate, was found to cause degassing during adhesive cure, resulting in adhesive “blow-out” at the bond (rigorous adhesive foaming). To resolve this problem, Baydur 420, a polyurethane based composite material was adopted and qualified with the 654 ETG adhesive for the FP.

A second composite substrate, consisting of s-SMC, was also identified for use in vehicle cross-sills (the cross-box structural reinforcements and sites for box/frame attachment) for FP II. The s-SMC was evaluated for bonding with the 654 ETG adhesive and found to have acceptable properties.

## **4.2.2 Specimen Fabrication**

### **4.2.2.1 Neat Adhesive Specimens**

It should be noted that although SIA 654 ETG adhesive was utilized in FP II, the research on adhesive bonding primarily considered BFG582E since this adhesive was considered a representative adhesive for most structural automotive SRIM applications. Additionally, a significant familiarity with this adhesive system, which will be detailed in the following sections, had been established prior to the onset of FP II. For example, processing suitable neat adhesive panels was found to be difficult due to physical characteristics of many adhesives, such as high viscosity and trapped air. The adhesive supplier provided samples that indicated that one-sided tooling resulted in surface voids and variations in thickness. To overcome these undesirable results, considerable effort had been expended in developing new methods for fabricating BFG EXP582E adhesive panels.

#### ***Casting with Two-Sided Tooling***

Initially, panels were fabricated by placing adhesive between two flat stainless steel plates. The steel plates were then clamped together with a spacer, which provided a fixed and uniform thickness of 3.175 mm (0.125 in). The fixture was then placed in an oven at 150°C for 1 hour to cure the adhesive. The panels produced using this method contained numerous voids, which led to premature failures in tensile tests.

A second approach for casting panels involved degassing the adhesive under vacuum to remove any dissolved air. After degassing, the adhesive was poured between stainless steel plates and cured. This method showed a slight improvement in panel quality; however, due to high viscosity the adhesive did not completely degas. Most likely, some air was also trapped in the adhesive during the transfer to the stainless steel plates.

Attempting to improve on the previous method, a thin layer of adhesive was applied to stainless steel plates and placed under vacuum in a chamber (both with and without heating). This method reduced the trapped air; however, the adhesive did not flow into the degassed voids.

Since the vacuum method was unsuccessful, the possibility of centrifugation for removing air from the adhesive was explored next. In this method, the adhesive was heated to 85°C and centrifuged at 1000 g's for 5 minutes. The resin was then reheated and poured onto an 85°C stainless plate. The plates were then bolted together and cured. This produced a significantly higher quality panel, although small voids were still present.

Encouraged by the success obtained with the centrifuge method, it was decided to reduce the adhesive viscosity further by heating the adhesive to 90°C after centrifugation. The adhesive was returned to a 100°C oven for an additional 25 minutes. Finally, upon removal from the oven

the adhesive was poured into a small mold followed by reheating for final cure. This procedure resulted in a void-free panel.

A full-sized panel was fabricated after making two additional modifications to the method outlined above. First, the centrifuge buckets were preheated to 120°C prior to centrifugation. At this temperature the heated buckets were no longer acting as heat sinks, to cool the adhesive, resulting in higher viscosity. This permitted the adhesive to be poured directly into the mold after centrifugation. Additionally, a “collapsible” gasket was developed increasing the area of the adhesive introduction port of the panel mold, thereby lessening the need for a lower adhesive viscosity. These changes significantly improved the quality of the panel and provided a more direct fabrication method.

After producing several panels using the previous method it became apparent the adhesive was partially curing prior to being transferred to the mold. In order to lessen the curing effect it was determined that a suitable viscosity could be achieved by heating the material to 77°C in an 82°C oven for approximately 1.5 hours. Once at 77°C, the adhesive could be centrifuged at 1000 g's in a 90°C centrifuge bucket for three minutes while maintaining a viscosity low enough to pour into a preheated 90°C mold with a “collapsible” gasket. This method for fabricating BFG EXP582E adhesive panels has proven to be an acceptable process for consistently producing quality panels.

### ***Fabrication with Injection Molding***

Injection molding was also investigated for the production of BFG EXP582E adhesive panels. The first attempt at fabricating a panel involved placing adhesive in a preheated 70°C reservoir and slowly introducing it into a warm stirring chamber under vacuum. Once the adhesive was degassed, it was injected into a Lexan mold that was also under vacuum. Although the injection process went well, there was contamination introduced into the adhesive from the galvanized piping used in the system. Another problem encountered was sagging in the Lexan mold during the pre-cure phase of the operation.

A new Lexan/aluminum mold was prepared for a second attempt with injection molding. This attempt was successful except for some sagging in the Lexan during the pre-curing step. Although injection molding with BFG EXP582E was deemed viable, further development ceased since this process was found to be more labor intensive and did not provide any noticeable improvements in panel quality over the conventional centrifugation method.

### ***Adhesive Analyses***

After the procedure to fabricate acceptable adhesive panels was developed, several samples from a panel were analyzed using a differential scanning calorimeter (DSC), dynamic mechanical thermal analyzer (DMTA), and density measurements to determine the degree of non-homogeneity of the cast adhesive. The results from these preliminary tests indicated there was very little variation in the material property data. Micrographs of the fracture surface of several tensile coupons were also obtained. In spite of the significant efforts to reduce voids, failed specimens were found to contain some small voids or inclusions which appeared to serve as fracture initiation sites as shown in Figure 4.2.1.

During panel fabrication with the centrifugation method, some solids are partially removed due to the processing technique. Initially it was believed these particles were fillers. However, after running Fourier transform infrared spectroscopy (FTIR), it was determined this material was actually dicyandiamide, a curing agent used with epoxy resins. Possibly the

dicyandiamide was acting as a potential failure initiator in tensile specimens. Reduction of the amount of dicyandiamide, through the centrifugation process, did not inhibit curing but did provide better properties due to the removal of failure initiators.

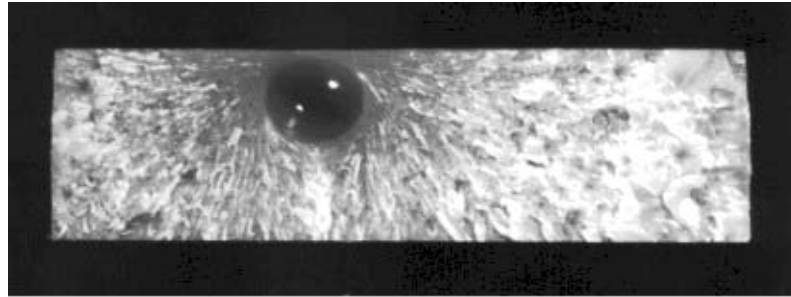


**Figure 4.2.1. Bubble in the Cross-Section of a Failed Specimen**

#### 4.2.2.2 Bonded Composite Specimens

When the first composite lap-shear samples were bonded using the epoxy-based adhesive, the composite blistered and the adhesive “blew out” of the joint during the curing cycle. The resulting samples were warped and the joints had no adhesive on the interior. Instead, a significant amount of adhesive was bonded onto the edges of the joint. After careful inspection, the source of the problem became readily apparent. Since the composite resin is a polyisocyanurate it has a large affinity for absorbing atmospheric moisture. Upon heating to 150°C, the absorbed fluid was constrained from escaping the composite due to microscopic, localized, thermal constriction of the capillary defects in the composite. This resulted in sufficient pressure to build inside the composite to produce blistering. Similarly, the thixotropic adhesive was constraining the surface and sub-surface moisture from escaping due to its high viscosity. As heating progressed, the adhesive's viscosity decreased, while the gas pressure increased, until the adhesive was forced out of the joint by the escaping gas. This resulted in foaming of the adhesive and a large percentage of disbonds in the joint.

The obvious solution to these problems was to eliminate the water before bonding. To accomplish this, a conservative drying temperature of 101°C was chosen to avoid burning or overheating the composite. Tests were then run for varying lengths of time (1 to 144 hours) to determine the total moisture content of the material and the removal rate by heating [1]. Of interest was not only the effect of moisture absorption in samples stored at room conditions, but also on samples that had been subjected to very wet and very dry conditions. To obtain this information, three sets of samples were considered: (1) stored at ambient conditions (69% relative humidity, RH); (2) stored in distilled water (100% RH) for six days; and (3) stored in a desiccator (5% RH) for six days. All samples were maintained at 21°C (72°F). The samples were then dried as described above and weight loss measurements were made. The samples stored at 69% RH had a weight loss of 0.9% during drying. The samples stored in water gained 0.4% by weight while submerged and then lost a total of 1.3% upon drying. The samples stored in the desiccators lost 0.3% by weight while in the desiccator and an additional 0.6% upon drying. In each case, the samples were almost completely dried in 48 hours. Therefore, all neat resin samples were dried at 101°C for 48 hours prior to bonding. This successfully eliminated the composite blistering and adhesive “blow out”.

### 4.2.3 Long-Term Environmental Testing

A long-term phase of the project was initiated at the Ford Scientific Research Laboratory to evaluate the properties of bonded joints when subject to mechanical stresses along with environmental exposure. It is expected that these conditions occurring simultaneously are considerably more severe than either mechanical loading or environment alone. Fixtures and grips were designed to allow bonded lap shear specimens to be loaded in tension and then submerged in an environmental chamber. Specimens were preloaded to predetermined load levels based on percentages of “ultimate failure” loads, and then placed in water at different temperatures. Samples loaded to high levels (50% and 40% of ultimate strength) all failed within a short period of time, while many of the lower load specimens (10%, 20%, 30%) had not failed after extensive exposure times. Interpretation of these results is under discussion, especially since there is little field data available for correlation for these new materials. The goal is to develop an understanding of what type of durability can be expected of this more realistic loading with exposure conditions. For example, accelerated test methods exist for metals, based on industry experience, that correlate a specific environmental exposure for a short time period is equivalent to long-term aging without the environmental exposure.

### 4.2.4 Static Tensile Testing of BFG582E Adhesive Specimens

An in-house built servo-hydraulic test machine with high temperature capabilities was employed to conduct the static tensile tests. The four-post test frame has a capacity of approximately 445 kN (100 kip), for extreme rigidity. However, the actuator and load cell were chosen to be 125 kN (28 kip) and 44.5 kN (10 kip) respectively for better machine control and measurement resolution at lower load levels. The control system was an MTS 407 controller with an MTS MicroProfilor function generator. The data acquisition system consists of a Hewlett Packard 3852A data acquisition and control unit for real time data collection and graphical display. Both control and data acquisitions systems were interfaced with a Macintosh PowerPC computer for consistent automated testing and real time displays of all measured test parameters. Control and data acquisition software was written in-house with a LabView development system. Temperature control was maintained with an in-house designed ATS oven with a two-zone LFE 3000 bi-modal heating/cooling temperature controller. The temperature range of the oven was approximately -84°C (-120°F) to 315°C (600°F). Custom features of the oven include an optical grade quartz port for specimen observation and liquid nitrogen capability for rapid heating/cooling cycles.

A summary of all static tensile tests at room temperature and 80°C is given in Tables 4.2.1 and 4.2.2. Several interesting observations concerning this data can be made. For the average material strength, the trend is increasing strength with manufacture date. This can be attributed to improvements in material processing. Specifically, as the number and size of what appeared to be air bubbles in the adhesive were reduced, material strength tended to increase. Unfortunately, this adhesive system also contains randomly distributed particulates consisting of non-dissolved hardener that are inherent in the composition of this epoxy. Microscopic inspection revealed that these bubbles and inclusions resulted in stress concentration sites that served as sources for crack initiation. These characteristics are most likely significant sources

for material property scatter in this adhesive. Examples of these bubbles and inclusions are shown in Figures 4.2.1 and 4.2.2.

**Table 4.2.1. Room Temperature (21°C) Tensile Test Data**

<u>Manufacture Date</u>	<u>Number of Specimens</u>	<u>Ave. Strength [ksi]</u>	<u>Ave. Strength [MPa]</u>	<u>Ultimate Strain [%]</u>
Prior to 9/95	3	7.82	53.9	2.3
9/21/95	3	8.43	58.1	3.0
1/05/96	8	9.04	62.3	2.7
2/06/96	3	11.0	76.2	4.5
9/20/96	3	11.8	81.7	9.8
11/05/96	3	11.4	78.8	9.7
02/21/97	3	10.9	75.1	6.3

**Table 4.2.2. Elevated Temperature (80°C) Tensile Test Data**

<u>Manufacture Date</u>	<u>Number of Specimens</u>	<u>Ave. Strength [ksi]</u>	<u>Ave. Strength [MPa]</u>	<u>Ultimate Strain [%]</u>
1/05/96	4	7.72	53.3	3.8
2/06/96	4	8.06	55.6	6.2
9/20/96	2	7.11	49.0	6.7
11/05/96	2	6.78	46.8	7.0
2/21/97	3	7.80	55.0	6.3

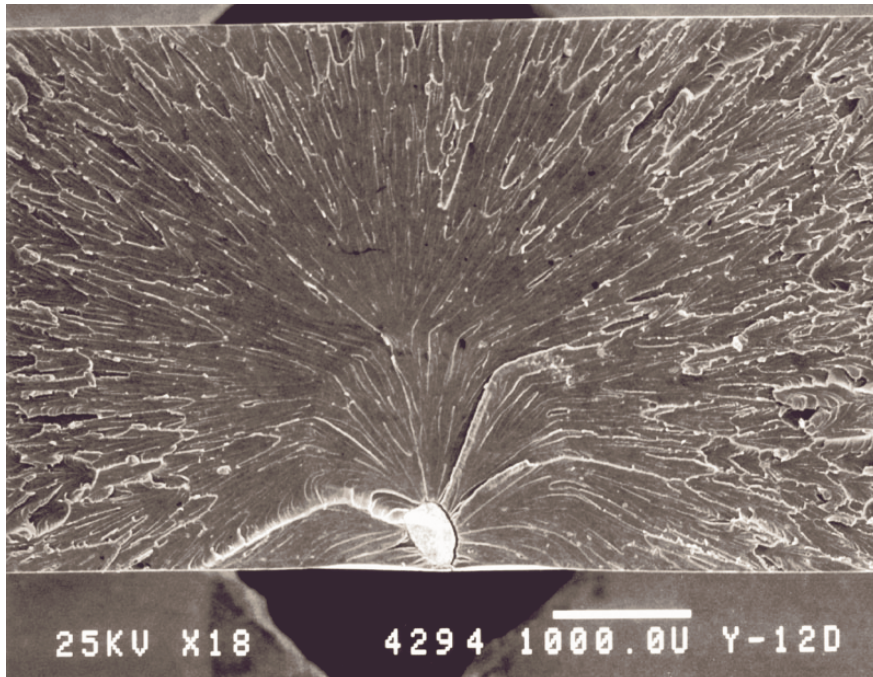


**Figure 4.2.2. Particle Inclusion in the Cross-Section of a Failed Specimen**

Typical stress-strain curves at room and elevated temperatures are plotted in Figures 4.2.3 and 4.2.4, respectively. These data represent a random selection of specimens from three different specimen panels (manufacture dates are 9/20/96, 11/05/96 and 2/21/97). It is obvious that the scatter (ultimate stress and strain levels) in the room temperature data is relatively small compared to that in the elevated temperature data set. There is also a noticeable increase in the scatter for the specimen stiffness from the room temperature to the elevated temperature data.

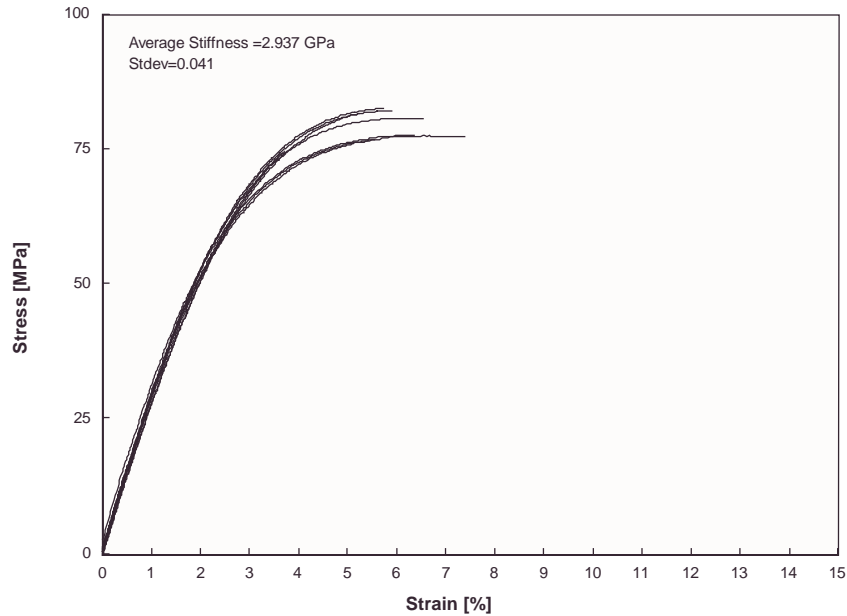


**Figure 4.2.3. Stress-Strain Curves for BFG EXP582E, T=21°C (68°F)**

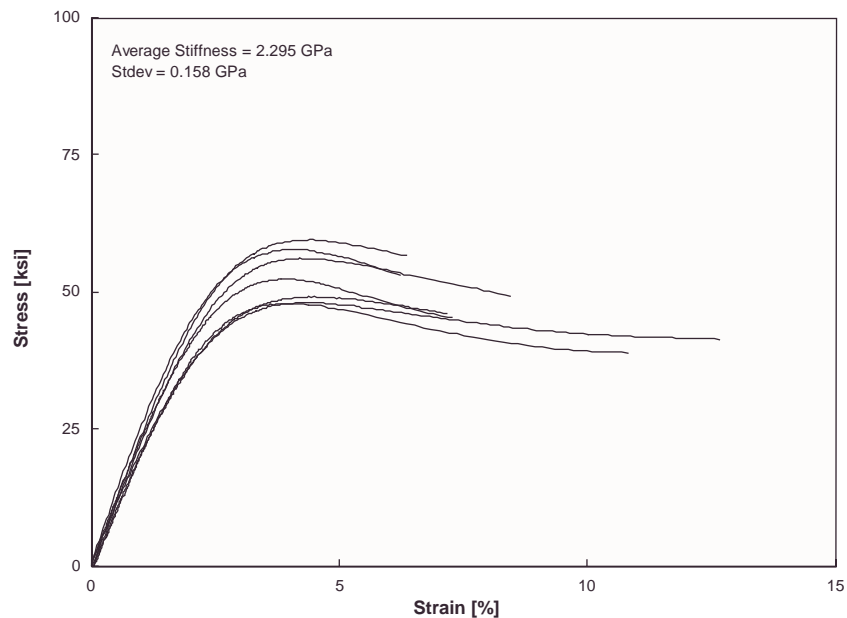


**Figure 4.2.4. Stress-Strain Curves for BFG EXP582E, T=80°C (176°F)**

#### 4.2.5 Creep Testing of BFG582E Adhesive

Creep testing was not originally a focus area of this CRADA. However, upon the request of the ACC, ORNL investigated the creep response of the BFG EXP582E epoxy.

Creep tests were conducted on four “dead weight” ATS creep machines. Loading was applied through manually operated weight platforms that could be lowered and raised smoothly by a lever-screw mechanism. Dead loads were verified by inserting a load cell in each machine prior to testing. Specimen gripping was accomplished with manual clamping grips that were attached to the load frames with a clevis-pin connection. The temperature was maintained with ATS clamshell ovens and LFE 2000 temperature controllers. Strain measurements were obtained with standard gages that were conditioned through a Hewlett Packard 3497 data acquisition and control unit. All measurements of strain and temperature were automated employing in-house developed software written in LabView.

As a starting point for the creep testing, a total of 18 possible testing conditions consisting of three applied stress levels at two different temperatures were chosen. Stress levels were calculated as percentages of the ultimate strength measured in tensile tests. To expedite the completion of the testing matrix, the creep tests were terminated when the strain levels reached a certain percentage of the average strain at failure determined from tensile tests. The two temperatures selected were room temperature, 21°C, for baseline data and 80°C, which was believed to be a conservative temperature level, well below the glass transition temperature of the adhesive (approximately 120°C). The original proposed test matrix is shown in Table 4.2.3.

**Table 4.2.3. Creep Test Matrix**

<b>Temperatures:</b>	<b>20°C (68°F)</b> <b>80°C (176°F)</b>
<b>Stress Levels:</b>	<b>0.2 <math>\sigma_{ult}</math></b> <b>0.4 <math>\sigma_{ult}</math> (<math>\sigma_{ult}</math> determined for each temperature)</b> <b>0.6 <math>\sigma_{ult}</math></b>
<b>Test Duration:</b>	<b>Time to reach 30%, 55% and 80% of ultimate strain</b>

Sixteen traditional creep tests were conducted at applied stress levels of 40% and 60% of the ultimate stress levels at room and elevated temperature. The strain vs. time behavior is shown in Figures 4.2.5, 4.2.6 and 4.2.7 for different stress levels and temperatures. It should be noted that the negative strain values in these plots are those for transverse measurements. The results of these tests are listed in Table 4.2.4 with the experimentally determined power-law parameters described in Equation [4.2.1].

$$\varepsilon(t) = \varepsilon_0 + mt^n \quad [4.2.1]$$

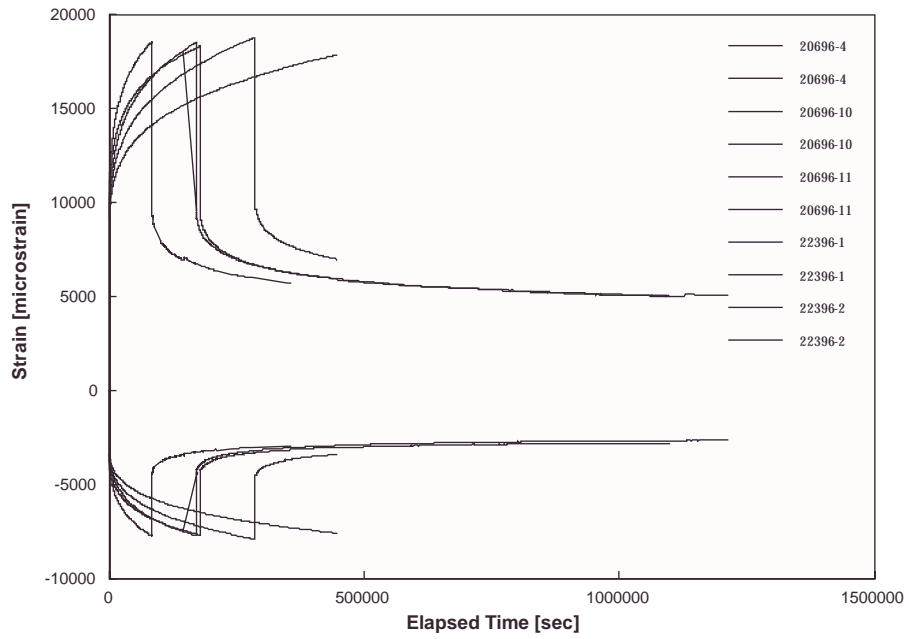


Figure 4.2.5. Creep Results for Loads at 40% of Ultimate Strength, 80°C

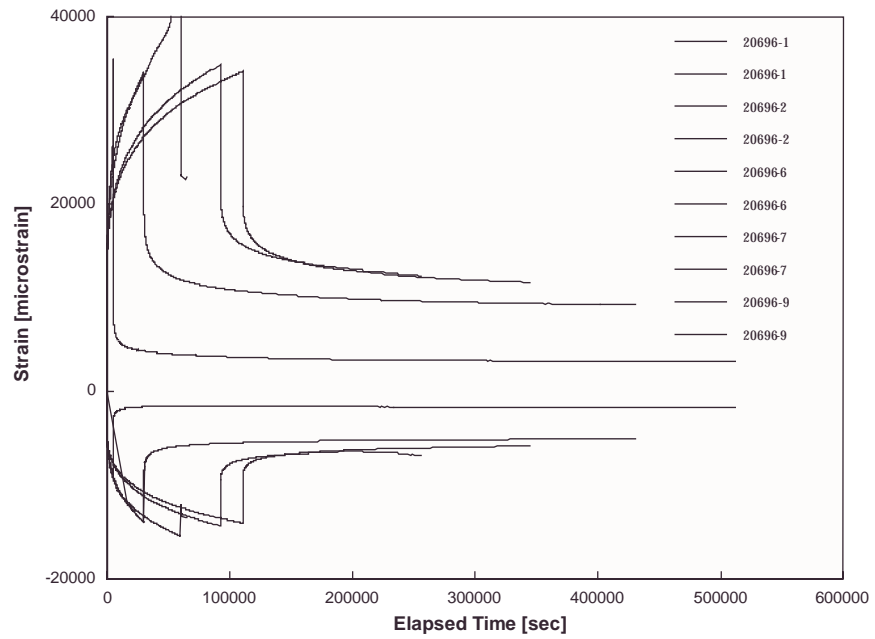
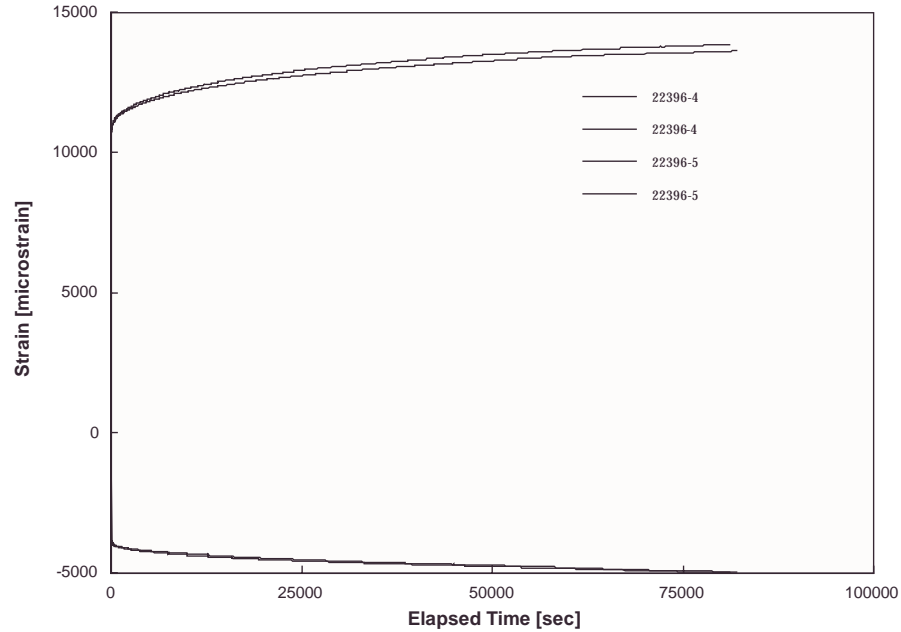


Figure 4.2.6. Creep Results for Loads at 60% of Ultimate Strength, 80°C



**Figure 4.2.7. Creep Results for Loads at 40% of Ultimate Strength, 21°C**

**Table 4.2.4. Tensile Creep Power Law Fit Parameters**

<u>Specimen</u>	<u>Temp. °C</u>	<u>Applied <math>\sigma_{ult}</math></u> <u>%</u>	<u>Initial Strain</u>	<u>m, multiplier</u>	<u>n, exponent</u>
20696-4	80	40	7890	234	0.320
20696-10	80	40	7350	634	0.237
20696-11	80	40	6880	730	0.246
22396-1	80	40	8070	199	0.318
22396-2	80	40	7750	250	0.285
22396-4	21	40	9790	354.	0.208
22396-5	21	40	9800	361	0.211
10596-24	80	60	13300	252	0.434
10596-27	80	60	9200	1380	0.240
20696-1	80	60	12500	418	0.383
20696-2	80	60	14100	52.8	0.636
20696-6	80	60	11900	610	0.311
20696-7	80	60	12100	807	0.320
20696-9	80	60	12100	478	0.340

The creep tests at elevated temperature for both 40 and 60% levels of applied stress exhibited large scatter. This could be expected considering the significant scatter in the static tensile results at elevated temperature. The scatter indicates that temperature may play a

significant role in the material behavior. For this case, the ramifications of temperature sensitivity can be observed by recalling the power law fit in Equation 4.2.2, which includes temperature effects. Notice that the term  $t/a_T$  significantly affects the shape of the strain-time curve and  $a_T$  is a function of temperature.

$$\varepsilon(t, T) = \varepsilon_0(T) + m \left( \frac{t}{a_T} \right)^n \quad [4.2.2]$$

To further complicate matters, there are a significant number of locations within the material that potentially serve as crack initiation sites. Under creep loading, random opportunities for cracks to initiate under the load application and then progress slowly within the softened material over time may exist. This would lead to artificially high instantaneous strain levels (see Table 4.2.4), which would have a cumulative effect over the test duration, resulting in inaccurate strain-time response curves.

Another noticeable feature of the creep response for this material is the large permanent strain present when the load was removed. When the specimens were unloaded, the bottom clevis attachment was removed; hence the specimens were essentially “load free” and should have recovered to a zero strain level. Permanent strain indicates that the elastic limit of this material has been exceeded, or alternatively there was damage introduced at the relatively high stress levels. In either case, it is desirable to determine if a threshold stress level exists for this material in which perfect elastic material behavior is observed. This was accomplished by conducting two incremental load tests at room temperature in which a sequence of increasing load cycles were applied to a specimen.

In the first test, the loading was applied in a series of increasing stress levels with a zero-load recovery time period between the successive cycles as depicted in Figure 4.2.8. These loads were applied in a very systematic manner, starting with low initial stress levels (approximately 5% of the ultimate strength). For each load cycle, the recovery time period lasted ten times longer than the time period required to complete the previous loading. Strain was monitored throughout the test, employing an extensometer as well as longitudinal and transverse strain gages.

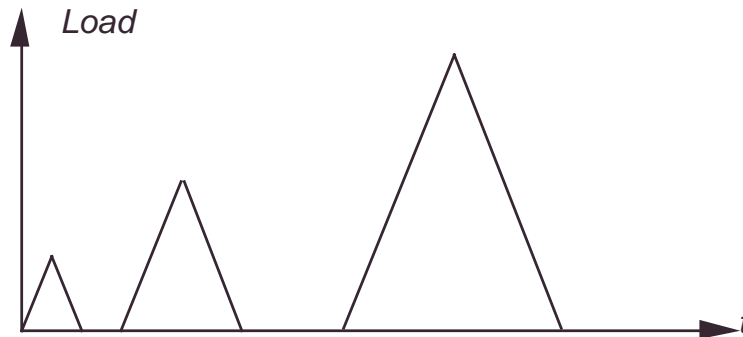


**Figure 4.2.8. Incremental Loading/Recovery Test, Increasing Stress Levels**

The second test consisted of loading cycles that had the same stress amplitude (approximately 30% of the ultimate strength), and a soak period at maximum stress as shown in Figure 4.2.9. As in the previous test, the recovery period in the unloaded state was ten times longer than the previous soak period at maximum stress.

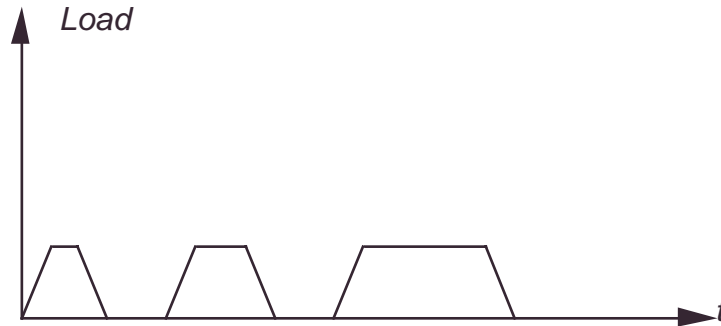


**Figure 4.2.9. Incremental Loading/Recovery Test, Constant Stress Levels**

In the incremental loading test with increasing stress, there appeared to be a continuous increase in permanent strain making it difficult to identify a precise stress level where the elastic limit of the material was exceeded. Slight differences between the extensometer and strain gage readings were noted and may be attributed to slight bending (specimens are not perfectly flat), or there may have been slight misalignment of the load train. Additionally, the resolution and sensitivity of an extensometer is much less than that of a strain gage that contributes to this discrepancy. Overall, it appears that this material exhibited permanent deformation at very low stress levels. Hence the basic equations of viscoelasticity may not be valid, and it may be necessary to separate the elastic and irrecoverable components of strain.

The incremental loading/recovery test with constant stress level indicated that there was a cumulative build-up of the permanent deformation with time. This agrees, for the most part, with the data from the creep tests. Specifically, the longer creep tests exhibited larger permanent strains.

### ***Discussion and Recommendations***

The results from the creep tests clearly indicate that the BFG582E adhesive is a complex material system with a number of undesirable interrelated characteristics. Specifically, there is substantial scatter in both the strength-elongation measurements and the inelastic time dependent response, and the likelihood exists that these characteristics may be influenced by the sensitivity of this material to temperature.

This material behavior presents a challenge in the design and implementation of material characterization techniques. However, with the knowledge gained through these preliminary static tensile and creep tests, it is possible to tailor subsequent tests to eliminate or substantially reduce some of the simultaneously occurring effects. In view of this, the following recommendations are made and are expected to be incorporated in a follow-on research program.

- Since the particulates in the adhesive cannot be eliminated, new procedures should be adopted to better estimate strength and ultimate strain levels from static tests at elevated

temperatures. This will probably require a greater number of static tensile tests to obtain an acceptable level of statistical significance. Additionally, in view of temperature sensitivity, the scatter in the static tensile data may be reduced with improved temperature control.

- Since the creep test results at room temperature exhibit little scatter, a time commitment should be made to dedicate several creep testing frames for additional long-term tests. These results will help identify the role temperature plays in the creep response of this material.
- Reducing the scatter in the static tensile tests should contribute to the improvement of elevated temperature creep tests. However, it may also be necessary to employ stress conditioning of specimens prior to creep testing. Essentially, this involves systematic fatigue cycling of the specimen to “activate” the flaws in the material to achieve a more consistent average material response
- Clearly, additional tests should be conducted to determine the stress level corresponding to the elastic limit of this adhesive and to establish the relationship between non-recoverable strain and applied stress levels/creep test duration. If this is accomplished, it should be possible to separate the elastic and inelastic responses necessary for material characterization.

#### **4.2.6 Additional Materials Efforts**

In addition to the efforts discussed previously, the ORNL/ACC project team prepared many types of test specimens needed for other joining activities. For example, the group designed and fabricated “known flaw” specimens for Nondestructive Testing (NDT) investigations, prepared the specimens required by the modeling sub-contractor (University of Texas), and designed SRIM hat-section specimens to be used in the fatigue durability work and in some NDT studies.

Finally, the group has planned, and is initiating two other adhesive joint testing sub-projects. The first project will include in-depth evaluation of the Sovereign 654 ETG to Baydur 420 bonded joint to determine the effects of bond thickness, loading rate, impact and fatigue durability, thermal fatigue, etc. This work will be carried out at the Chrysler test lab. The second project is a review of potential adhesives for bonding SRIM substrates. This is being revisited since the substrate was changed from the Dow material to the Baydur SRIM. The substrate will be sent to various adhesive suppliers for a first level screening of any off-the-shelf adhesives that might have acceptable properties. No development efforts will be requested at this time.

### **4.3 Fracture Mechanics**

#### **4.3.1 General Considerations**

Comprehensive fracture toughness characterization of a material requires determining its resistance to crack propagation for three modes of deformation shown in Figure 4.3.1— Mode I (cleavage or opening), Mode II (forward shear or sliding) and Mode III (transverse shear or edge

tearing). Additionally, the combination of these modes (mixed-mode) must be considered. Propagating cracks in isotropic metals subjected to mixed-mode conditions will typically turn to grow under Mode I conditions, making Mode I toughness of primary interest. For bonded joints in which the crack initiates in the adhesive, however, the adherend may confine the crack to the bond line, unable to turn, so that Mode II and mixed-mode crack propagation may become a much more relevant issue. It is generally accepted that most joints are designed such that the Mode III contribution is negligible. Accordingly, the fracture mechanics task was restricted to Modes I, and II and in-plane mixed-mode, a combination of Modes I and II.

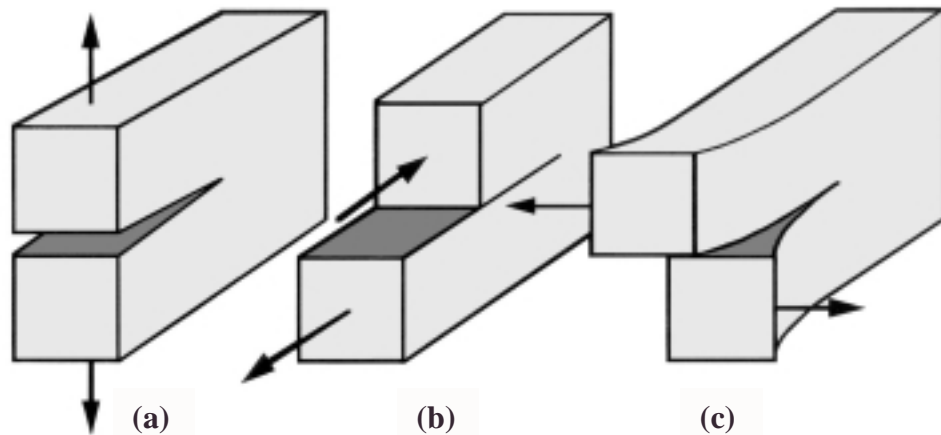


**Figure 4.3.1. The Three Modes of Fracture: (a) Opening or Mode I, (b) Sliding Shear or Mode II and (c) Transverse Shear or Mode III**

The goal of the fracture mechanics task was to develop testing procedures applicable to a broad range of automotive materials, not to characterize specific materials [1-3]. Therefore, to evaluate the test methods, materials were chosen that are believed to represent some of the most challenging substrates: a standard e-coated thin-section steel, and a glass-fiber, polymer matrix composite. The specific e-coating considered used for corrosion resistance had a Ford Motor Co. designation of J28. The composite was made from a continuous-strand mat preform infiltrated with an isocyanurate (Dow MM364) resin by a SRIM process. The composite was considered to be transversely isotropic, although slight differences in modulus were observed in the two principal directions. Fiber volume content was approximately 25%. The adhesive chosen for this study was a non-commercial thixotropic epoxy.

## 4.3.2 Mode I Fracture Toughness Testing

### 4.3.2.1 Mode I Fundamentals – the Double Cantilever Beam Test

Mode I fracture toughness defines a material's resistance to crack propagation while under tensile forces normal to the crack surface. Several standard methods exist for testing composites, metals and plastics in Mode I fracture. For composite delamination and adhesive joint studies, most methods are based on the double cantilever beam (DCB) specimen [4,5]. In its simplest configuration, the DCB specimen geometry consists of a uniform thickness rectangular specimen with a crack starter at one end. The specimen is visualized as two cantilevered beams, fixed at the crack tip. Opening load is introduced to the specimen, through piano hinges or end blocks with clevis holes, by specifying a constant-rate opening displacement. As the crack extends, the compliance of the specimen increases. The Mode I fracture toughness can be determined from load, displacement, and crack length measurements according to the relationship

$$G_{Ic} = \frac{P_{cr}^2}{2b} \frac{dC}{da} \quad [4.3.1]$$

where  $G_{Ic}$  is the Mode I critical energy release rate,  $P_{cr}$  is the load required to extend the crack,  $b$  is the specimen width,  $a$  is the crack length measured from the load line, and  $C$  is the compliance defined as the load-line deflection divided by the load.

Although the DCB is the subject of ASTM standards [6,7], a casual review of the literature quickly indicates that the practice of these tests is far from “standard”. Specimen size, length-to-width ratio, method of tabbing, etc., seem to be subject to personal preference of the individual conducting the test. Perhaps a little more troublesome is the choice of the data reduction method.

Several data reduction schemes are in use including: the area method, elementary beam-analysis, generalized empirical, and corrected beam-analysis methods [5,8-10]. Each method is subjected to assumptions, simplifications, limitations and/or special testing considerations. Not surprisingly, individual schemes can yield significantly different toughness values depending on how they treat factors such as shear strain energy, rotation at the crack tip, geometric non-linearities, anticlastic curvatures, width variations of the strain energy and crack profiles. Regardless of data reduction scheme used, the DCB specimen geometry permits multiple measurements for fracture toughness from each specimen. For the current work, an appropriate data reduction scheme was adopted which will be discussed below.

### 4.3.2.2 Limitations of the DCB for Automotive Materials

The approaches to determine fracture toughness mentioned above have been successfully applied in numerous studies involving aerospace-grade composites and adhesive joints. These test methods, however, have limitations that preclude their use for testing adhesive joints comprised of the automotive materials of interest for this program. Two specific limitations are substrate failures and the use of dissimilar substrates. The problematic issues with current test methods and the approach taken to mitigate them will be addressed in the following sections.

### ***Substrate Failures***

In contrast to composites utilized in aerospace applications, typical low-cost composites used in the automotive industry have higher void contents, lower fiber-volume fractions, and randomly oriented reinforcement. Consequently, they have a lower flexural rigidity that leads, in part, to substrate damage when tested using “standard” DCB geometries (Figure 4.3.2). Similarly, DCB specimens comprised of thin-section sheet metal will generally deform plastically prior to or during crack extension. In either case, inelastic contributions to the energy release rate are present and, consequently, erroneous toughness values will be obtained if modifications are not made to the specimen geometry. The propensity for inelastic effects to occur can be determined from the material and geometry of the substrate, as discussed below.

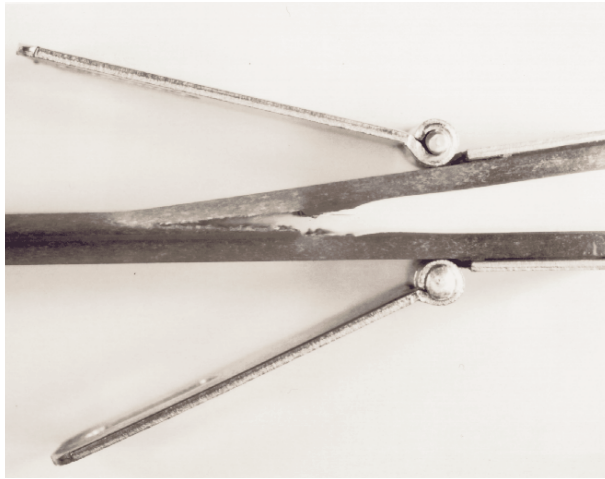


**Figure 4.3.2. Flexure Failure of the Substrate During Mode I Fracture Tests of SRIM Composites with Traditional DCB Geometry**

*Flexural Stresses in Substrates:* As opening forces are applied to the DCB specimen, the unbonded portion develops flexural stresses as the strain energy in the specimen increases. If the unbonded portion is assumed to be rigidly fixed at the crack tip, elementary beam theory can be used to determine the flexural stresses, as well as the strain energy release rate, as a function of the applied load. As the load increases the specimen may deform elastically, the crack may extend, and/or the substrates may develop damage or plasticity (as in the case of metal substrates). Comparing the critical load for the latter two cases provides an estimate of the minimum required substrate height that will ensure crack extension before substrate damage, which is given by

$$h > \frac{6E(G_{Ic}^{est})}{\sigma_{critical}^2}, \quad [4.3.2]$$

where  $E$  is Young’s modulus of the substrate,  $\sigma_{critical}$  is the stress at which damage or plasticity in the substrate occurs, and  $G_{Ic}$  is the Mode I critical energy release rate. Since  $G_{Ic}$  is the property to be determined by the test, it must be estimated from the best available data to determine the height requirement. If the height of the substrate is insufficient to satisfy equation 4.3.2, as is the

case of the materials discussed here, then the relation suggests that the substrate height (thickness of the composite or steel material) be increased. Unfortunately, due to processing limitations, this is not a practical solution for many of the materials of interest. Additionally, the modulus, critical stress, and critical strain energy release rate are not parameters that can be selected for a given material system. To mitigate substrate failures, a backing beam concept, as discussed in Section 4.3.2.3 was developed.

### ***Dissimilar Substrates***

One of the chief advantages of adhesive bonding is the ability to join dissimilar materials. The potential exists for bonding steel to aluminum, steel to polymer composite, or aluminum to steel. However, when the substrates have different flexural rigidities from geometric and/or material differences, then the DCB specimen does not deform symmetrically and the tensile forces are no longer normal to the crack surface. Consequently, the problem becomes one of mixed-mode (i.e., opening and shearing) fracture. Although this may provide useful data, assuming inelastic effects are avoided and mode-mix determined, it does not permit determination of the Mode I fracture toughness, which is needed for complete characterization of fracture. Modifications to test procedures to handle joints with dissimilar substrates will be discussed in Section 4.3.2.4.

### **4.3.2.3 Backing Beam Concept**

To circumvent the problem of substrate failures, a bonded-on backing beam concept was developed. Two types of backing beams were considered for Mode I testing: beams of uniform and contoured cross-section. For backing-beams with a uniform cross-section, the fracture toughness can be calculated from the same relationship used in the standard DCB with the exception that the equivalent mechanical properties of the combined beam must be used. Alternatively, a contoured backing-beam may be used. Contoured (or height-tapered) substrates were originally proposed by Mostovoy [11] to circumvent the need for crack-length measurements. The fracture toughness is determined solely from the load vs. displacement data. Unfortunately, for the “composite” (i.e., substrate-backing beam) beam, the independence of fracture toughness on crack length is lost when using the Mostovoy taper due to the contribution of the substrate to the overall compliance of the specimen. However, using the tapered beam does weaken the sensitivity to errors in crack length measurements.

### ***Additional Advantages of Backing Beams***

Several advantages arise with the use of backing beams:

- *Small Displacements:* In many applications of the DCB geometry, large displacements of the cantilever ends are encountered. This introduces two primary error sources that must be accounted for in the analysis of the results. Firstly, large deflections cause an effective shortening of the cantilever. Secondly, if end blocks (rather than hinges) are used to introduce the load and if deflection is measured at the load-line, then end block rotation reduces the deflection. As a practical testing matter, the correction factors required to account for these two effects are problematic. Incorporating the backing beam concept can circumvent both correction factors. Now, the stiffer backing beam limits the

deflection to acceptably smaller values. In addition, since the backing beams provide the majority of the overall stiffness, the deflections from tests with a wide range of adherend stiffness will exhibit a much narrower range of load-line displacement, eliminating the need to change the test setup for the variety of different adherends of interest to the automotive industry.

- *Anticlastic Curvatures:* It has been reported [12] that thin (perpendicular to the crack surface) adherends develop anticlastic curvatures. As a result, strong variations of the strain energy release rate as a function of width develop. By bonding the backing beams to the specimen, it is believed that the curvature and the subsequent variation in the strain energy are significantly diminished. This may lead to crack growth profiles that are more uniform through the specimen width.
- *Load Introduction:* Backing beams can be machined with clevis holes for convenient application of loads.

#### 4.3.2.4 Compliance Matching for Dissimilar Substrates

Mode I fracture in adhesive joints can be achieved employing double cantilever beam specimens. The symmetry of the applied loading and material properties about the fracture surface results in a symmetric stress distribution in front of the crack tip (normal to the fracture path). Hence the crack will advance in the opening manner, Mode I. However, for the case of dissimilar materials bonded together (the top and bottom beams are different materials), there is no guarantee that the stress distribution ahead of the crack tip will be symmetric, and in most cases, there will be shearing stresses at the crack tip, which result in a Mode II fracture component. Similarly, a crack not located at the mid plane between two beams of equal height would result in mixed-mode conditions. With this in mind, backing beams of varying heights above and below the fracture surface were used to counter the effect of the dissimilar materials and develop a pure Mode I stress distribution.

From a physical standpoint, if the heights of the two backing beams are chosen such that symmetric bending is achieved, then conditions for Mode I are established. Geometrically, this suggests that the cantilevered portion of each substrate must have the same load-line displacement during loading. Consequently, each portion contributes equally to the work done during the test since, from equilibrium, the same forces are acting on each substrate. The deflection,  $\delta$ , of a cantilever beam of length,  $a$ , with a concentrated load,  $P$ , at the free end is given by

$$\delta = \frac{Pa^3}{3(EI)}, \quad [4.3.3]$$

where  $EI$  is the flexural rigidity. Clearly, for each substrate to have the same deflection requires both must have the same flexural rigidity as given by

$$(EI)_{top\ beam} = (EI)_{bottom\ beam}. \quad [4.3.4]$$

### Determination of the Backing Beam Heights

Elementary mechanics of materials can be used to determine the requisite heights for the uniform cross-section backing beam in the following manner.

**Step 1** Choose the height for one of the backing beams.

**Step 2** Using Equation 4.3.5, determine the location of the neutral axis,  $\bar{Y}$ , of the composite beam which consists of the backing beam with known height and its corresponding substrate (see Figure 4.3.3).

$$\bar{Y} = \frac{h_b \left( h_a + \frac{h_b}{2} \right) + \frac{E_a h_a^2}{2E_b}}{h_b + h_a \frac{E_a}{E_b}} \quad [4.3.5]$$

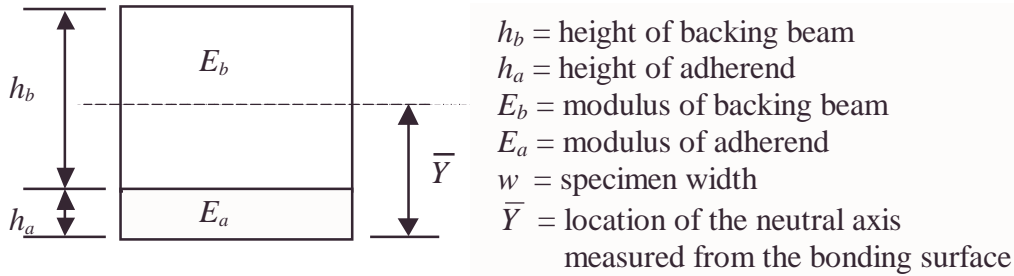


**Figure 4.3.3. Composite Beam Cross-Section Consisting of Backing Beam Rigidly Attached to a Substrate**

**Step 3** Calculate the value of  $EI$  for the composite beam.

$$EI = \frac{wE_a h_a^3}{12} + wE_a h_a \left( \bar{Y} - \frac{h_a}{2} \right)^2 + \frac{wh_b^3 E_b}{12} + wE_b h_b \left( h_a + \frac{h_b}{2} - \bar{Y} \right)^2 \quad [4.3.6]$$

**Step 4** Determine the height of the backing beam required for the other substrate that will result in a second composite beam of equal flexural rigidity as the first composite beam. This requires iteration on Equations 4.3.5 and 4.3.6 to solve for  $h_a$  with a common spreadsheet program. A similar formulation, albeit much more complex, can be developed for the height-tapered backing beam.

### Accuracy of the Compliance Matching Approach

The compliance matching approach is a practical approximation for minimizing the shearing contribution that is inherent in specimens with dissimilar substrates. To assess its validity, a finite element analysis was conducted to determine the mode-mix as a function of

substrate height for a simplified case, steel bonded to aluminum. The results of this analysis are shown in Figure 4.3.4. Using the compliance matching approach, the ratio of the height of the steel to aluminum was calculated as 0.693 for pure Mode I. Although the finite element analysis results show the ratio for pure Mode I loading to be closer to 0.4, the Mode II contribution for a height ratio of 0.693 is less than 5%. This was considered acceptable.

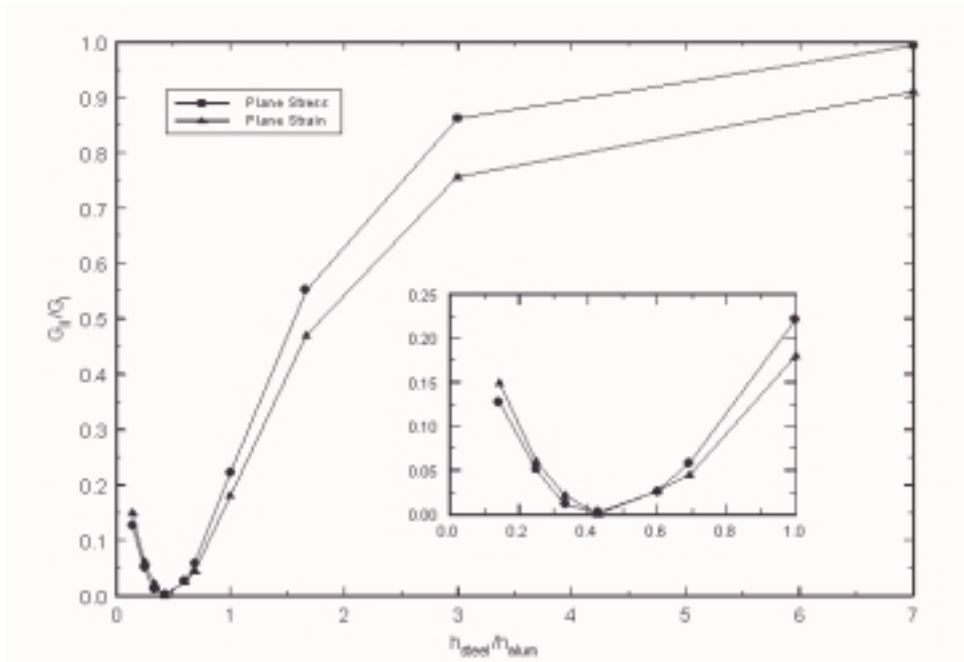


**Figure 4.3.4. Finite Element Analysis Depicting Mode-Mix Versus the Ratio of Substrate Heights for a Steel-Aluminum Specimen**

#### 4.3.2.5 Mode I Experiments

The typical adhesive joint may consist of a combination of composite materials, metals and adhesives. Since fracture can occur in the adhesive, composite or at the interface, it is necessary to have a measure of the fracture toughness of each component independently in addition to the bonded joint for design purposes. Accordingly, steel-steel, composite-steel, and composite-composite joints were tested along with epoxy specimens, where the backing beams were bonded together with the test adhesive, and composite specimens, where the composite adherend was bonded directly to the backing beams.

Specific details on specimen preparation for each configuration are given in the Draft Mode I testing procedure [13]. Both uniform and height-tapered backing beams (Figures 4.3.5 and 4.3.6) were used during the Mode I tests.

Equation 4.3.2 can be used, with modification to account for the “composite” backing/substrate beam to ensure the stresses in the outer fibers of the backing beam do not exceed the yield stress. However, from the authors’ experience, aluminum or steel backing beams of 12.7 mm height are generally sufficient and practical. After the testing was complete, confirmation that the relationship in equation 4.3.2 is satisfied was done. When the stresses

exceed the yield strength of the backing beams, there is often obvious permanent deformation of the beam after unloading.

### ***Test Procedure***

For all of the Mode I tests, specimens were mounted in clevis-pin fixtures on a servo-hydraulic test machine. The edge of the specimen was coated with a thin layer of white correction fluid ahead of the crack tip starter in order to observe the crack extension during loading. Opening forces were applied under displacement control at a rate of 1.27 mm/min until the crack began to grow. For each test specimen, the crack length was visually measured prior to testing and monitored for each loading cycle of the test. The crack was allowed to grow approximately 6.35 mm, at which point the displacement was reversed and the specimen unloaded to approximately 5 percent of the maximum load occurring during crack extension. The extent of crack growth was recorded and the specimen was reloaded for subsequent measurements. Force and displacement data was acquired using a custom LabView application via a National Instruments data acquisition (DAQ) card. The process was repeated until 15 to 20 crack extensions had occurred or until the crack growth resulted in separation of the two halves of the specimen. A continuous record of load versus load-line displacement was obtained for each crack extension. A detailed account of this procedure can be found in the draft standard given in [13].

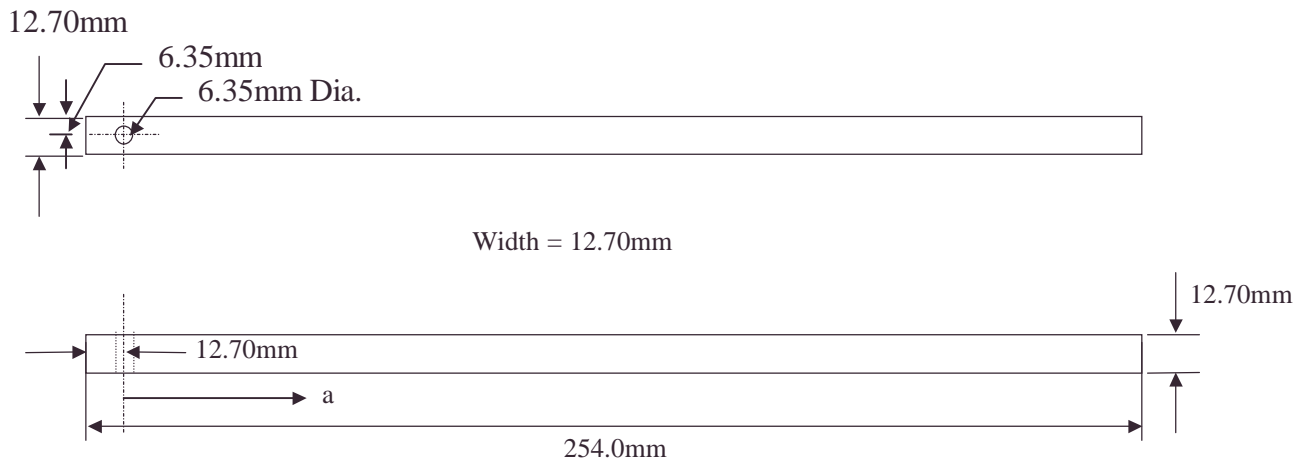
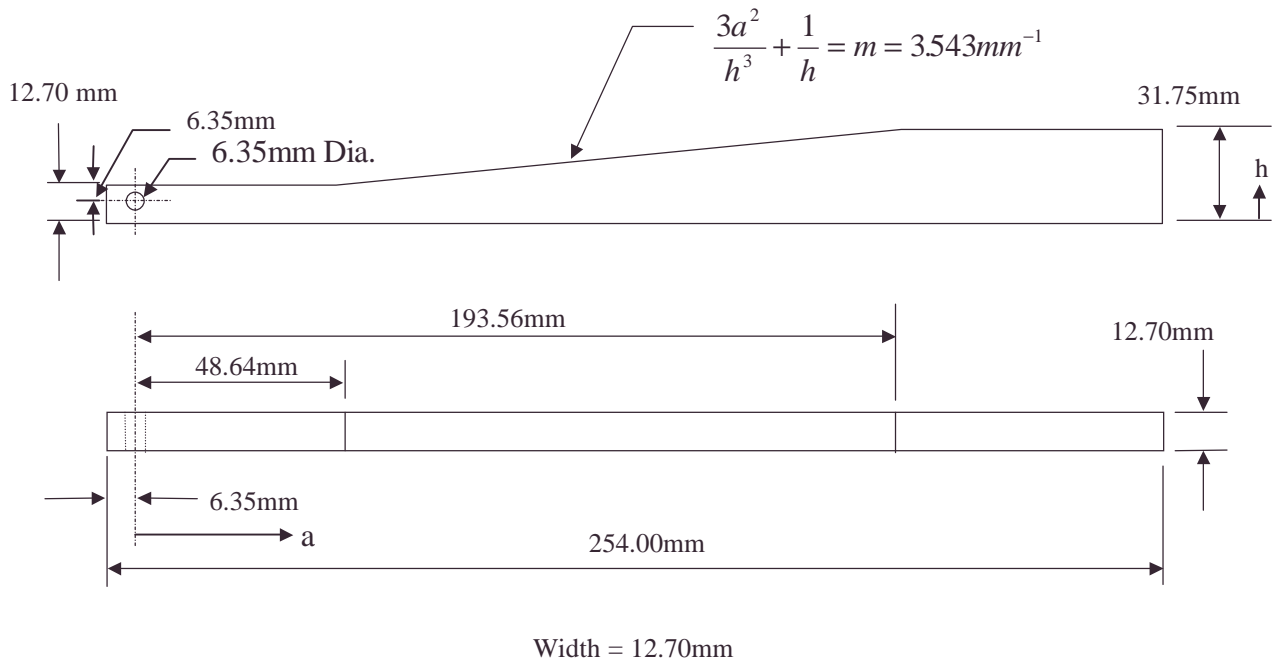


**Figure 4.3.5. Uniform Backing Beam**



Width = 12.70mm

a (mm)	h (mm)						
48.64	12.7	85.82	18.5	131.03	24.5	182.21	30.5
56.35	14	96.52	20	143.30	26	193.56	31.75
65.71	15.5	107.63	21.5	155.92	27.5		
75.54	17	119.14	23	168.90	29		

**Figure 4.3.6. Contoured Backing Beam**

*Dissimilar Substrate Tests*

The compliance-matching formulation discussed in Section 4.3.2.4 was used to size the backing beams for the composite bonded to steel specimens depicted in Figure 4.3.7. Dimensions and properties used to determine the backing beam requirements are shown in Table 4.3.1.

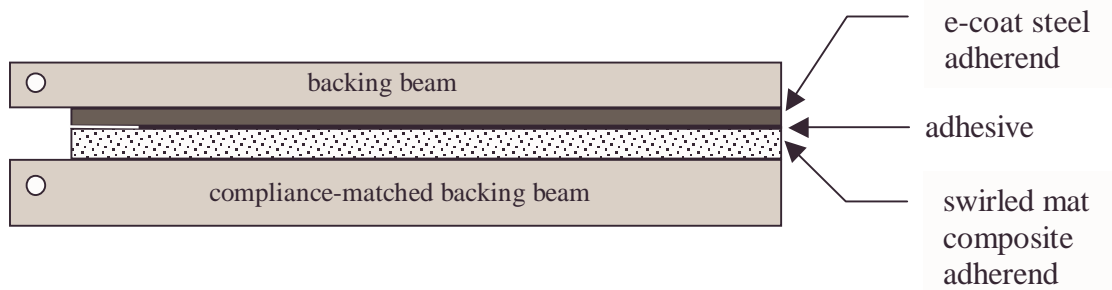


**Figure 4.3.7. Schematic Representation of a Test Specimen with Dissimilar Substrates and Backing Beams**

**Table 4.3.1. Dimensions and Properties of Substrates for Backing Beam Determination**

	<b>Composite Substrate</b>	<b>Steel Substrate</b>
<b>Width</b>	12.7 mm (0.5 in)	12.7 mm (0.5 in)
<b>Height, <math>h</math></b>	2.175 mm (0.125 in)	0.085 mm (0.0335 in)
<b>Young's Modulus, <math>E</math></b>	13.8 GPa (2 Msi)	207 GPa (30 Msi)

For convenience, the height of the backing beam for the steel substrate was selected as 12.7 mm (0.5 in). This ensured that the height of the backing beam for the composite substrate would be greater than 12.7 mm, which is considered to be a practical minimum dimension. From equation 4.3.5, the neutral axis,  $\bar{Y}$ , for the steel/backing beam combination is 6.06 mm (0.2562 in). The flexural rigidity,  $EI$ , from Equation 4.3.6 is 482,900 GPa-mm<sup>4</sup> (168,300 psi-in<sup>4</sup>).

#### 4.3.2.6 Mode I Results

All of the Mode I specimens exhibited very controlled slow-stable crack growth such as indicated in typical load-displacement curves depicted in Figures 4.3.8-4.3.12. Adhesion of the substrates to the joint adhesive and adhesion of the substrates to the backing beams were excellent.

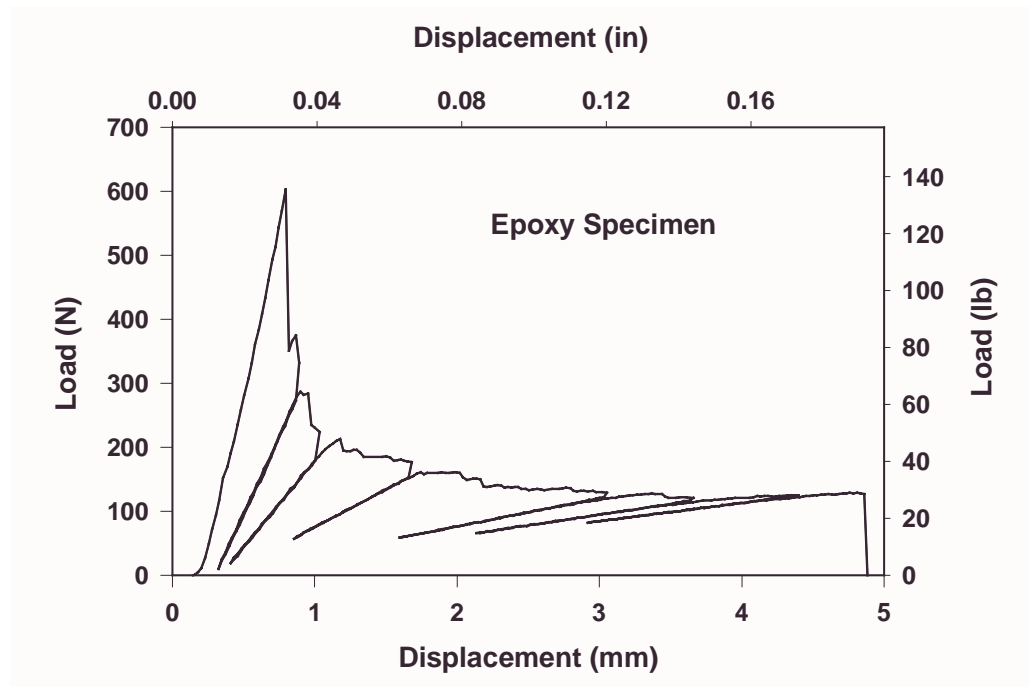


**Figure 4.3.8. Load-Displacement Record for an Epoxy Mode I Test**

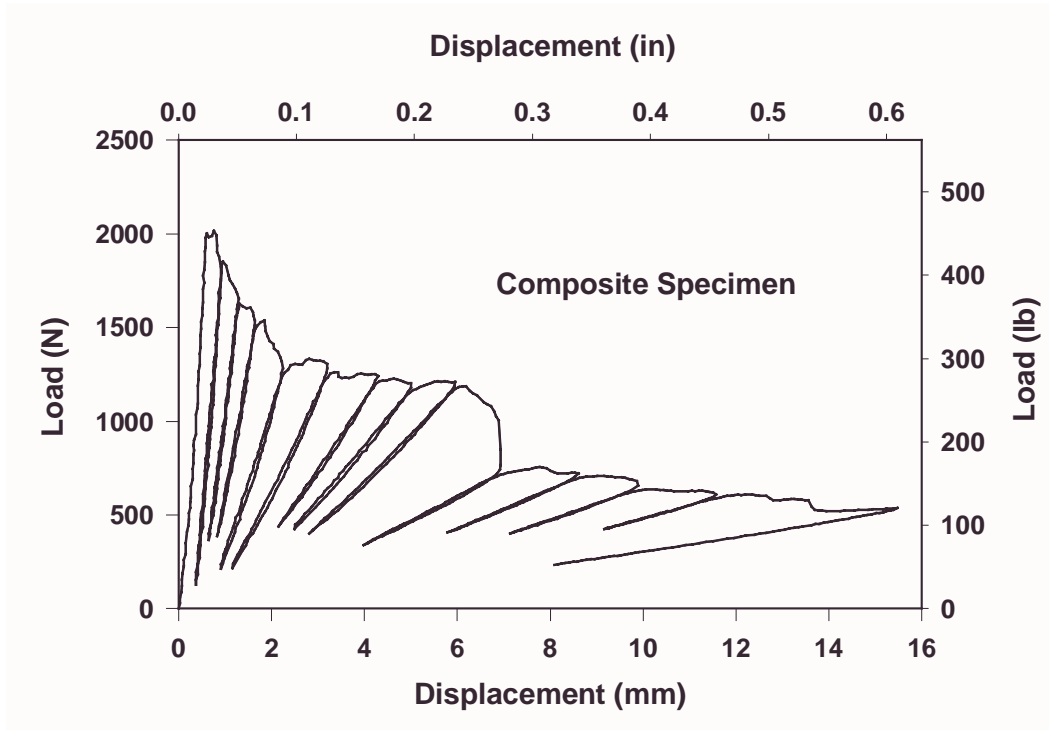


Figure 4.3.9. Load-Displacement Record for a Composite Mode I Test

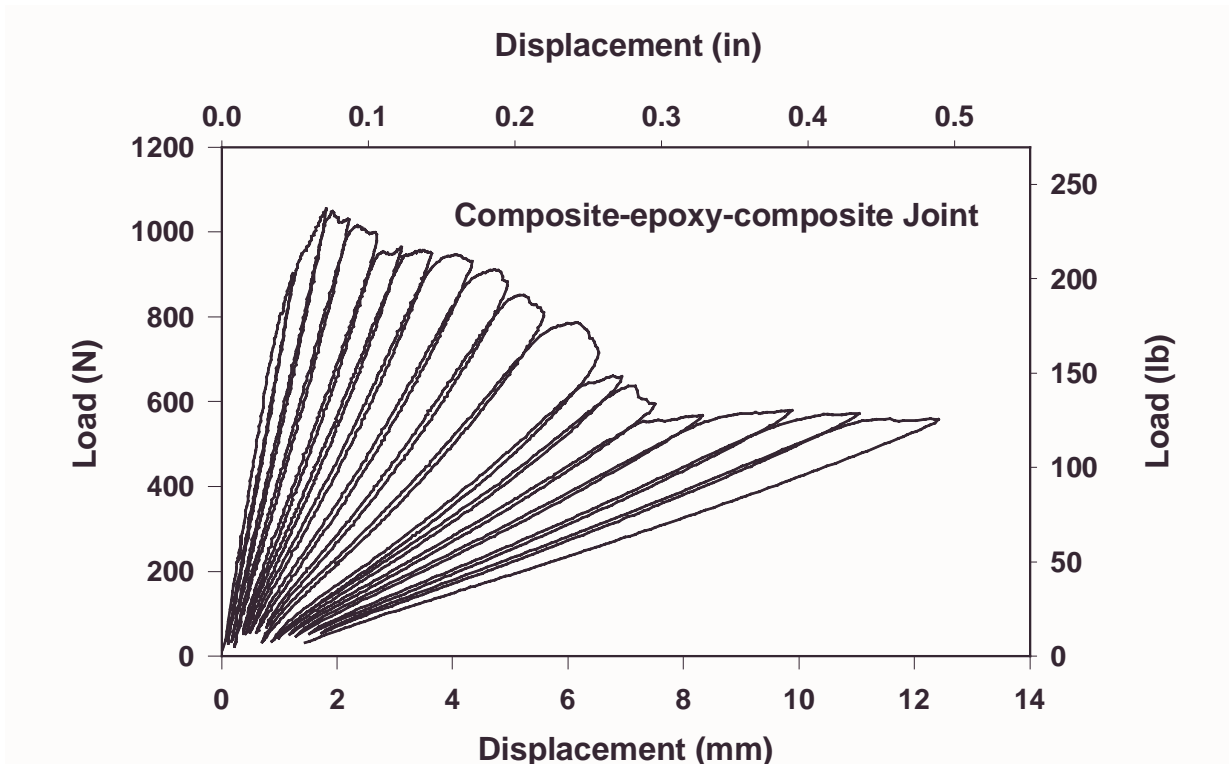


Figure 4.3.10. Load-Displacement Record for a Composite-Epoxy-Composite Mode I Test

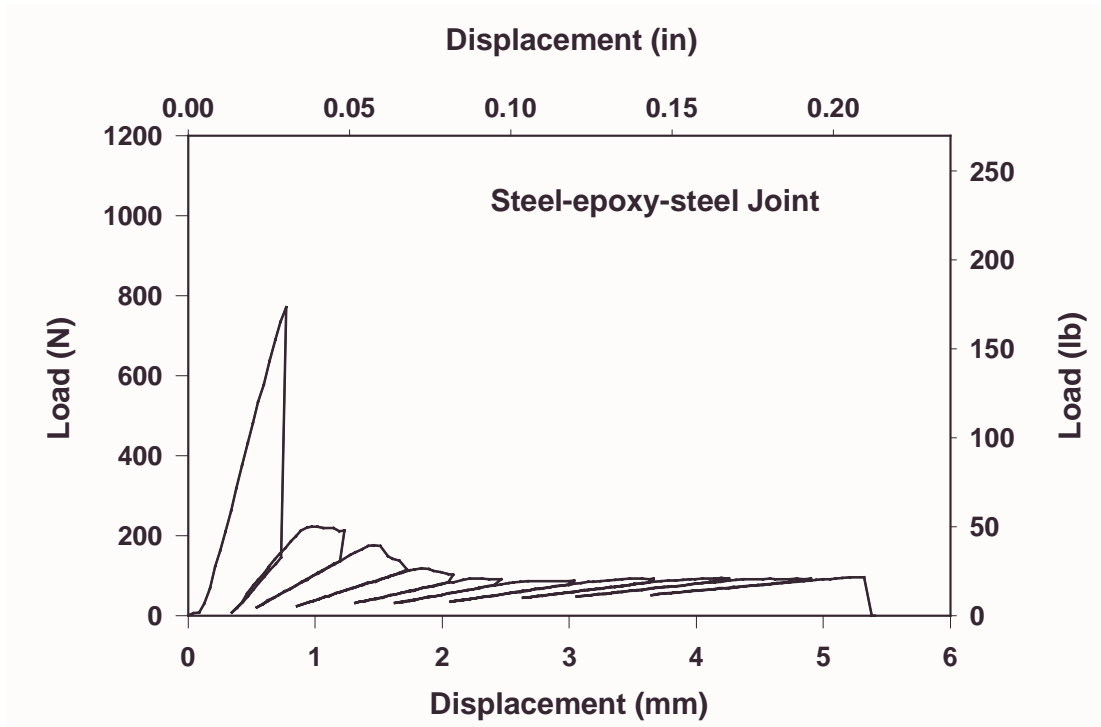


Figure 4.3.11. Load-Displacement Record for a Steel-Epoxy-Steel Mode I Test

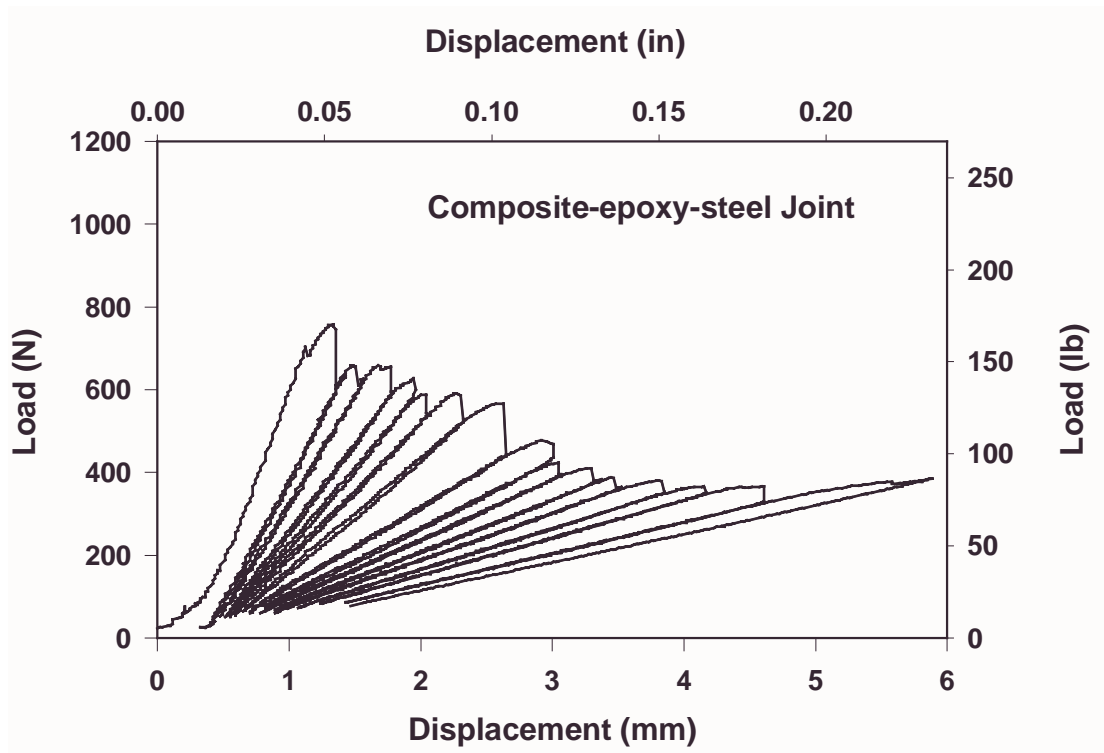


Figure 4.3.12. Load-Displacement Record for a Composite-Epoxy-Steel Mode I Test

### ***Failure Modes and Crack Paths***

*Epoxy and Composite Specimens:* For the epoxy bonded directly to the backing beams, the crack growth initiated in the epoxy and rapidly grew into the adhesive/beam interface. The fracture surface morphology was quite rugged.

For the composite specimens, the crack path stayed within the composite away from the backing beam interface but there was extensive fiber bridging and a rugged fracture surface.

*Composite-Composite Joints:* These specimens showed excellent composite/adhesive interfacial adhesion. The crack grew in the composite near the surface resin-rich composite interface, following the fiber bundles. There was significant fiber bridging across the crack surface as shown in Figure 4.3.13. Fiber/matrix interfacial failure was the dominant factor in crack propagation indicating that the adhesive and adhesive/adherend interface have higher fracture toughness than the composite.

*Steel-Steel Joints:* The crack propagated through the protective e-coat layer, indicating that both the adhesive and the adhesive/coating interface have higher fracture resistance than the coating. Thumbnail crack fronts were visible in the steel-steel fracture surfaces, which provided verification of the crack length measurement technique.

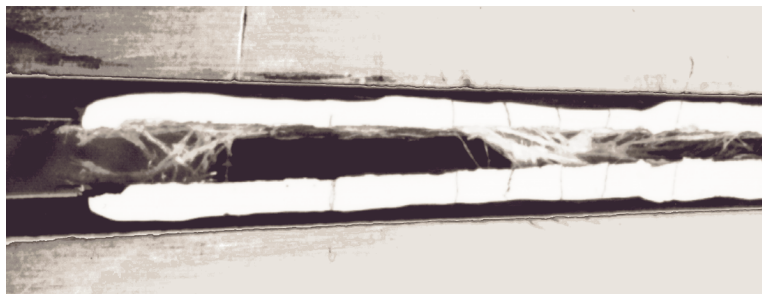


**Figure 4.3.13. Fiber Bridging in a Composite-Epoxy-Composite Mode I Test**

*Composite-Steel Joints:* A total of nine exploratory tests were conducted to collect Mode I data for the dissimilar adherend joints. The load-displacement behavior was similar to other Mode I specimens conducted on the same set of materials when both substrates were identical. A photograph of the resulting failure surface is shown as Figure 4.3.14. Failure occurred alternately in the e-coat layer of the steel and the resin-rich surface layers of the composite in a remarkable periodic fashion. The top half of the specimen has islands of adhesive on the steel substrate, whereas the bottom half has the remaining adhesive on the composite substrate. Bare fibers in the composite are exposed as the resin-rich layer, as well as a few loose fibers, adhere to the adhesive islands on the e-coat substrate.

### ***Determination of Critical Load, $P_{cr}$***

The critical load for each loading cycle is defined as the load required to initiate crack extension. For run-arrest crack growth, the critical load is the maximum value for each loading. For slow-stable crack growth, the value is taken where the load-displacement curve deviates from linearity by approximately 5%.

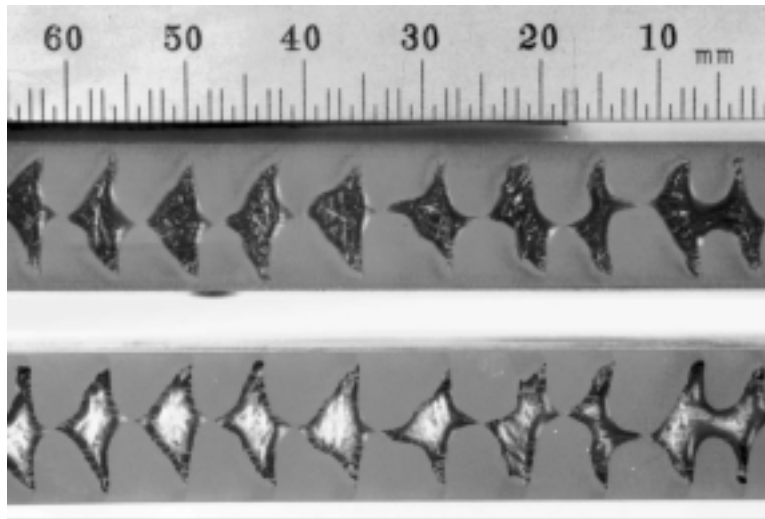


**Figure 4.3.14. Failure Surface for Mode I Fracture of Composite-Epoxy-Steel Specimen**

### *Data Analysis*

The load versus load-line displacement data together with the crack length measurements were used to calculate the fracture toughness using three techniques: the area method, beam theory analysis, and experimental compliance method. The area method provides a direct approach for calculating the fracture toughness. The energy required to grow the crack is determined from the area enclosed by each loading and unloading curve. This method, although the most fundamental, was found to provide results with significant scatter.

Beam theory analysis is based on the assumption that each cracked half of the double cantilever beam specimen is a perfect cantilever beam and that no deformation occurs in the specimen ahead of the crack tip. Deflection of each cantilever beam is calculated by elementary beam theory.

The experimental compliance method using a third-order compliance fit was chosen for this work because it provided the best trade-off between reproducibility and fundamental formulation. The slope in N/mm of the initial linear portion of each loading curve was determined from linear regression. The compliance,  $C$ , was calculated for each loading cycle and plotted versus crack length. The coefficients for a third-order polynomial were determined from internal routines of a commercial spreadsheet program. The change in compliance as a function of crack length,  $dC/da$ , was determined through differentiating the polynomial fit. The critical energy release rate in for each loading cycle was then calculated from Equation 4.3.1.

Figure 4.3.15 shows a comparison of the fracture toughness values as a function of crack extension obtained from each of the methods for a composite/composite joint with uniform backing beams. In addition to being a fundamental approach resulting in low-scatter and reproducible results, the experimental compliance method has another definite advantage over beam theory approaches; it eliminates the need to calculate the flexure characteristics of a “composite beam” from material property values that may not be known.

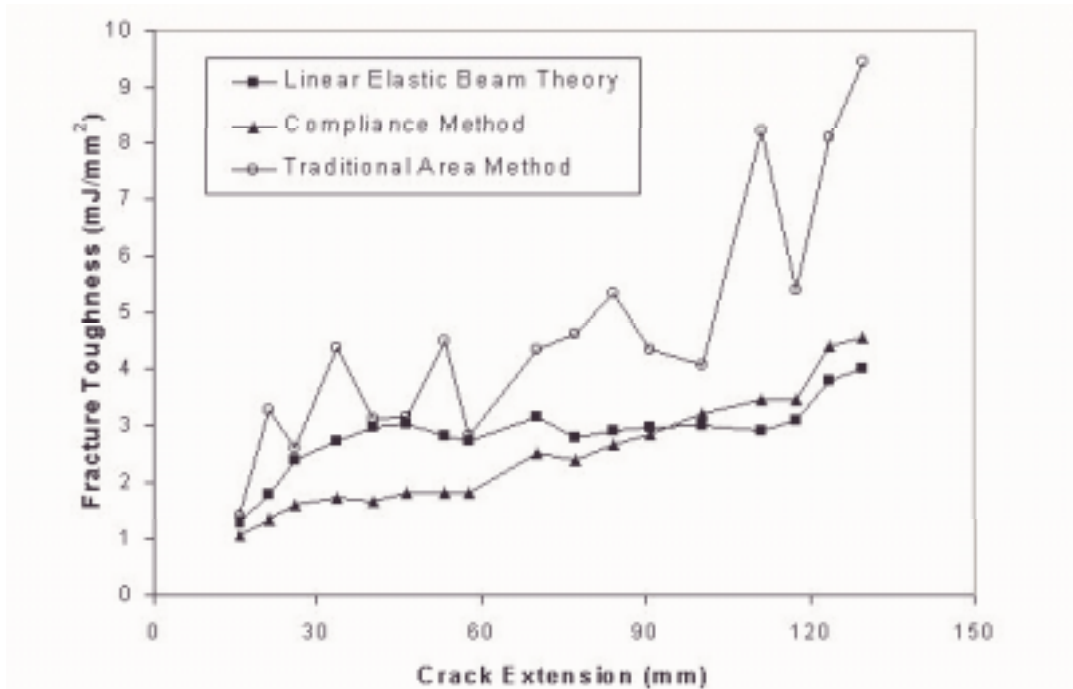


**Figure 4.3.15. Fracture Toughness Values Calculated with Several Analysis Methods**

Initially, both uniform and tapered backing beams were tested with good agreement between fracture toughness measurements. Uniform backing beams were chosen for the remaining Mode I fracture tests because they are easier to prepare, require less machining, and are, consequently, less expensive. The small gain in accuracy of  $G_{Ic}$  was not worth the additional cost and complexity associated with using tapered backing beams. However, the tapered beams could prove useful for test environments where visual measurements are not accurately obtainable.

A compilation of the results for the Mode I toughness of the various configurations is shown in Figure 4.3.16. As expected, the  $G_{Ic}$  values for the composite specimens and the composite-composite joints increase with crack extension due to the fiber bridging effects. The values at initial crack length are artificially high due to pop-in.  $G_{Ic}$  for the composite range from 1.2 to 6.6 mJ/mm<sup>2</sup>. The epoxy adhesive specimens had low fracture toughness between 0.18 and 0.6 mJ/mm<sup>2</sup>. The composite-composite specimens had a range of fracture toughness values increasing with crack extension from 0.7 to 4.6 mJ/mm<sup>2</sup>. The fracture toughness of the steel-steel joints and the composite-steel joints were fairly uniform with average values of 0.096 and 0.58 mJ/mm<sup>2</sup> respectively. The fracture toughness for the composite-epoxy-steel joint is higher than the steel-epoxy-steel joint owing to the crack branching and slight fiber bridging that occurs due to the presence of the composite.

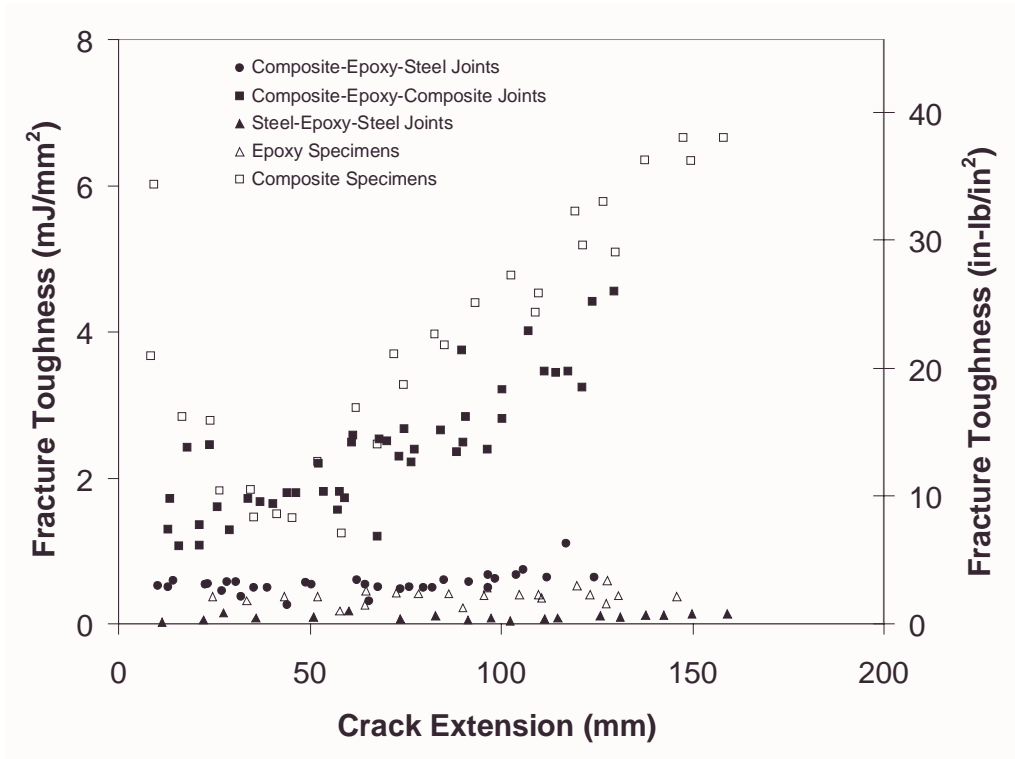
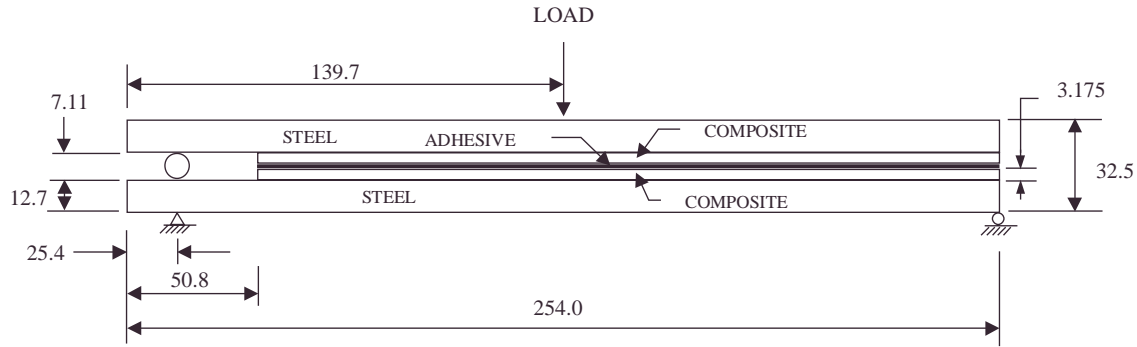


**Figure 4.3.16. Fracture Toughness as a Function of Crack Length (Each Case Represents Several Specimens)**

### 4.3.3 Mode II Fracture Toughness Test

#### 4.3.3.1 Mode II Fundamentals – the End Notched Flexure Text

Mode II fracture toughness ( $G_{IIc}$ ) defines the resistance of a material to crack propagation while under in-plane shear loading which is characterized by crack face sliding over each other. The end-notched flexure (ENF) is the most common specimen configuration used for determining the Mode II fracture toughness of adhesive joints and laminated composites [1-3,14]. Essentially, the ENF specimen is a derivative of the Mode I DCB specimen whereby the specimen is loaded in three-point bending (see Figure 4.3.17). With a mid-plane delamination at one end, the flexure loading results in shearing deformation at the crack surface. As in the Mode I testing, the standard geometry proved to be inadequate for the materials of interest here. The standard geometry lacked sufficient stiffness to allow for crack extension within a linear range. In actuality, the case is more severe where excessive curvatures are obtained to the point that the specimen becomes unstable in the bend fixture. Based on the success of the Mode I test developments. The same general approach was taken for Mode II. Specifically, backing beams were employed and the experimental compliance method of data analysis was used.



Note: All dimensions in mm.

**Figure 4.3.17. Modified ENF Specimen**

#### 4.3.3.1 Preliminary Findings for the ENF

Preliminary tests were conducted that identified several problematic issues with the ENF specimen.

- During the preliminary tests for the steel - steel joints, the specimens failed by sudden debonding between the steel and the backing beam with no crack propagation through the adhesive joint. Loading the specimens in Mode I and allowing the crack to propagate with an initial pop-in (sudden crack growth) accompanied by a short crack extension remedied this problem. This Mode I pre-cracking served to introduce a sharp crack initiator instead of the blunt crack in the joint as fabricated. When the pre-cracked specimens were subsequently tested in Mode II, the crack propagated in the joint as desired and allowed for the determination of fracture toughness value. Mode I pre-cracking was utilized for the remaining Mode II tests, including composite-composite and adhesive specimens.
- The toughness values in Mode II were found to be sufficiently high to require loads exceeding the yield point of aluminum backing beams. Consequently, high-yield-point steel (approximately 2000 MPa) was used as the backing beams for Mode II and mixed-mode, mitigating the yielding problem.
- Considerable hysteresis was encountered between the loading and unloading curves as shown in Figures 4.3.18 - 4.3.20. Due to this hysteresis, the loading and unloading compliances do not appear to be equal for a given crack length. Additionally, with each successive loading, accumulative permanent deformation was evident. These effects were believed to be a result of friction acting on the cracked surface of the specimen. To investigate the potential frictional effects, a finite element analysis was conducted and a modification to the test geometry was introduced as discussed in the following sections.

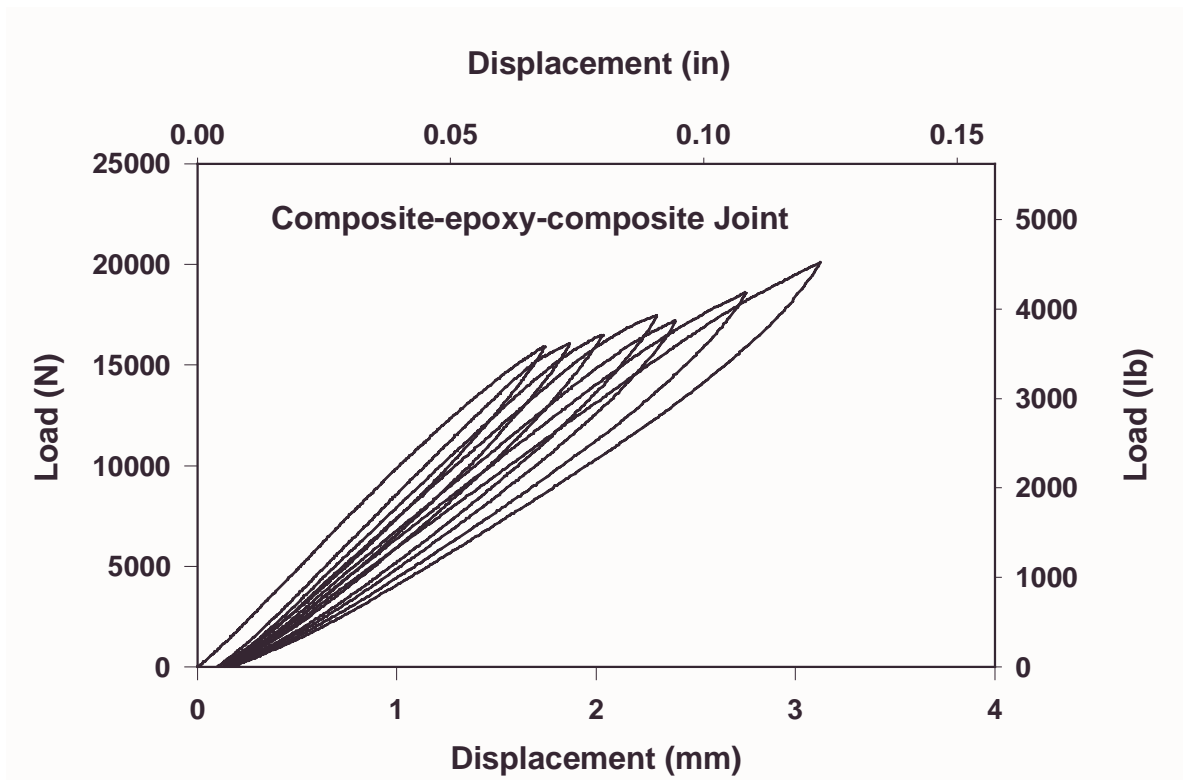


Figure 4.3.18. Load-Displacement Record for Mode II Composite Joint Test

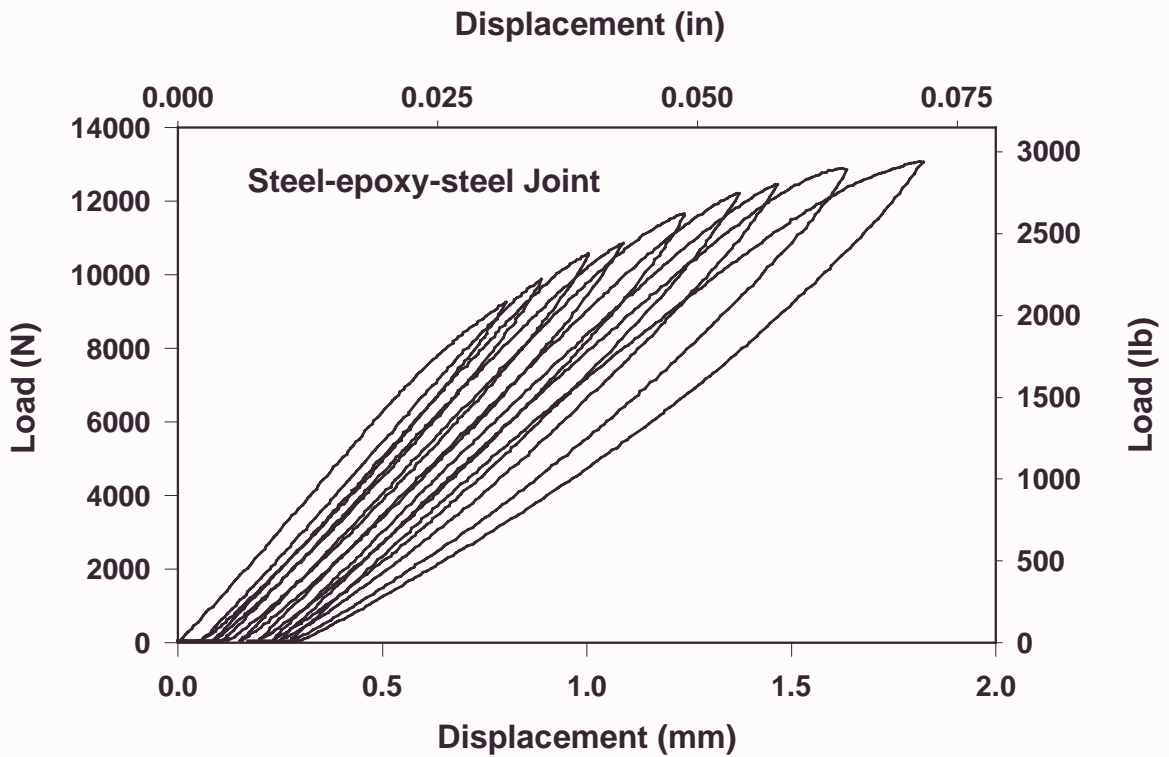


Figure 4.3.19. Load-Displacement Record for Mode II Steel Joint Test

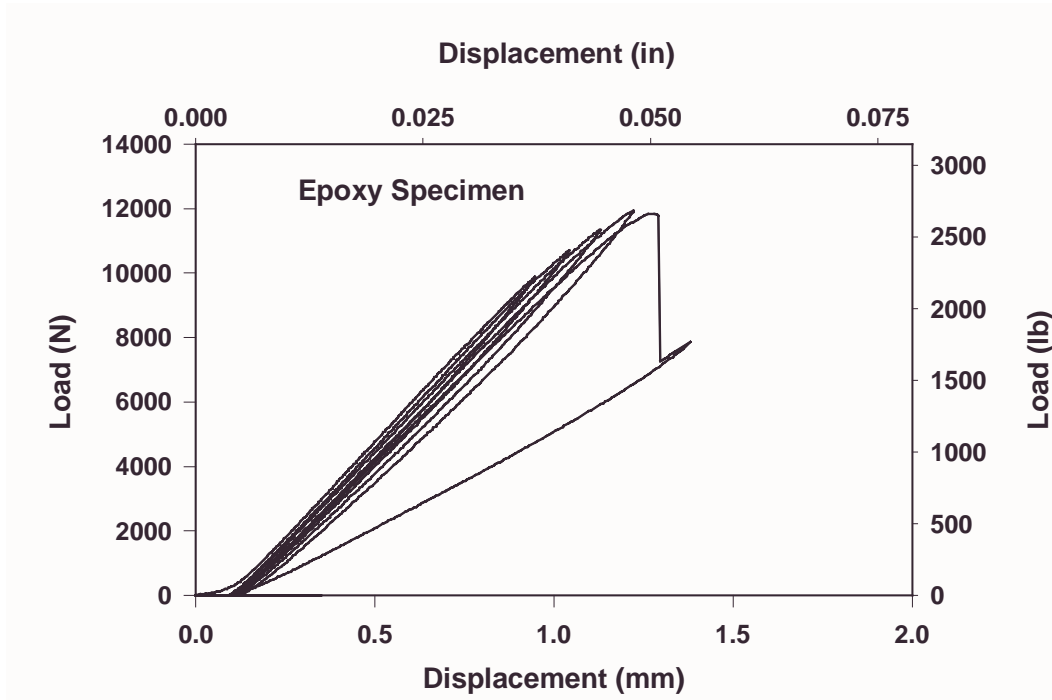


Figure 4.3.20. Load-Displacement Record for Mode II Epoxy Test

#### 4.3.3.2 Finite Element Analysis of Mode II Fracture Test

A finite element analysis (FEA) for the Mode II compound beam was performed using the Engineering Mechanics Research Corporation (EMRC) NISA finite element code to quantify the frictional forces due to crack closure. Initial results from the analysis of two steel beams subjected to three-point bending, without adhesive or initial crack, indicated a strong effect of friction on the loading and unloading compliance (see Figure 4.3.21). A more detailed analysis of the actual Mode II test specimen configuration was warranted.

##### *ENF Test Specimen*

The FEA geometry consisted of a compound beam, that included inner composite beams sandwiched between two steel backing beams, subjected to three-point bending with a starter crack at the mid-plane. The analysis considered two coefficients of friction,  $\mu=0.0$  (frictionless) and  $\mu=1.0$ , and varied the initial crack length. For both the friction and frictionless cases, the load-displacement curves were determined from the FEA results and plotted as a function of initial crack length for the loading cycle only. As expected, for both cases, an increasing compliance was demonstrated for increasing crack lengths. The effect of friction was demonstrated by a reduction in the beam compliance. Also, the results showed that the compliance was not a linear function of the initial crack length. Instead, the compliance was approximately proportional to the square of the crack length.

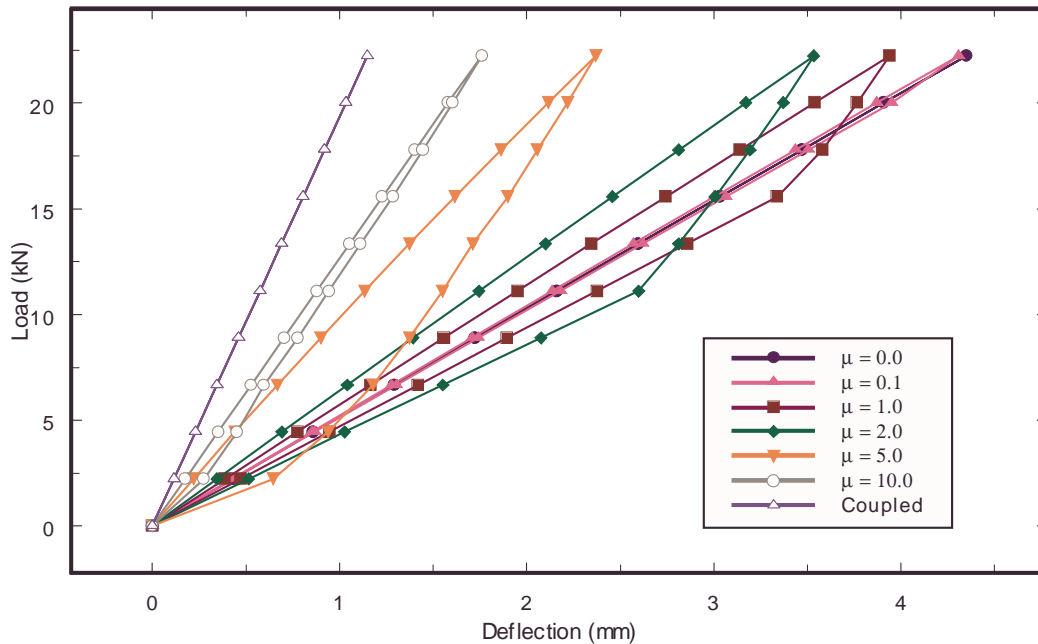


**Figure 4.3.21. FEM Mode II Load-Displacement Results (No Adhesive or Initial Crack)**

The finite element analyses were also performed using a model that included the adhesive layer. The results for compliance as a function of crack length were calculated and plotted for both friction and frictionless cases, and compared to the results without the adhesive layer. The relationship between compliance and crack length was the same with and without the adhesive layer. The overall effect of the adhesive was shown to be an increase in the compound beam compliance.

Another analysis considered the case of the adhesive layer with a 95.25 mm (3.75 in) initial crack length. The load-deflection curve was then determined from the FEA results considering various loading and unloading cycles. The results showed a nonlinear unloading behavior similar to that seen in the steel beam analyses. Also, the cyclic loading-unloading behavior was similar to that observed experimentally.

### ***Modified ENF Test Specimen***

The FEA model used to study the effects of friction on beam deflections was modified to consider an alternative test configuration. In the initial modeling and analyses efforts, the lengths of the composite and steel beams were equal. The compound beam was simply supported on each end at the bottom corner nodes and the load was applied at the mid-span between support points. The modifications to the model consisted of extending the steel backing beams two inches beyond the end of the composite beams. In addition, a 6.35 mm (0.25 in) diameter pin was placed between the gap that was generated by the steel beam extension. The pin was placed 25.4 mm (1 in) from the end of the steel beams, directly above the bottom support point (see Figure 4.3.17). In the modified model, the beam was still simply supported on the bottom surface but the distance between support points was equal to 228.6 mm (9 in). In addition, the point of load application was at the middle of the supports, which made the loading

un-symmetric about the midpoint of the composite/adhesive beam. The longer span resulted in a larger moment being applied ( $M = PL/4$ ) for the modified model than in the initial equal beam length model.

FEA runs were completed on seven different cases. The cases are identified as:

- |           |  |
|-----------|--|
| Case I.   | Equal length composite/steel beams 203.2 mm (8 in) with friction |
| Case II.  | 254 mm (10 in) steel beam without the pin and with friction      |
| Case III. | Case II but without friction                                     |
| Case IV.  | Case II but with the circular pin                                |
| Case V.   | Case IV but with no friction at the pin/steel interface          |
| Case VI.  | Case IV but with a longer crack length                           |
| Case VII. | Case IV but with a square pin                                    |

The coefficient of friction was set equal to 1.0 in all cases that considered friction. The crack length in all cases was 44.45 mm (1.75 in), with the exception of Case VI where the crack length was 95.25 mm (3.75 in). The average nodal stresses from the FEA output were used to plot stress profiles along the mid-plane of the adhesive. Stress profiles were plotted for the normal stress,  $\sigma_{yy}$ , and the shear stress,  $\tau_{xy}$ , over a range of the x-coordinate that encompassed the crack region.

The effect of the steel beam extension was an increase in the magnitude of the normal stress and shear stress at the crack opening and at the crack tip. These increases in stress magnitude were likely due to the increased bending moment for the extended beam case. In both of these cases, the crack actually closed up over a finite length starting at the crack opening. This produced a normal compressive stress and a shear stress along this length. For the case of no friction (Case III), the shear stress along the crack was zero but there was still a compressive normal stress at the closed end. The magnitude of the shear stress at the crack tip was greater when there was zero friction (Figure 4.3.22).

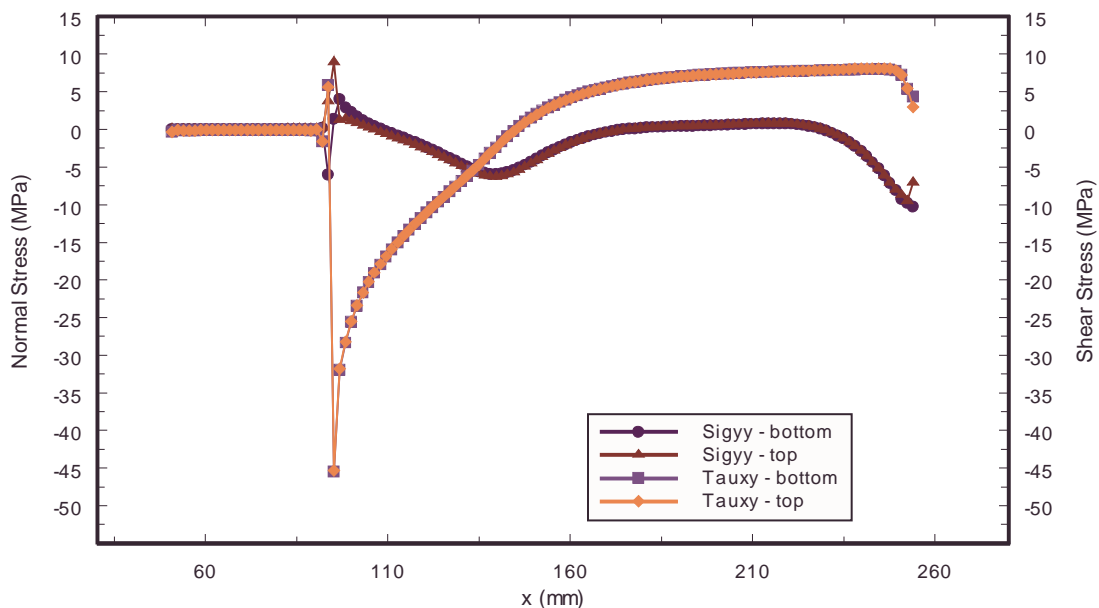


**Figure 4.3.22. FEM Determined Stresses  
(Case III:  $a=45\text{mm}$ , 1.75 in, No Insert, with Friction)**

The effects of inserting a pin between the two steel beams (Case IV) were the crack remained open along its entire initial length and the maximum shear stress at the crack tip was nearly as large as the frictionless case without the pin. Additionally, since the crack remained open, the normal and shear stresses were negligible along the entire length of the crack surface. The effects of modeling the contact between the pin and the top steel beam as a frictionless interface (Case V) were negligible, compared to the Case IV stress profile results. However, there was a slight increase in the shear stress magnitude at the crack tip (Figure 4.3.23).

The effect of a longer crack length (Case VI) was a reduced maximum shear stress at the crack tip relative to the shorter crack length. Also, due to the close proximity of the crack tip to the point of load application, the crack closed up in this vicinity and compressive normal stresses and shear stresses developed. This is likely the reason why the maximum shear stress at the crack tip was reduced. The effect of using a square pin (Case VII) versus a round pin (Case IV) was a slight reduction in the maximum shear stress at the crack tip (Figure 4.3.24).

Cases II and IV, the extended steel beam cases with and without a circular pin, respectively, were further analyzed by plotting load versus displacement as a function of crack length. The curves were plotted for both loading and unloading and the results are shown in Figure 4.3.25 for the case without a pin and in Figure 4.3.26 for the case with a pin. As previously discussed, the effect of friction along the crack interface produced a different loading and unloading path. However, this effect was only seen when the crack closed up and normal and shear stresses were developed along the crack faces. For the case without a pin, there was always some portion of the crack where the gap elements were closed, independent of the crack length. Consequently, for all crack lengths considered there was a different load and unload path. For the case of inserting a pin between the two steel backing beams, there were closed gap elements only for the two longest crack lengths. As described above, the closed elements were near the crack tip, which for the longer crack lengths, were in the vicinity of the applied load.

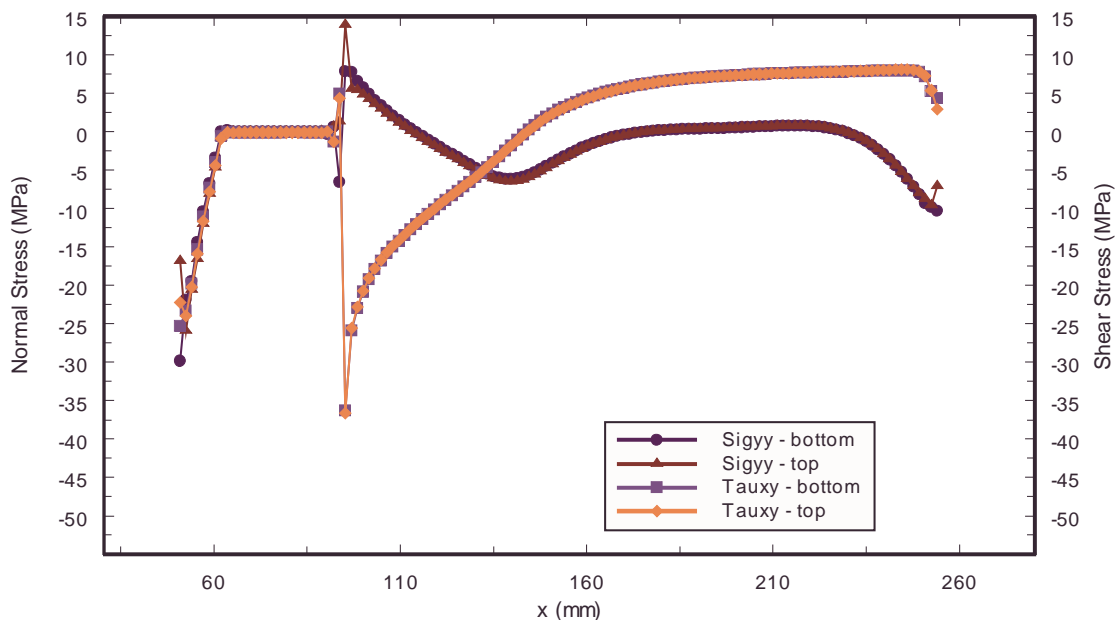
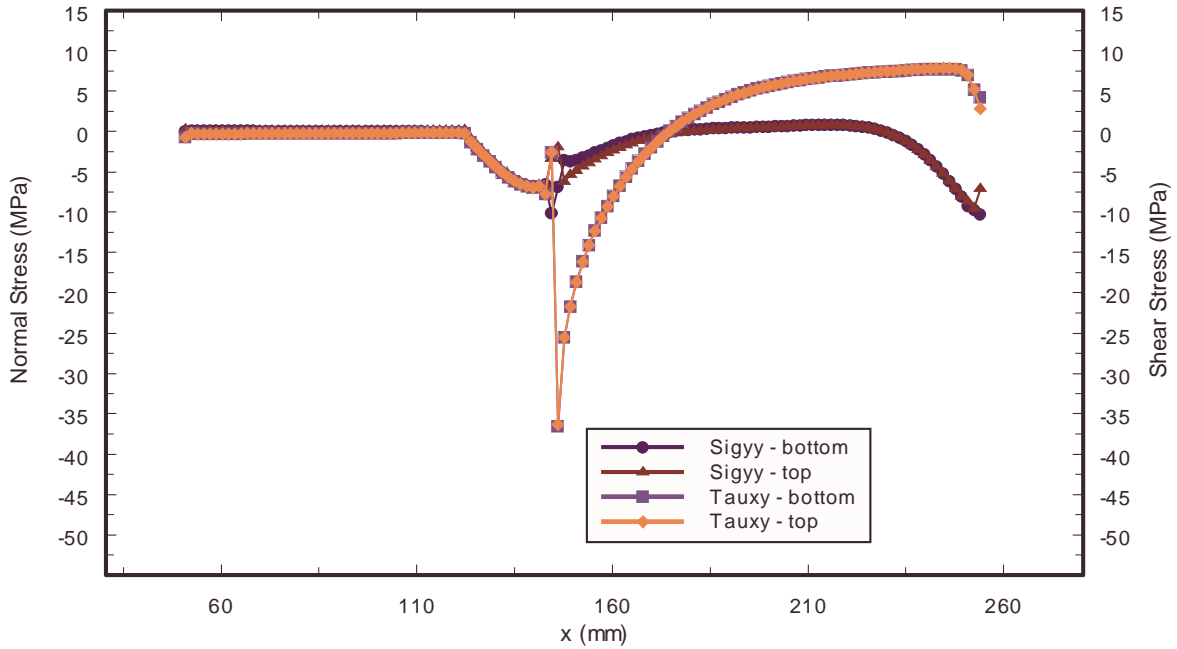
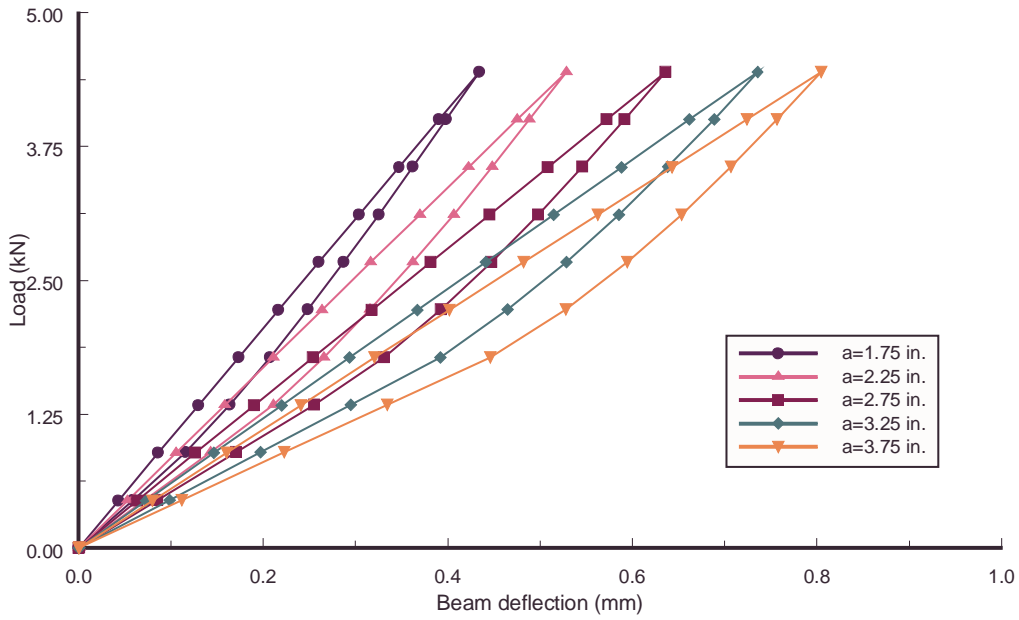


Figure 4.3.23. FEM Determined Stresses (Case V:  $a=45$  mm, 1.75 in, Insert, with Friction)



**Figure 4.3.24. FEM Determined Stresses (Case VII:  $a=95$  mm, 3.75 in, Insert, with Friction)**



**Figure 4.3.25. FEM Mode II Load-Displacement Results (No Insert)**

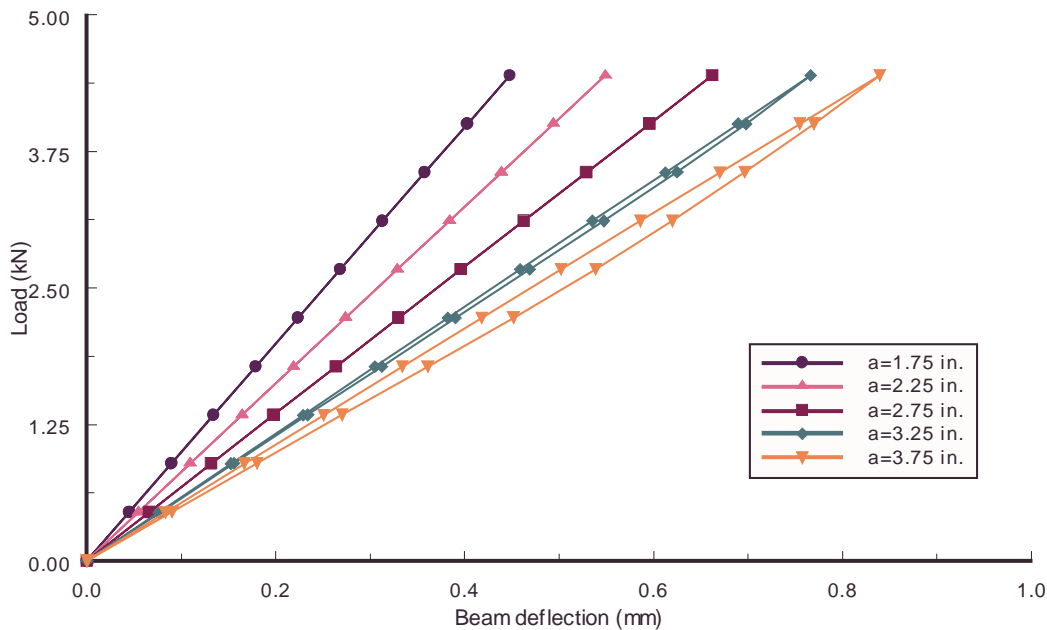


**Figure 4.3.26. FEM Mode II Load-Displacement Results (Insert)**

The FEA results comparing the modified Mode II test specimen geometry to the original configuration showed the modified geometry, at least for small crack lengths, eliminates the problems associated with friction. Also, the FEA results provide valuable insight about the stresses and displacements resulting from three-point bending of compound beams.

#### 4.3.3.3 Mode II Experiments

Two compliance calibration specimens were tested in an attempt to quantify the magnitude of the frictional forces and determine the best way to account for the frictional effects in the calculation of Mode II fracture toughness. The calibration specimens consisted of a composite-composite joint with a 1.27 mm (0.05 in) bondline. The adhesive behind the crack tip was removed prior to testing by sawing the specimen up to the crack tip. The removal of the adhesive should result in a complete elimination of friction along the cracked interface. For the first test, a shim was placed behind the crack tip to prevent the backing beams from collapsing towards each other. For the second test, a dowel pin was placed between the beams aligned with the loading pin behind the crack. Both specimens were loaded in Mode II in the three-point-bending fixture to a load below that required to grow the crack. The specimen was unloaded, at which point the specimen was sawed, thereby increasing the crack length. The specimen was again loaded and unloaded and the procedure was repeated. The resulting load displacement information yielded compliance vs. crack length information for a specimen with no friction.

Because of the finite element modeling predictions, the remaining Mode II tests were conducted with a dowel pin inserted between the backing beams just above the loading point. Several comparison tests were conducted to determine if the pin should be placed in a notch in one of the backing beams to hold the pin in place or if it should be free to roll between the

backing beams. These tests were run with specimens with identical geometries and similar original crack lengths.

The typical load vs. displacement behavior for the Mode II tests are shown in Figures 4.3.18-4.3.20 for the composite-composite, steel-steel and epoxy specimens respectively. The crack lengths were difficult to visually identify for the adhesive specimens and may have significant error. Some of the Mode II tests may need to be repeated with crack gages to improve the accuracy of the crack length measurement. Another problem with the adhesive specimens was that the crack tended to grow too far during the Mode I pre-cracking, resulting in higher loads and fewer number of crack extensions until the crack propagated under the center loading pin. Because the load dramatically increases as the crack grows toward the center-loading pin, the joint geometry was altered slightly. The crack initiator was shortened to make the initial crack length as short as possible. The crack extensions were kept as short as possible in order to get several data points for measurement of  $G_{IIc}$ .

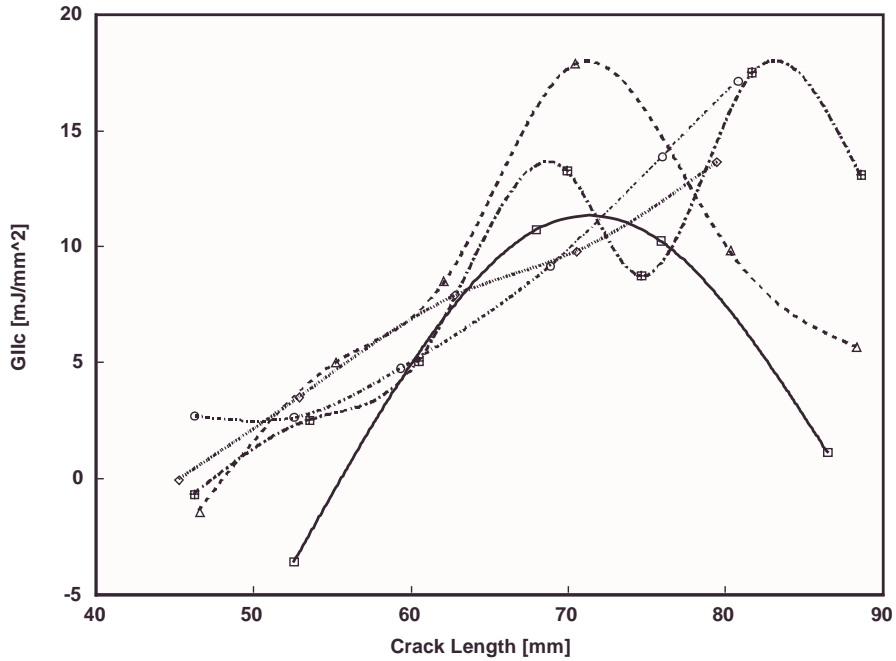
There appears to be a reduction in the hysteresis between the loading and unloading curves due to the insertion of the pin propping the crack open slightly. However, the hysteresis is not completely eliminated. Methods to quantify the improvement in the tests with the pin propping the crack open are currently being evaluated.

The method chosen for data reduction was the compliance method using a third order compliance fit, the same method used for the Mode I calculations. However, both the critical load and the compliance were not straightforward to obtain from the load vs. displacement data because of the large amount of hysteresis and associated non-linearity of the load-displacement curves. With this in mind, it was decided that the compliance should be determined from the slope of the initial linear portion of the loading slope for each loading cycle. The critical load was calculated the same way as for the Mode I tests, from the point of deviation from linearity of the loading curve.

Figures 4.3.27-4.3.29 show the results for several composite-composite specimens demonstrating the effects of pre-cracking and employing the friction-reducing roller. The large scatter in  $G_{IIc}$  may be attributed to errors in determining the critical load. As an improvement,  $G_{IIc}$  will be recalculated with a different method for determining the critical load. The critical load for each loading/unloading cycle will be defined as the load just prior to unloading from the previous loading/unloading cycle. This means that a  $G_{IIc}$  will not be calculated for the first crack extension. The rationale behind this definition of the critical load results from the load-displacement curve for a Mode II specimen tested without unloading. If the specimen is not unloaded, the crack continues to grow as the displacement increases. Therefore, it is assumed that after the specimen is unloaded and reloaded, the crack will begin to grow at the load level prior to unloading.

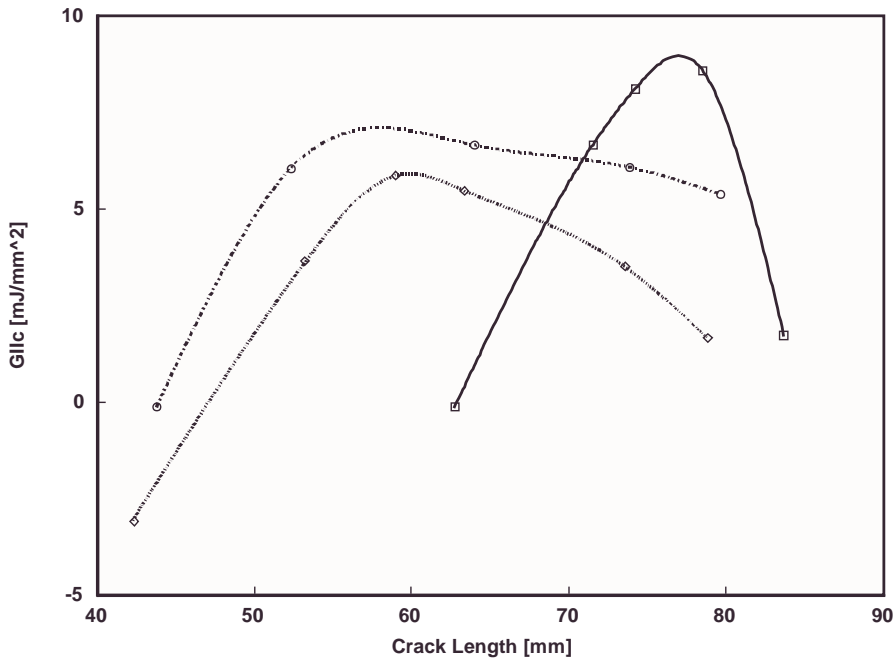
As expected, the  $G_{IIc}$  values are significantly higher than the  $G_{Ic}$  values for the same joints. In general, most materials are more susceptible to fracture by normal tensile stresses than by shear stresses.

The first draft of the Mode II testing procedure has been completed and will be reviewed by the ACC Joining Group. When finalized, the procedure will be submitted for external validation. The Mode II test has been automated using LabView to control the specimen loading as well as data acquisition. Future enhancements will also consider utilization of crack gages to provide further enhancements to the test automation. The data analysis will be fully automated with LabView as well.



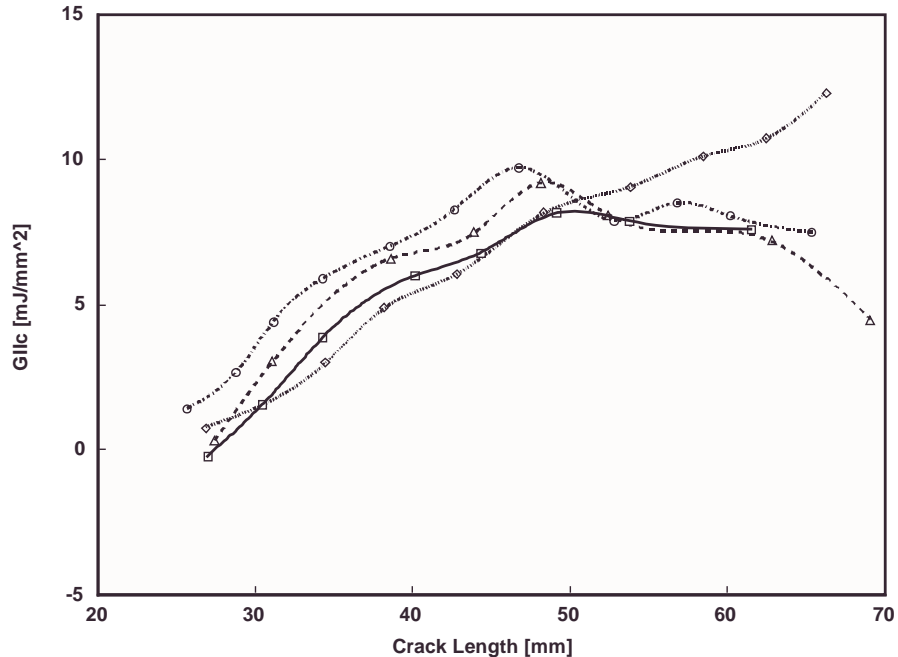
Notes: Pre-crack in Mode I, without friction reduction pin roller.

**Figure 4.3.27. Mode II Fracture Toughness vs. Crack Length for Five Composite-Composite ENF Specimens**



Notes: Pre-crack in Mode I, with friction reduction pin roller.

**Figure 4.3.28. Mode II Fracture Toughness vs. Crack Length for Three Composite-Composite ENF Specimens**



Notes: No pre-crack in Mode I, with friction reduction pin roller.

**Figure 4.3.29. Mode II Fracture Toughness vs. Crack Length for Four Composite-Composite ENF Specimens**

#### 4.3.4 Mixed-Mode Fracture Toughness

This area of the adhesive joining project was concerned with the circumstance of mixed-mode fracture (simultaneous Mode I and Mode II). Mixed-mode fractures are generally encountered in combined loading conditions where both normal and shearing stresses act to generate crack growth. For the case of adhesive joints, there are often dissimilar materials present which, when exposed to loading conditions that would normally result in Mode I crack growth, can yield a mixed-mode fracture. With this in mind, it is important to understand the mode mix, and to develop analysis techniques to design pure Mode I and Mode II tests to evaluate the bonding of dissimilar materials.

##### 4.3.4.1 A Brief Overview of Mixed Mode Specimen Geometries

There are several approaches employed to achieve mixed-mode loading conditions. The goal is to introduce a combination of both normal and shear stress components at the crack tip in such a way that the mode mix can be calculated. One of the simplest specimens is the mixed mode flexural (MMF) specimen depicted in Figure 4.3.30 below.

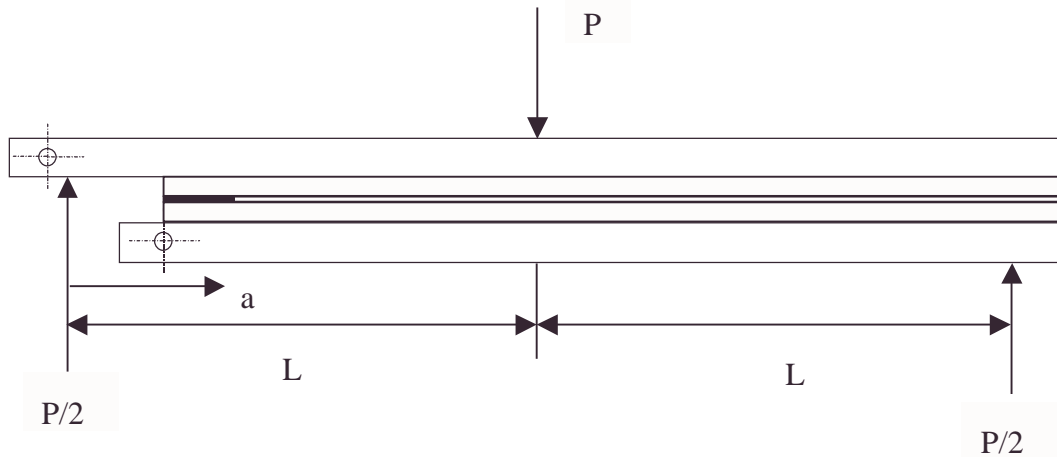


**Figure 4.3.30. Typical MMF Specimen**

This specimen is convenient from a manufacturing standpoint. However, only one mode mix ratio is achieved if the top and bottom beams are the same height and material. In the absence of a Mode III component of crack growth, this ratio is given as:

$$\frac{G_I}{G_{tot}} = 4/7 \quad [4.3.7]$$

Since  $G_{tot} = G_I + G_{II}$ , the mode mix can also be expressed by:

$$G_I = 4/3G_{II} \quad [4.3.8]$$

In the above expressions,  $G_{tot}$ ,  $G_I$  and  $G_{II}$  are the total, Mode I, and Mode II energy release rates respectively. The total strain energy release rate of the specimen can be calculated using the following expression, which is derived from energy considerations and beam mechanics:

$$G_{tot} = \frac{21P^2 a^2 C}{2L^3 + 7a^3} \quad [4.3.9]$$

Again,  $C$  is the specimen compliance, which can be determined from the slope of the load-displacement curve prior to crack extension. All other parameters are defined in Figure 4.3.30.

#### 4.3.4.2 Mixed-Mode Fracture Toughness Testing

Exploratory mixed-mode tests using the MMF specimen were carried out on several different adherend combinations to evaluate the specimen's usefulness with adhesive joints. Specifically, steel-steel, composite-composite and pure adhesive joints (adhesive layer between two backing beams) were tested with varying degrees of success.

In the case of the steel-steel and purely adhesive specimens, the crack did not grow steadily with increasing load. Instead, the crack growth initiated abruptly and arrested beyond the location of the center-loading pin. A typical load-displacement curve (Figure 4.3.31) shows

a sudden drop in load with little or no corresponding change in displacement, which is indicative of run-arrest behavior. Several modifications were made to the test procedure in an attempt to avoid run-arrest behavior. First, the test speed was slowed by two orders of magnitude. Next, Mode I pre-cracking was employed to develop a sharp crack, and mixed-mode pre-cracking by cycling the specimen at reduced dynamic load levels was investigated. In spite of these attempts stable crack growth could not be achieved.

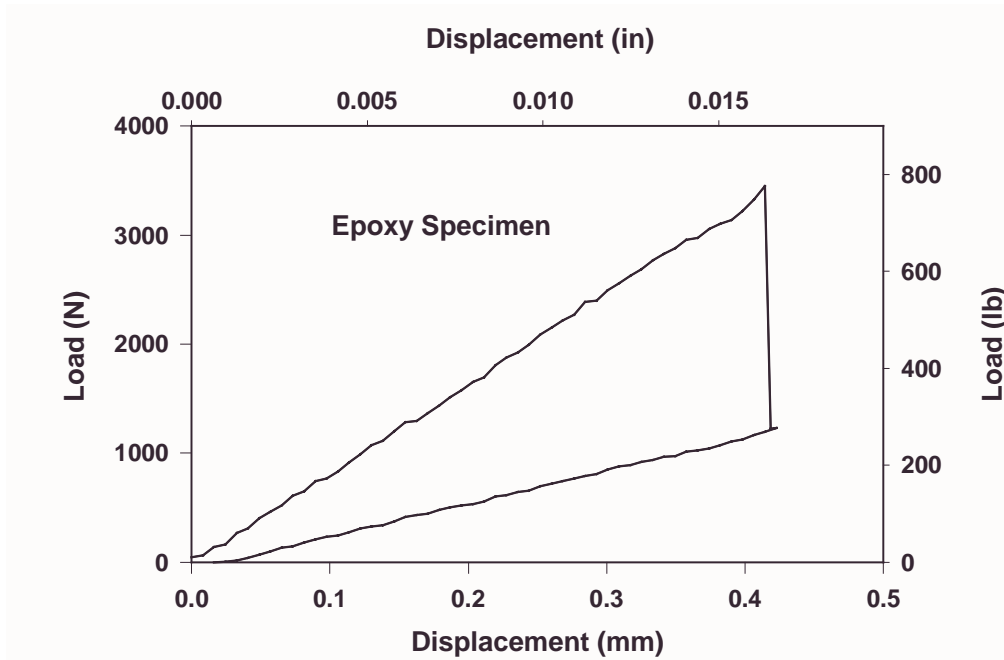


**Figure 4.3.31. Typical Load-Displacement Curve From a Pure Adhesive MMF Specimen**

This type of run-arrest behavior excludes using a single specimen energy analysis such as that described in Section 4.3.2.1 (Equation 4.3.1) since it is impossible to establish a relationship between specimen crack length and compliance ( $dC/da$ ). Therefore, to measure energy release rate it is necessary to consider employing Equation 4.3.9.

For the composite-composite specimens, the specimen geometry was found to be lacking since there was interface failure between the composite and top-backing beam in addition to crack growth in the adhesive joint. This dissipative interface failure invalidates any method to determine a fracture toughness value. In view of the difficulties and limitations associated with the MMF specimen, alternate specimen geometries are being evaluated using finite element modeling.

#### **4.3.5 Mixed-Mode Fracture Testing of Adhesive Joints with Dissimilar Substrates**

##### **4.3.5.1 Mode I Fracture with Dissimilar Materials**

Examination of the fracture surfaces in the e-coat/composite joints revealed that the fracture path consistently remained within the region of the e-coat and adhesive layers for most of the crack extension. Although this fracture pattern gives the indication that the failure was primarily Mode I, it is not conclusive evidence that there was no Mode II component. The idea

of balancing the flexural stiffness outlined in section 4.3.2.4 may have some conceptual shortcomings for certain beam configurations, in spite of the good agreement with finite element results. Specifically, by definition, the mode mix ratio is determined from the stress distribution and associated displacement fields at the crack tip. Determining these stress and strain fields are beyond the scope of the mechanics of materials approach used in the compliance-matching scheme, and require more detailed fracture mechanics analysis.

#### 4.3.5.2 Mixed-Mode Fracture with Dissimilar Materials

For the case of dissimilar beams (different material or beam heights), a variety of mode mixes can theoretically be obtained with the MMF specimen. Unfortunately, a rational scheme for designing for specific mode mixes with this specimen is not available at this time. Therefore, it is necessary to consider different specimen geometries.

Similar to the strategy for matching beam compliance to obtain pure Mode I, it has been shown by Suo, Hutchinson, et al that it is also possible to obtain a range of mode-mixes employing double cantilever beam type specimens with different materials and/or beam heights as depicted in Figure 4.3.32. General axial and shear loading conditions in addition to the applied moments shown can be considered for this type of specimen, however, for the sake of brevity the current discussion will focus on the case shown below.

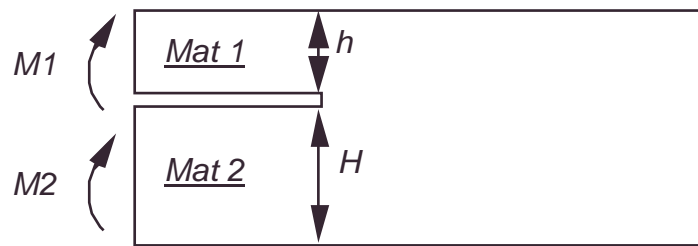
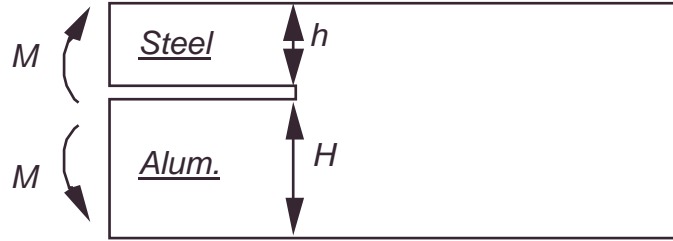


Figure 4.3.32. Mixed Mode Model Geometry

There are several existing mode-partitioning models for calculating the fracture toughness components ( $G_I, G_{II}$ ) for this specimen geometry. Generally these models are based on fundamental energy principles along with fracture mechanics; hence the details of the stress field at the crack tip are taken into account. The inputs to these models consist of material properties and the heights of the two beams, and the result is the mode-mix ratio. Unfortunately, the analysis involved in the actual mode-mix ratio can be extremely complex, and only a limited number of data sets for various material combinations are available. Therefore, to find the mode-mix ratio for a specific material/beam height combination that is not published, it is necessary to interpolate the results from the existing data, or re-run the analysis for the material and specimen geometry under consideration.

With this in mind, it was decided to compare results between the aforementioned flexural stiffness matching technique (mechanics of materials approach) and one of the mode-mix models. As a test case, it was decided to calculate the beam height required to obtain the pure Mode I condition between steel and aluminum beams (see Figure 4.3.33).



**Figure 4.3.33. Test Case Specimen Geometry**

It is simple to show that matching the flexural stiffness with typical values for the moduli of steel and aluminum ( $E_{alum}$ ,  $E_{steel}$ ) requires the ratio of the two beam heights to be:

$$\frac{h}{H} = \left( \frac{E_{alum}}{E_{steel}} \right)^{1/3} \approx 0.693 \quad [4.3.10]$$

From the mode-mix model the approximate beam height ratio was found to be 0.76, approximately an 8% difference. Some error in this calculation may be introduced by interpolating the solution from tabulated data.

Although several comprehensive DCB mixed-mode models exist at the current time, they may not be appropriate for practical evaluation of the complex joint configurations that would be encountered in automotive applications. For example, these solutions do not readily lend themselves to determination of the correct beam height for a desired mode-mix. Rather, they solve the inverse problem, providing the mode-mix for a given joint geometry. Additionally, the solutions to these models are not closed form and need to be evaluated numerically on a case-by-case basis. Finally, it is difficult to validate these models experimentally due to the idealized loading conditions, which cannot be implemented in the laboratory. With this in mind, it will be necessary to develop a new practical methodology to evaluate a variety of mixed-mode adhesive joints, which address these shortcomings.

#### 4.4 Modeling/Characterization

The objective of this task was to develop design procedures for cracked adhesively bonded joints with fiber-reinforced polymer matrix composites. The main focus of this task was to determine the resistance to quasi-static mixed-mode crack growth under short term, monotonic loading. The final report, by Leichti et al, detailing this work can be found in References 19 and 20.

A wide variety of material properties of adhesively bonded joints were analyzed and non-linear finite element analysis models were developed to accurately simulate the fracture behavior of three test geometries: (1) the double cantilever beam geometry which allows a determination of the fracture behavior when the loading is such that the crack is opened (Mode I) (2) the end notched flexure test, which loads the crack in a pure shear fashion (Mode II) and (3) the mixed-mode flexural test configuration (Modes I and II), since most “real world” failures are a combination of these two loading types.

To develop accurate models, the behavior of the adhesives and adherends were characterized together and independent of each other. This was a partial duplication of the work conducted in the bulk materials task but was necessary due to the different task schedules and the need for dynamic behavior information.

Adhesive and adherend characterization was carried out to determine properties such as Young's modulus, Poisson's ratio, shear modulus, shear relaxation behavior, etc., under near-static conditions. In addition, dynamic properties such as shear moduli, Poisson's ratio, and tensile moduli were determined using three different frequencies. These tests were repeated for bonded composite/adhesive/composite sandwich samples. Included in this evaluation was a full complement of tests to determine quasi-static properties and dynamic properties as well as specialized shear testing. Following this characterization, the three fracture test geometries indicated above were evaluated.

For the three test geometries, information was sought on the interfacial fracture properties, compliances, strain energy release rates, stress distributions, relaxation moduli and viscoelastic behavior. Characterization of the plastic zone was conducted including crack tip displacement measurements. The effects of anti-clastic bending, fracture behavior, and location of the initial crack tip were examined. After completion of material testing, finite element models were constructed for each of the three test geometries and verified using different adherends and adhesives (for example see Figure 4.4.1). This included a determination of the fracture envelope for each adherend/adhesive pair.

The long-range goal of this project task was to develop an analytical method for predicting the fracture response of "real world" joints, which required interaction between the modeling/characterization, fracture mechanics and bulk materials sub-task researchers. This development process can be repeated for understanding the fatigue, creep, fatigue fracture and creep fracture behavior of joints.

## **4.5 Process Control and Nondestructive Evaluation**

### **4.5.1 Nondestructive Evaluation**

Nondestructive analysis (NDA) is a means of validating a component or structure without the expense and waste of destructive testing. Validation is particularly important when the structure or part in question is manufactured using new materials, such as SRIM composites, and/or new processes, such as structural adhesive bonding.

At the onset of the program, a survey of the current state-of-the-art in NDA was performed. The survey consisted of contacting university and research centers, National Laboratories working on nondestructive test (NDT) methods, commercial suppliers of NDT equipment, and reviewing the literature and product bulletins. Several contacts requested samples to use to demonstrate their methods. Two types of specimens were prepared to help evaluate NDT methods for bonded composites (and for the composite itself): a sandwich of corrugated composite (to simulate a truck box) with many different "known" flaws incorporated into the bonds, and a thick sheet (19 mm, 0.75 in) of composite with drilled holes of varying depth and diameter to measure the sensitivity of the NDT methods. These specimens were circulated to the following labs and test facilities:

Recognition Technology, Inc. (shearography/holography)  
 Laser Technology, Inc. (shearography)  
 Thermal Wave Imaging (thermography)  
 Digital Wave (pitch/catch ultrasound)  
 UltraOptec (laser ultrasound)  
 Failure Analysis Assoc. (array ultrasound)  
 Wright Patterson Materials Labs (various)  
 Wayne State University (vibration damping)  
 NASA Langley (various).

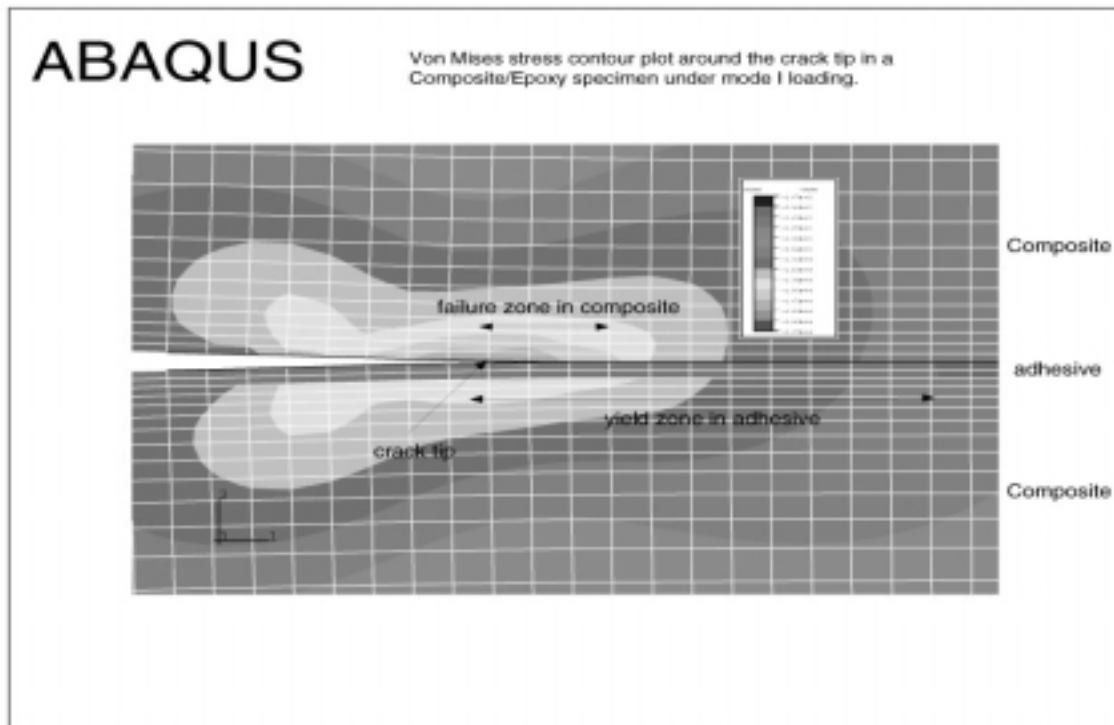


**Figure 4.4.1 Von Mises Equivalent Stress Contours in a Composite/Epoxy Specimen with a Trapezoidal Interface Separation Law Under Mode I Loading**

The specific NDT method required for production must be rapid, simple to use (capable of automation; capable of use by non-technical personnel), robust (practical to operate in a plant environment), and of reasonable cost. These requirements can best be met by “full-field” NDT methods - techniques that can interrogate large areas of a structure rapidly using non-contact methods. Additionally, in many circumstances, a structure will offer only single-side access and the NDT method must still be able to perform its evaluation. From the survey and results from the circulating “known-flaw” specimens, it appeared that, of all the methods considered, thermography and shearography would most likely have the necessary attributes for automotive applications. For many of the methods (e.g., ultrasound) obtaining results was very difficult due to the damping/dispersive characteristics of composites being studied. Results from the survey

and testing are documented in ACC Technical Report TR J94-01 and in the Technical Review Report from the ACC Off-Site - XIV (May 14, 1996).

While the laboratory-scale “known-flaw” specimens were being circulated, larger bonded composite structures, representative of automotive applications, were evaluated using thermography, thermal wave imaging (a “next-generation” thermography method), and commercial shearography. Ultimately, a destructive teardown of the structures was performed to check the NDT results.

Thermography was used to evaluate a bonded SMC mini-van door. A flaw was introduced into the bond by prying apart the inner and outer door panels, thus destroying the bond in a known location (SMC fiber tear). In two other locations, adhesive was drilled out of the bond through the outer edge of the door assembly. Thermography was able to locate the areas where drilling had removed adhesive, but this method was not successful in locating the region where the bond had been damaged between the inner and outer door panels. Since heat transfer is the means by which thermography detects a good or bad bond (a good bond allows good heat transfer), a damaged bond where two surfaces still remain in close contact, allowing heat transfer to occur, will not be detected.

Professor Bob Thomas (Wayne State University) and Steve Shepard of Thermal Wave Imaging, Inc. (Lathrup Vill, MI) also analyzed the SMC door. Their results were similar to those of the first thermography testing. Further refinement of their method should allow for location of the unbonded region not initially detected. Also, applying a small mechanical agitation to separate the unbonded parts, which would interrupt heat flow, would most likely enable the method to identify this damage site.

Thermography was also used to evaluate a bonded composite pick-up box from a previous GM program (the Sedona S-10 pick-up). The part was evaluated as received and then again after being subjected to hot and cold weather durability exposure. No bond degradation was apparent after environmental exposure.

Laser Technology, Inc. was contracted to perform a shearography analysis of the P/U box after the final environmental exposure. The results (shown in Figure 4.5.1) were consistent with the results from the thermography testing, but the shearography data was easier to interpret. Physical teardown of the P/U box confirmed the NDT results.

It was decided to examine the potential production capability of shearography as a rapid, full-field, non-contact inspection method in more detail. A research project was arranged with Oakland University, Prof. Michael Hung P.I. This project is funded by the DOE/ United States Automotive Materials Partnership (USAMP) Cooperative Agreement. The first year deliverable is demonstration of the capability of a lab-scale system to analyze composite structures of interest. The second year deliverable is a demonstration of a plant-capable shearography unit (in a plant environment). When the shearography project has been completed, results from shearography and thermography (thermal wave imaging) can be compared again in the plant.

Quarterly Progress Reports from Year 1 of the shearography project, submitted to ORNL and ACC by Professor Michael Hung of Oakland University, have been included with the appropriate quarterly reports for this CRADA project. These reports detail efforts to determine the proper method for applying stresses to the materials and structures of interest (bonded SRIM composites), and the development of software to optimize and help automate testing and analysis. The method was shown to be capable of detecting flaws in a new pick-up box replica fabricated from the composite and adhesive materials to be used in ACC FP II (bonded composite P/U box). With appropriate image analysis software, shearography data collection

and interpretation (go/no-go) has the potential to be automated. The one concern with the method is that, to date, the best method of stressing these large composite parts is acoustic vibration (other methods include mechanical vibration, vacuum, and thermal stressing). Because the parts are so large and stiff, the sound level needed to provide surface deformation is intense. This could be a concern in a plant environment. Ear protection, and/or soundproofing may be required. Vacuum application also appears to have potential as a stressing method, however a method of applying vacuum to a large irregular surface, or part with a complex shape, has not been successfully demonstrated (for this project). It should be noted that vacuum stressing is a common method successfully used to inspect aircraft fuselage sections that are smooth and easy to seal against.

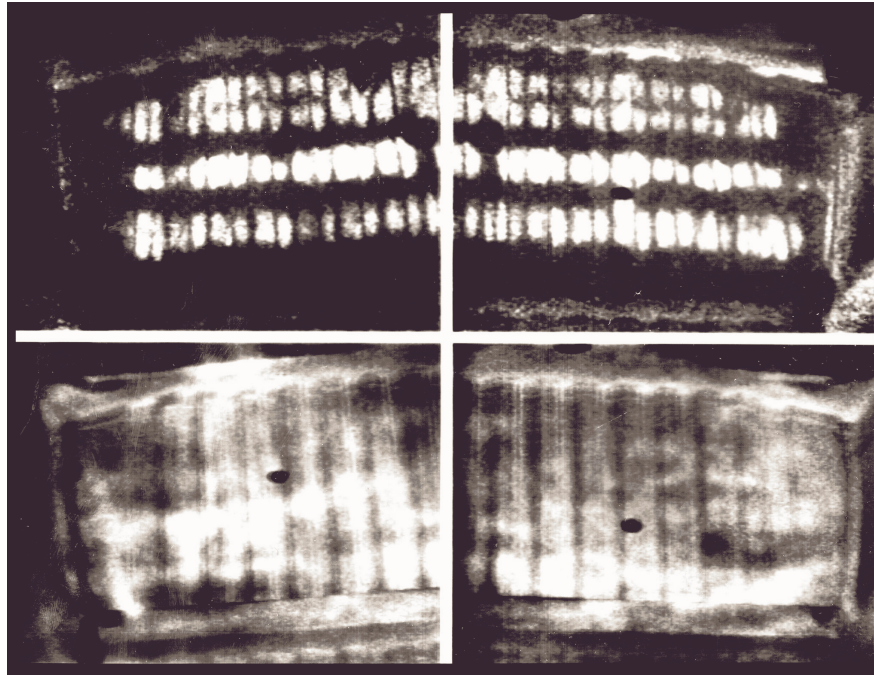


**Figure 4.5.1. Photo Results from Shearography NDT Trial: Dark Areas Indicate Good Adhesion. Small Black Circles Indicate Where Core Samples Were Removed**

After review of the first year results, it was decided that there was sufficient potential in shearography to continue the project. The second phase of the research program will be to build and demonstrate a plant-functional prototype instrument. This work will not be carried out under this CRADA but will be part of future collaboration between the ACC and the ORNL under the master DOE/USAMP cooperative agreement.

#### **4.5.2 Process Control**

Process control is the means by which an efficient manufacturing process is maintained, and a product is manufactured according to specification (quality and reliability). Critical process parameters must be identified, along with their control limits, for each step in the

bonding process. The technology required to provide real-time feedback and control may not be available (for reasons including cycle time and/or cost). The intent of this effort was to identify critical processing parameters for adhesive bonding and determine whether the technology to measure and control the parameters is currently available. If the technology is not available, the effort should be directed towards determining: 1) what is required to develop such technology, and 2) whether it is appropriate for the automotive industry to be involved in the required technology development.

The group started by developing an outline of a generic methodology for production process control:

1. Product Research and Development
  - Product Definition and Design
  - Performance Specifications
  - Material Choices
  - Preliminary Plant Process
2. Process Development
  - Identification of Plant Processing Issues
  - Establishment of Critical Parameters
  - Determination of Limits of Critical Parameters
  - Confirmation of Results in Lab and Pilot Plant
3. Manufacturing Development
  - Determine if New Technology is Required to Implement Controls
  - Implement Required Controls

It is clear from this outline that effective process control begins with product concept and design. Attempts were made to contact personnel at production bonding facilities, such as automotive assembly plants and supplier facilities, to determine what steps in the control process the plant personnel felt were lacking. These interactions were not particularly fruitful. Feedback indicated all control methods required, regardless of technical sophistication, were deemed to be in place or could be implemented if desired. Additionally, those contacted felt that current control process was sufficient and any new problems would be addressed when required. Thus, it was not clear what approach the group should try next.

Work in this area was suspended for a period of time to concentrate on other pressing areas related to FP II. When work on this topic resumed, it was suggested that the group prepare a document detailing issues critical to structural bonding (identify critical process parameters). Examples of such issues include substrate cleaning and maintaining clean surfaces, assembly without wiping out adhesive, knowing the required time at cure temperature of the adhesive (a function of substrate heat transfer, different for all substrates), etc. This type of document would serve as an introductory guide to bonding for any program or manager that needed to implement adhesive bonding with little or no previous experience.

#### **4.6 Crash Energy Management of Bonded Composites**

Investigating the energy management capability, not only of composite structures, but also of bonded composite structures (such crush rails used in front end applications), was identified as an important area of interest. The need for bonded energy management structures

arises if repair is required of the structure, or if the vehicle is designed to have a modular front end.

The ACC Joining and Energy Management (EM) Groups developed an approach to investigate various joint configurations and a series of test specimen geometries using both static and dynamic tests. The test geometries are based on composite crush tube investigations already completed by the EM Work Group. Scaled down hourglass rails were designed which were to be bonded, or mechanically fastened and bonded, in either the vertical or the horizontal plane of the rail. Fifty-four bonded rails, and six one-piece controls were fabricated by an outside molder (Excel Pattern). These parts were molded from a vinyl ester with glass mat and directed glass fiber reinforcement. Since this material was also used in the initial crush tube work by the EM group, there is a corresponding database for comparison. Four types of longitudinal joints (Figure 4.6.1) and five types of transverse joints were evaluated. All specimens were bonded using an Ashland urethane using a method recommended by the molder.

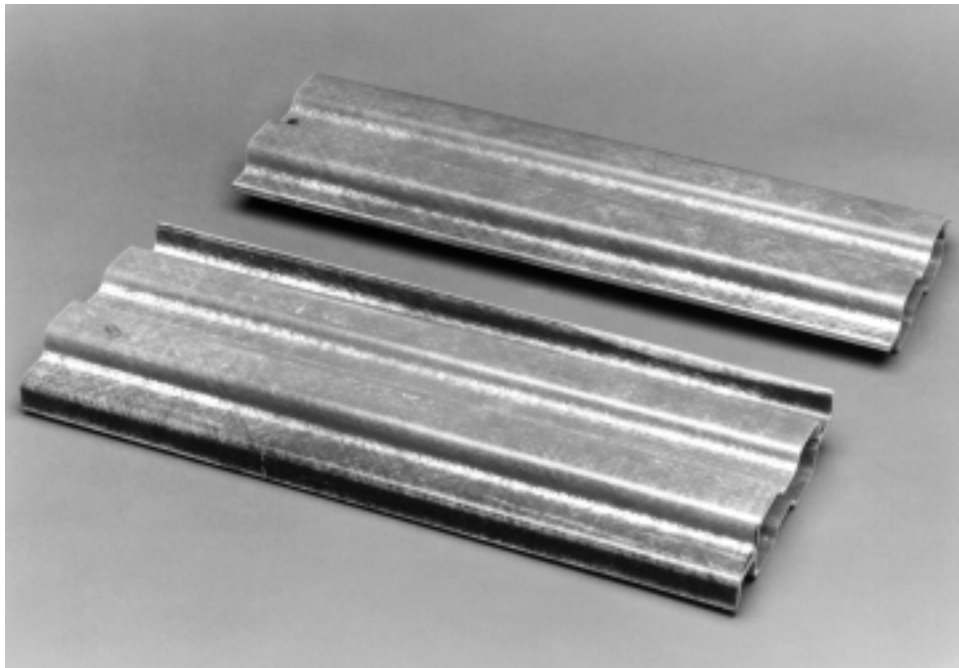


**Figure 4.6.1. Longitudinally Bonded SRIM Composite Hourglass Rails**

Drop tower testing of the specimens revealed, for the longitudinal joints, that stable crush was achieved in all cases and all bonded tubes were stiffer than the non-bonded control (Figure 4.6.2). At least some of the increase in stiffness results from the additional material (adhesive and extra layer of composite). In some cases the part may turn out to be too stiff, resulting in a “brittle” catastrophic failure. Reduction in stiffness may require the use of less composite material. Some of these joint geometries were considered potentially useful. For transverse joints, stable crush occurred up to the point where the initiator reached the bonded joint. This was immediately followed by a significant reduction of load (Figure 4.6.3), which was deemed unacceptable. Thus, the decision was made to continue working only with longitudinal geometries.

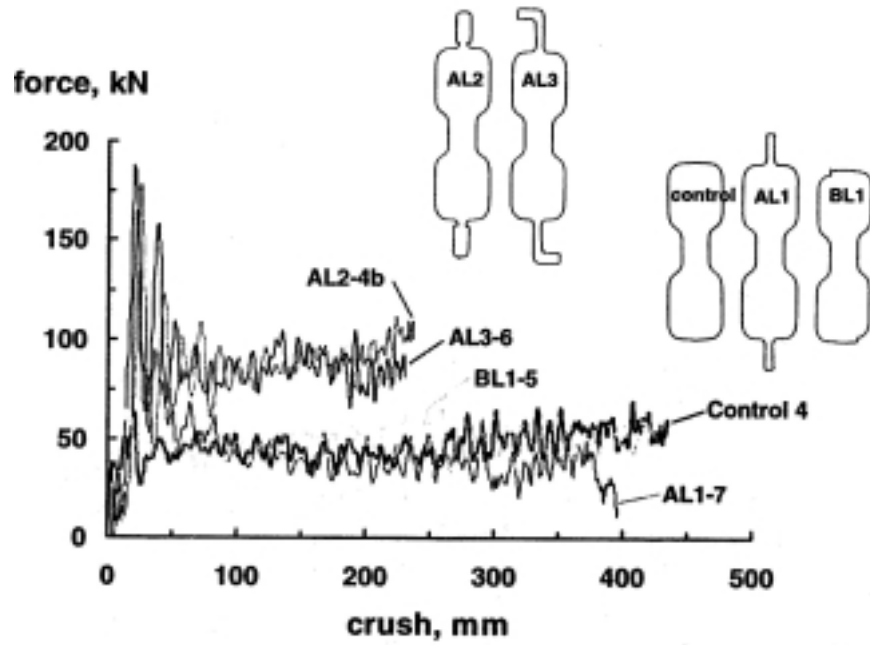


Figure 4.6.2. Dynamic Response Curves for Four Longitudinally Bonded Crush Rails

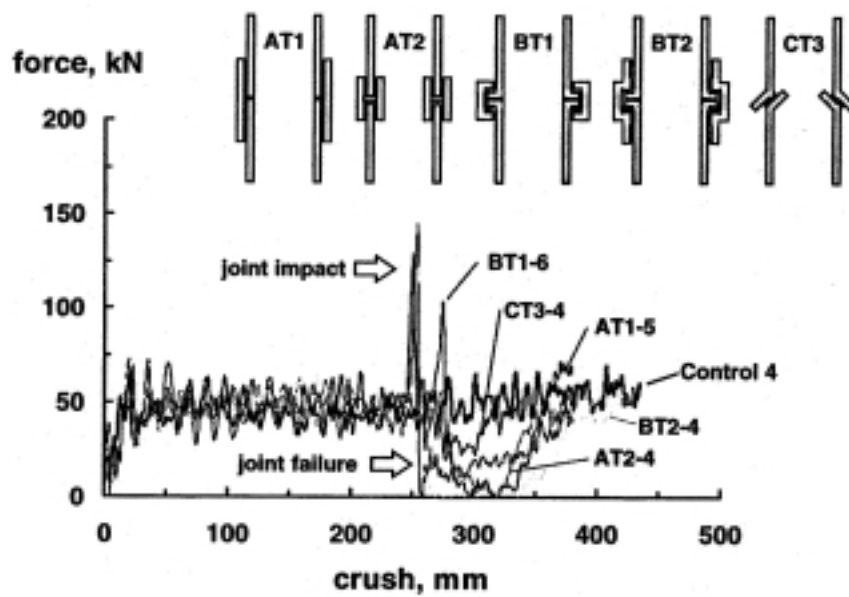


Figure 4.6.3. Dynamic Response Curves for Ten Transversely Bonded Crush Rails

Investigating the effects of temperature and bond-line thickness on dynamic crush performance for the shear joint geometry (BL1 in Figure 4.6.2) is planned for future work. For the peel geometry (AL1 in Figure 4.6.2), the addition of mechanical fasteners will be studied. Specimens will only be tested dynamically since the EM group has not seen any correlation between static and dynamic behavior.

#### **4.7 Fatigue Durability of Bonded and Hybrid Joints**

The fatigue durability (fatigue life) of bonded composite structures is another key issue when considering such materials for automotive applications. Composites, such as SMC, have been shown to exhibit a variety of problems such as fretting or wear near fastener holes when exposed to fatigue loading. In certain circumstances, if the fastener is located close enough to the edge of the part, catastrophic failure of the attachment point may occur. Thus, this part of the project was initiated to investigate the fatigue performance of bonded and hybrid (bonded and/or mechanically fastened) composite joints, and to determine methods and joint designs for improving the fatigue life. This work is being performed at the University of Michigan, Dearborn under the direction of Professor P.K. Mallick. The ACC and the Michigan Materials and Processing Institute (MMPI) are jointly funding the project.

Agreement was obtained between ACC and the principle investigator to perform the initial study of bonded lap joints with both a commercial SMC and an ACC-identified SRIM as substrates. The ACC FP II adhesive was to be used in the work. In the first year, the overall work plan included a baseline study of parameters, such as lap length, bond thickness, and substrate taper angle, (which all affect bonded joint performance in static loading) and then compare these effects on joint performance during fatigue loading. These comparisons were made with SMC (GenCorp 7144, a "structural" SMC) and SRIM (Dow MM 364 with continuous strand mat (CSM) glass reinforcement). Tensile and flexural fatigue loadings were studied. Joint modeling was performed for the lap joints, including evaluating stresses through the thickness of the substrate as well as stresses within the adhesive layer.

Similarly, the goal of the second year of the program was to perform a comparative parametric study of the static versus fatigue performance of mechanically fastened SRIM joints. In this case, the parameters were to be the size, thickness, and edge shape of washers for a single bolt size. These joints were to be modeled as well.

The goals of the third year of the program were to review the performance results for the bonded and mechanical joints and, using this information, determine the best design(s) for a hybrid composite joint. This work is to include experimental verification and modeling. Additionally, during the second year of the program, the ACC requested that the PI study a more realistic automotive joint. For this, SRIM "hat-sections" were provided for the project. Bonded and hybrid joints of this geometry will be experimentally studied and modeled. This work would be initiated in the second year and completed in year three.

Progress to date has been documented in detail in MMPI-required quarterly progress reports. Year 1 was completed and several papers have been published in the open literature. Year 2 was in progress at the completion of this CRADA, with further publications being planned. Work on the bonded hat sections has begun, both experimental and analytical.

The ACC Joining Group is the technical monitor for this effort and has been pleased with the progress of the work to date, and funding for the third (and final) year of the program has been approved and paid to MMPI.

## **4.8 Alternate Processing**

The overall objective in this task was to conduct preliminary studies of advanced processing techniques that might lead to dramatic improvements in bonding efficiency or performance. Bonding via both microwave and electron beam radiation were investigated as well as ultrasonic technology. Additionally, potential improvements in surface preparation techniques were investigated.

### **4.8.1 Adhesive Bonding via Exposure to Microwave Radiation**

Adhesive bonding/joining through microwave radiation curing was evaluated as an alternative processing technology. The intent of this work was to produce high quality bonds, with mechanical and physical properties equivalent to conventionally cured samples, with a substantial reduction in the required cure time. The bond strength in the processed samples was characterized using single lap-shear tests. A standard Instron tensile testing machine was used to perform this testing. The substrate studied was the aforementioned Dow MM364 SRIM material.

Microwave curing significantly reduced the required curing time for the adhesive while maintaining equivalent physical characteristics as the adhesive was polymerized (cross-linked). The overall result is an improvement in the economics of the process. Testing of samples cured via microwave radiation for evaluation of mechanical properties indicated that the obtained values from the single lap-shear test are in the range of the conventionally cured samples. Furthermore, the ultimate load for the microwave-processed samples subjected to this single lap-shear test was slightly higher than for conventionally cured samples [21-23]. Figure 4.8.1 depicts force-displacement curves from lap-shear tests for specimens prepared under several variable-frequency processing conditions.

Variable frequency microwave processing appeared to yield a slight reduction in the required adhesive cure time when compared to processing by the application of single frequency microwave radiation [23]. In contrast to the single frequency processing, the variable frequency methodology does not readily produce localized overheating (burnt or brown spots) in the adhesive or the composite. This makes handling and location of the sample in the microwave oven less critical for producing high quality bonds and allows for a more homogeneous distribution of the cure energy. Variable frequency microwave processing is a valuable alternative method for rapidly curing thermoset adhesives at low input power levels [23]. These technologies show promise for being applicable to a wide range of high volume, consumer goods industries, where plastics and polymer composites will be processed. This technology may also be extended to multiple-layered panels or components.

### **4.8.2 Ultrasonic Bonding**

Ultrasonic assisted bonding was investigated at ORNL as a means to increase the adhesive cure rate for joints comprised of the MM364 SRIM composite and the BFG EXP582E epoxy adhesive [24]. Bonding was accomplished by exposure to a 20 kHz acoustic energy source. Initial efforts directed at bonding with the acoustic energy proved to yield unsatisfactory results only because the substrates experience localized overheating and displayed low lap-shear

strengths. Subsequent efforts were directed at combined thermal and acoustic energy. The thermal energy was supplied via a heating tape. Although some improvement was noted, the combined energy approach also proved ineffective for the composite substrates. This may result from low thermal conductivity of the substrate. In this work, it was not feasible to use energy directors at the interface of the joining area as is typically done for thermoplastic welding.

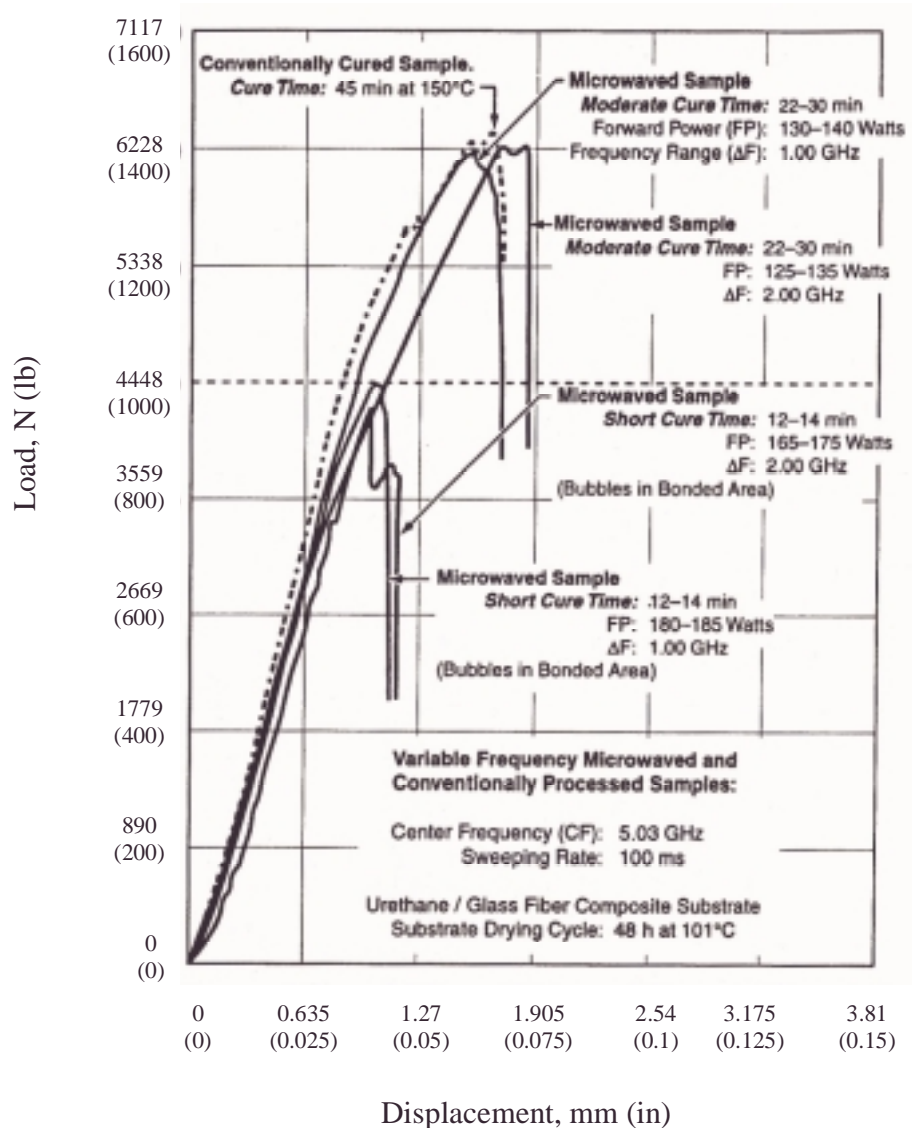


**Figure 4.8.1. Comparison of Lap-Shear Test Results for Adhesive Cured with Microwave Energy Under Various Operation Conditions**

### 4.8.3 Electron Beam Bonding

The bond strength for lap-shear specimens comprised of electron beam curable resins and the MM364 SRIM composite substrate was investigated. This was a small effort that leveraged the e-beam curable resin development efforts from another CRADA at ORNL. A wide array of

adhesive systems that cure by a free radical and/or cationic cure mechanism were investigated. These included metal and glass filled systems, as well as thermoplastics, elastomers, acrylics, and proprietary toughened adhesives. Approximately 35 different adhesives were cured with lap-shear strengths ranging from 1558-14,410 kPa (226 to 2090 psi), which indicates that this method may be a viable alternative for curing adhesive joints from a mechanical performance viewpoint.

#### 4.8.4 Laser Ablation for Surface Preparation

Laser ablation was evaluated as a surface pretreatment prior to adhesive bonding of the SRIM composites [25]. The objective was to remove the resin-rich surface layer and expose the fibers. It was postulated that in a subsequent bonding step, better adhesion would be afforded through enhanced mechanical interlocking and removal of surface contaminants. The ablation was performed using a KrF excimer Laser with a wavelength of 248 nm. A pulse frequency of 10Hz was used with average pulse energy of 90-100 mJ and pulse duration of twelve nanoseconds. Various pulse durations and incidence angles were investigated. The ablation proved successful in selectively removing the resin while leaving the fibers in place as shown in Figure 4.8.2. After the composite substrate was ablated, lap-shear specimens were fabricated for testing. Additionally, three control sets were made: 1) no surface preparation, 2) solvent wipe, and 3) mechanical roughening. Results indicated that the lap-shear strengths for the laser-ablated samples were significantly higher than those for specimens with no preparation or with solvent only. However, the strengths for the laser-ablated samples were slightly lower than those for specimens that were mechanically roughened. Optimization of the process may lead to further improvements. Additionally, the technique holds promise for carbon-reinforced composites [25].



Figure 4.8.2. Glass Fibers Exposed Through Laser Ablation in a SRIM Composite

## 4.9 Manufacturability Demonstration

The purpose of this effort is to demonstrate that a “designed for composites” vehicle, or major vehicle sub-assembly, is manufacturable, meets defined performance criteria, and achieves weight savings (relative to a conventional steel structure) at minimum cost. A bonded composite pick-up truck box assembly was chosen for the demonstration; the composite manufacturing process is structural reaction injection molding (SRIM).

Several indicators of success were defined as:

- molding cycle time of 4 minutes
- dimensional stability, functionality, quality and performance as good as (or better than) steel
- cost to be competitive with a steel box plus bed-liner
- 25% weight savings vs. steel

With respect to bonding and assembly, this indicates a bonding process that will enable cycle time requirements to be met and structural joints that provide the strength and durability to meet product performance specifications.

### 4.9.1 Design

In the design phase of this effort, several concepts were reviewed by the FP II team (which included members of all the other ACC Work Groups: Materials, Processing, EM, and Joining). The Joining Work Group reviewed each concept with respect to apparent loading mode (design for shear loading is preferable) and ease of assembly (prevent adhesive wipe-out, maintaining specified bond thickness, etc.). Once the concept was chosen and the final design detailed (Masco Tech), the specific design drawings were reviewed. Design validation was performed by Altair Engineering using finite element analysis to determine if part stiffness and deflection would meet truck specifications (mutual performance specifications of Chrysler, Ford, and GM Truck). The Joining Work Group identified an adhesive for this application: a 1-part experimental Sovereign (originally BFGoodrich) epoxy compatible with the SRIM substrate. This adhesive was acceptable in terms of processing requirements. The bulk mechanical properties of the adhesive and substrates were provided to Altair for input into the model. According to the results from Altair’s global analysis, after certain adjustments such as relocation of cross-sills were made, the design of the pick-up box assembly was deemed acceptable.

After subsequent conversations with design and analysis personnel, the decision was made to take a closer look at the behavior of the bonded joints in the truck box assembly. The goal was to obtain stresses in the adhesive while the joint is under load, and then compare those stresses to the experimentally determined strength for the adhesive. The global model generated by Altair was not appropriate for this work, since it only provided stiffness and deformation information. Intelligent Structures, Inc. (Plymouth, MI) has been contracted to perform this work. Pending the results of this local analysis and evaluation of any required joint design changes, the Joining Work group will be able to endorse the design.

#### 4.9.2 Processing

Sovereign 654 ETG, an adhesive previously shown to provide good adhesion to SRIM, and which has an acceptable “production” cure cycle of 45 minutes at 121°C, was chosen for use in FP II. Next, a “strawman” assembly plant layout was developed by the FP II team. The layout includes pre-forming, molding, and post-cure stations, cleaning and assembly (bonding) operations, and subsequent body operations. The Joining Group developed the bonding process plan which includes substrate cleaning, part location and fixturing, adhesive application, assembly, clamping, and adhesive cure. The bonding fixture was designed and fabricated by MascoTech after discussion with the Joining Group. In some cases (adhesive dispensing, for example), suppliers were consulted to recommend appropriate equipment. Since a heat cure is required for the adhesive, it is intended that the substrate cure/post-cure ovens will be used for bond cure. For this, a second set of conveyors can be run through the oven, or the two processes can be performed at different times.

The Joining Group also participated in a Processing Failure Modes and Effects Analysis (P-FMEA). This type of review points out potential problems that might occur during the assembly process, the effects on the product any such problems might cause, and the criticality of the problem. This enables processing and/or design changes to be made before any tools or equipment are purchased. The P-FMEA has been documented in the ACC Technology Transfer Manuals.

Finally, an alternative adhesive curing method, induction curing, was investigated to determine the possibility of a more rapid process to shorten production cycle time. Equipment suppliers were not comfortable with the idea of induction curing of an adhesive between two non-conducting composite substrates. There was also some concern that the temperature spike, which would occur in the adhesive during induction heating, might damage the composite. This method of curing has not been studied further for the FP demonstration. It is expected that further rapid curing investigations will be possible when the work at the National Center for Composite Systems Technology (NCCST) facility begins.



## 5. INVENTIONS

The Alternate Processing task, detailed in Section 4, has proven to be a relatively fertile area for invention. Under this CRADA, ORNL personnel have submitted five invention disclosures and two patents have been issued to date. The invention disclosures and their status are found in Table 5.1.

**Table 5.1. Invention Disclosures Filed as a Result of CRADA Research**

<b>ESID/ERD</b>	<b>Title</b>	<b>Status</b>
1426-X	Adhesive Joining via Exposure to Microwave Radiation	In review
1427-X	Sealed Printed Circuit Board Fabricated via Exposure to Microwave Radiation	Combined with 1428-X
1428-X	Thermoplastic Joining via Coupling to Dielectric and Electrically Conductive Materials Under Suitable Loading	Granted
1679-X	Fiber-Reinforced Adhesive Bonding for Polymer Matrix Composites	In review
TBD	Bonding/Joining of Metal-Metal and Metal-Composite Substrates via Acoustic Processing	Pre-disclosure
1617-X/S-82298	Fiber Reinforced Bonding for Polymer Matrix Composites	In review



## **6. COMMERCIALIZATION**

Although none of the inventions discussed above have been licensed to date, several of the technologies developed under this CRADA are expected to see considerable use by the domestic automobile industry and their suppliers. Specific commercialization opportunities by technical area are described below.

### **6.1 Bulk Material Data**

Data obtained from the Bulk Materials Task will provide the basis for future material screening efforts. The data will be used by the ACC or their supplier when considering new materials. Additionally, material behavior documented in this task will be incorporated into a predictive methodology for the fracture behavior of adhesive joints under a variety of environmental conditions.

### **6.2 Structural Mechanics Test Development**

The aircraft/aerospace industry has invested many years in developing test methods for composites and adhesives. Many of those test methods are lacking for the evaluation of automotive materials. Prior to this CRADA, no established standard fracture test method (that is, test procedure along with data reduction scheme) was available to the automotive industry and its suppliers. The test methods developed in this CRADA are expected to be adopted by the ACC and see widespread use by the automobile industry and their suppliers. The ACC would like to require the test methodology to be used by automotive suppliers to assure uniformity in data reporting. In addition, the test methods will provide necessary data for the automotive industry to assess design robustness based on the design guidelines established in the predictive modeling task. It is also expected that these test methods will provide benefits to other industries including aircraft and aerospace.

### **6.3 Predictive Modeling**

Practical design guidelines will follow from the predictive methodology developed under the subcontract to the University of Texas at Austin. It is expected that they will be used by the automotive industry to assess competing designs of adhesively bonded joints from a fracture perspective. Extensive use of design guidelines and a predictive methodology will save considerable effort and money in testing. Utilization of the design guidelines will only require considering a few promising designs to be tested whereas many geometries would have required testing in the past.



## **7. FUTURE COLLABORATION**

Future collaborations between ORNL and the ACC Joining Group have already been identified in two areas. First, the present work will be extended in a DOE direct funded effort to address durability issues. Substrates, adhesives and joints will be characterized under static, cyclic and sustained loading conditions. Effects of temperature and solvents on mechanical properties will also be determined. Test procedures and fracture-based design guidelines for the automotive industry are being developed and will be transferred to the industry. Secondly, discussions are underway to validate the University of Texas at Austin's design guidelines. The ACC proposes to conduct the numerical modeling of a representative structural joint. ORNL proposes to conduct mechanical testing of the structural joints for comparison to the predicted results obtained by the ACC.



## 8. CONCLUSIONS

### 8.1 Bulk Materials

The process developed for casting neat resin test specimens for static tensile and creep tests minimized trapped air-bubbles and resulted in a significant reduction in scatter in the test data. The injection molding process did not yield superior results and was found to be more labor intensive. The drying process developed for the composite substrates eliminated the substrate blistering and adhesive voids resulting in more consistent specimen quality.

Static tensile results for the adhesive showed a high degree of sensitivity to elevated temperature. Large increases in ductility (strain to failure) and reductions in strength were measured at elevated temperature.

Creep data exhibited considerable scatter and permanent deformation even at low stress levels. Scatter, along with permanent deformation, was reduced but not eliminated by employing the preconditioning procedure. These effects were found to be more pronounced for the elevated temperature condition.

### 8.2 Fracture Mechanics

#### 8.2.1 Mode I

Double cantilever beam specimens employing backing beams were successfully used to carry out the Mode I fracture toughness test on adhesive joints comprised of automotive materials. The data reduction schemes outlined in the Mode I fracture toughness testing procedures were found acceptable for characterizing the performance of automotive adhesive joints. This procedure offers the best trade-off between practicality, reproducibility and fundamental foundation.

The compliance-matching scheme, developed for fracture testing of adhesive joints consisting of dissimilar adherends, provides an approximate, yet practical, approach to obtain the Mode I fracture toughness (to within 5%) for the joints considered in this study.

Fracture toughness data was successfully measured as a function of crack length for composite, composite bonded to composite, composite bonded to steel, steel bonded to steel, and neat adhesive specimens.

#### 8.2.2 Mode II

Test results indicate that significant levels of friction were present for the Mode II fracture toughness tests. These frictional effects resulted in artificially high Mode II fracture toughness values.

Modified Mode II test methods, utilizing various roller-pin geometries in conjunction with specimen pre-cracking, reduced, but did not completely eliminate, frictional effects. The best results were achieved for the case with the friction-reducing pin without pre-cracking. Overall, results were satisfactory but somewhat lacking due to the remaining influence of friction.

### **8.2.3 Mixed-Mode**

The MMF test specimen proved to be unsatisfactory for determining the mixed-mode fracture toughness for these materials. A novel approach utilizing dissimilar beams was proposed but not fully investigated in this work. Additional work is required to obtain the mode-mix accurately for such a specimen.

### **8.3 Nondestructive Evaluation**

Of the numerous techniques considered for nondestructive evaluation for on-line component/structural validation, laser shearography was selected as a primary candidate for rapid in-line inspection of bonded structures.

### **8.4 Crash Energy Management**

Drop tower testing of bonded rail structures demonstrated higher stiffness over unbonded structures. More work is warranted to utilize these results to determine methods to optimize joint design for crashworthiness.

### **8.5 Alternative Processing**

Microwave processing was shown to significantly reduce cure time without sacrificing mechanical performance. The ultimate strength of bonded lap joints increased by curing with microwave energy. Variable frequency radiation was found to be superior to single frequency radiation by virtue of faster cure rates and reduction in local overheating.

Laser ablation appears to be a viable candidate for a rapid, plant-ready surface preparation technique. Optimization of this process will be required to determine the full potential. The technique may provide better results for carbon-fiber composites than glass-fiber composites.

### **8.6 Summary**

This work has addressed many issues relevant to the acceptance of adhesive bonding as an enabling attachment technology suitable for a variety of new structural materials being considered for automotive applications. In particular a host of techniques and procedures were established during this research program to address new methods to quantify the performance of adhesive joints between polymeric composite materials.

The development of these methods revealed issues concerning practical information such as processing methods and joining procedures to maintain acceptable (mechanically suitable) and consistent bond characteristics. Additionally, unforeseen behavior of both the adhesives and adhesive joints were identified throughout the research and were incorporated into the characterization.

The culmination of these findings provides a basic guideline for future studies concerned with the design of actual composite automotive structural components.

## 9. ACKNOWLEDGMENTS

The authors wish to acknowledge the contributions of the past and present members of the Joining Group of the Automotive Composites Consortium which includes Tom Dearlove (GM), Mack Endo (Ford), Susan Ward (Ford), Ray Dickie (Ford), Ken Morman (Ford), Brent Larson (GM), Dave Biernat (Chrysler), Kurt Synder (Chrysler), Tom Brimhall (Ford), John Hill (Ford) and Bob Emerson (Chrysler). Their contributions were considerable in defining and executing this research. Hannes Fuchs (GM) of the ACC Energy Management Group conducted the investigations of the crash characteristics of bonded composites. The authors also wish to acknowledge the contributions of Fahmy Haggag, Ken Yarborough, and Dan Skidmore of ORNL. Professors Tom Meek of the University of Tennessee and Dallas Smith of Tennessee Technological University are gratefully acknowledged for the significant contributions to microwave processing and fracture test development respectively. Finally, C. Dave Warren is acknowledged for providing excellent direction as the original project manager and performing much of the early materials research.



## 10. REFERENCES

1. Warren, C. D., Boeman, R. G., and Paulauskas, F. L., "Adhesive Bonding of Polymeric Materials for Automotive Applications", *Proceedings of the Annual Automotive Technology Development Contractor's Meeting*, October 1993.
2. Warren, C. D., Boeman, R. G., and Paulauskas, F. L., "Adhesive Bonding for Automotive Applications", *Proceedings of the Annual Automotive Technology Development Contractor's Meeting*, October 1994.
3. Boeman, R. G., and Warren, C. D., "Fracture Testing and Analysis of Adhesively Bonded Joints for Automotive Applications", *Proceedings of the 10<sup>th</sup> Annual ASM/ESD Advance Composites Conference*, November 1994.
4. Whitney, J. M., Browning, C.E., and Hoogsteden, W., "A Double Cantilever Beam Test for Characterizing Mode I Delamination of Composite Materials," *Journal of Reinforced Plastics and Composites*, Vol.1, October 1982, pp.297-313.
5. Smith, D. G., "Fracture Toughness of Adhesive Joints in Automotive Composites," *Internal Report*, Oak Ridge National Laboratory, August 1993.
6. "Plain-Strain Fracture Toughness and Strain Energy Release Rate of Plastic Materials," D5045-93, *Annual Book of ASTM Standards, American Society for Testing and Materials*, Philadelphia.
7. "Standard Test Method for Fracture Strength in Cleavage of Adhesives in Bonded Joints," D3433-93, *Annual Book of ASTM Standards, American Society for Testing and Materials*, Philadelphia.
8. Williams, J. G., "The Fracture Mechanics of Delamination Tests," *Journal of Strain Analysis*, Vol. 24, No. 4, 1989, pp.207-214.
9. Blackman, B., Dear, J. P., Kinloch, A. J. and Osiyemi, S., "The Calculation of Adhesive Fracture Energies from Double-Cantilever Beam Test Specimens," *Journal of Materials Science Letters*, Vol. 10, 1991, pp 253-256.
10. Williams, J. G., "Large Displacement and End Block Effects in the 'DCB' Interlaminar Tests in Modes I and Mode II," *Journal of Composites Materials*, Vol. 21, April 1987, pp. 330-347.
11. Mostovoy, S., Ripling, E. J., and Bersch, C. F., "Fracture Toughness of Adhesive Joints", *Journal of Adhesion*, 3 (1971) 125-144.
12. Crews, J. H., Jr., Shivakumar, K. N. and Raju, I. S., "Strain Energy Release Rate Distributions for Double Cantilever Beam Specimens," *AIAA Journal*, October 1991, pp. 1686-1691.
13. "Test Procedures for Structural Automotive Adhesive and Adhesively Bonded Joints: Mode I Fracture Toughness," *Draft*, Oak Ridge National Laboratory, 1995.
14. Carlsson, L. A., Gillespie, J. W., Jr., and Pipes, R. B., "On the Analysis and Design of the End Notched Flexure (ENF) Specimen for Mode II Testing," *Journal of Composite Materials*, Vol. 20, November 1986, pp. 594-604.
15. "Test Procedures for Structural Automotive Adhesive and Adhesively Bonded Joints: Mode II Fracture Toughness," *Draft*, Oak Ridge National Laboratory, 1995.
16. Freda, T., "The Use of Laminated Beams for the Determination of the Pure and Mixed-mode Fracture Properties of Adhesives," *Engineering Mechanics Research Laboratory, EMRL 87-5*, University of Texas at Austin, June 1987.

17. "Test Procedures for Structural Automotive Adhesive and Adhesively Bonded Joints: Mode II Fracture Toughness," *Draft*, Oak Ridge National Laboratory, 1996.
18. "Test Procedures for Structural Automotive Adhesive and Adhesively Bonded Joints: Mix-Mode Fracture Toughness," *Draft*, Oak Ridge National Laboratory, 1996.
19. Liechti, K. M., et al, "Deformation and Fracture Mechanisms in Automotive Bonded Joints," *Final Report*, Engineering Mechanics Research Laboratory, EMRL 96-6, University of Texas at Austin, July 1996.
20. Liechti, K. M., et al, "Deformation and Fracture Mechanisms in Automotive Bonded Joints," *Final Report Design Supplement*, Engineering Mechanics Research Laboratory, EMRL 96-6, University of Texas at Austin, July 1996.
21. Paulauskas, F. L., Meek, T. T., and Warren, C. D., "Adhesive Bonding/Joining via Exposure to Microwave Radiation," *Proceedings of the 27<sup>th</sup> International SAMPE Technical Conference*, Albuquerque, N. M., October 1995.
22. Paulauskas, F. L., Warren, C. D., and Meek, T. T., "Adhesive Bonding Via Exposure to Microwave Radiation and Resulting Mechanical Evaluation," *Proceedings Spring Materials Research Society (MRS) Meeting*, San Francisco, CA., April 1996.
23. Paulauskas, F. L., McMillan, A. D., and Warren, C. D., "Adhesive Bonding Via Exposure to Variable Frequency Microwave Radiation," *Proceedings Spring Materials Research Society (MRS) Meeting*, San Francisco, CA., April 1996.
24. Paulauskas, F. L., and Meek, T. T., "Bonding of Thermoset Substrates Using Ultrasonic Technology," *in preparation*.
25. Warren, C. D., Paulauskas, F. L., and Boeman, R. G., "Laser Ablation Assisted Adhesive Bonding of Automotive Structural Composites", *in preparation*.

**DISTRIBUTION****INTERNAL**

R. G. Boeman (5)  
M. A. Brown  
L. B. Dunlap  
D. L. Erdman (5)  
E. C. Fox  
E. T. Grostick  
L. B. Klett  
R. D. Lomax  
S. R. McNeany  
R. E. Norris  
F. L. Paulauskas  
J. M. Starbuck  
Dave Warren  
G. E. Wrenn  
R. E. Ziegler  
Central Research Library  
Laboratory Records – RC (2 for transmittal to OSTI)

**EXTERNAL****General Motors**

T. J. Dearlove  
E. M. Hagerman  
J. F. Quinn  
J. A. Schroeder  
K. C. Taylor

**DaimlerChrysler**

D. L. Denton  
A. Rich

**Ford**

J. DeVries  
R. Jeryan  
S. Ward

**USCAR -file**